FERNANDA CRISTINA NASCIMENTO SILVA

Thermodynamic study of oxyfuel gas turbines: from O_2 production to CO_2 abatement

São Paulo

2021

FERNANDA CRISTINA NASCIMENTO SILVA

Thermodynamic study of oxyfuel gas turbines: from O_2 production to CO_2 abatement

Corrected Version

Dissertation submitted in partial fulfillment of the requirements of the Degree of Master in Science at the Polytechnic School of the University of São Paulo.

Area: Mechanical Engineering – Energy and Fluids

Supervisor: Prof. Dr. Silvio de Oliveira Júnior

São Paulo
2021

Este exemplar foi revisado e corrigido em relação à versão original, sob responsabilidade única do autor e com a anuência de seu orientador.

São Paulo, 18 de Junho de 2021

Assinatura do autor: _____

Assinatura do orientador: _____

Catalogação-na-publicação

Silva, Fernanda Cristina Nascimento
Thermodynamic study of oxyfuel gas turbines: from O2 production to CO2 abatement / F. C. N. Silva -- versão corr. -- São Paulo, 2021.
134 p.

Dissertação (Mestrado) - Escola Politécnica da Universidade de São Paulo. Departamento de Engenharia Mecânica.

1.Offshore 2.Plataformas offshore 3.Oxyfuel 4.Carbono 5.Captura de carbono I.Universidade de São Paulo. Escola Politécnica. Departamento de Engenharia Mecânica II.t.

AGRADECIMENTOS

Concluir esse mestrado foi um longo e tortuoso caminho. Muitas vezes achei que iria nadar, nadar e morrer na praia. Felizmente e aparentemente não foi isso que aconteceu. E estou convicta que isso só foi possível por conta das inúmeras pessoas que, de diversas formas, contribuíram para a realização dessa empreitada.

Gostaria de agradecer ao meu orientador, Silvio. Além de me guiar por esse processo inédito para mim com discussões e aporte teórico, foi também imensamente paciente e compreensivo com as dificuldades que enfrentei. Dificuldades essas que nem sempre soube articular bem. Por todo direcionamento, suporte, ajuda e oportunidades, sou muito grata!

Agradeço a minha mãe, Rita, e a meu pai, Joel. Minha maior torcida desde o primeiro dia. Em absolutamente todos os desafios, independente de discordâncias, o suporte incondicional de meus pais esteve lá. Obrigada e espero que saibam que os amo muito. E sempre.

Agradeço meus irmãos de sangue, Marina e Leonardo, e amigas-irmãs e amigos-irmãos adquiridos ao longo da vida. Lis Barreto, Bruno Lima, Érica Tirzah, Ingrid Araújo, Carol Martins, Lucas Gomes. Parceiros que chegaram em diferentes momentos mas que agradeço imensamente a disposição de me ouvir, acolher e aconselhar. E nesse momento não foi diferente. Muito obrigada pelo carinho e força.

Um agradecimento especial a Daniel Flórez-Orrego. Sua contribuição, principalmente nos estágios iniciais desse trabalho, foi de grande importância para o seu desenvolvimento. Obrigada pelas discussões, ajuda na confecção do texto, trocas e parcerias.

No mais, gostaria de agradecer à banca avaliadora, muito solicita e que contribuiu com valiosos *insights* para a dissertação. Agradeço ao Programa de Pós-Graduação de Engenharia Mecânica da Universidade de São Paulo e seus funcionários que também viabilizaram o presente trabalho assim como o Conselho Nacional de Desenvolvimento Científico e Tecnológico, CNPq.

ABSTRACT

On conventional offshore petroleum platforms, the combined heat and power production (CHP) currently depends on simple cycle gas turbine systems (SCGT) that operate at a lower efficiency and increased environmental impact compared to modern onshore thermoelectric plants. Additionally, the reduced space and the limited weight budget in offshore platforms have discouraged operators from integrating more efficient but also bulkier cogeneration cycles (e.g. combined cycles). In spite of these circumstances, more stringent environmental regulations of offshore oil and gas activities have progressively pressured companies to lean towards the integration of advanced cogeneration systems together with either customary or unconventional carbon capture approaches to maintain both higher power generation efficiencies and reduced CO_2 emissions. Accordingly, the performance of a conventional offshore petroleum production platform (without a carbon capture system) is assessed and compared to other configurations based on either an amines-based chemical absorption system or oxyfuel combustion concepts (e.g. S-Graz and Allam Cycles) for CO_2 capture purposes. Since the original power and heat requirements of the processing platform must be satisfied, an energy integration analysis is performed to determine the waste heat recovery opportunities, whereas the exergy method helps quantifying the most critical components that lead to the largest irreversibility and identifying the thermodynamic potential for enhanced cogeneration plants. As a result, the oxyfuel gas turbines cogeneration based plants, the Allam and the S-Graz cycles, present competitive exergy performances such as power exergy efficiencies of 42.63% and 27.10% compared to 25.41% and 23.59% exhibited by SCGT and post-combustion systems, respectively. Furthermore, those advanced systems allow for significant cutting down of atmospheric CO_2 emissions while maintaining similar unit exergy costs and higher rates of heat recovery as shown by the pinch and exergy analysis.

Keywords: Offshore platforms, oxyfuel, carbon capture

RESUMO

Em plataformas de petróleo *offshore* convencionais, a produção combinada de calor e potência depende atualmente de sistemas de turbina a gás de ciclo aberto que operam com menor eficiência e maior impacto ambiental em comparação com as modernas termelétricas terrestres. Além disso, o espaço reduzido e peso limitado nessas plataformas desencorajam os operadores de fazer uso de ciclos de cogeração mais eficientes, mas também maiores (por exemplo, ciclos combinados). Apesar disso, regulamentações ambientais mais rigorosas das atividades de petróleo e gás *offshore* provocaram renovado interesse em sistemas de cogeração avançados e técnicas de captura de carbono. Sejam essas técnicas convencionais ou não, sua integração a sistemas avançados de cogeração buscam manter as eficiências de geração de energia altas à medida que reduz emissões de CO_2. Em conformidade com esses objetivos, o desempenho de uma plataforma convencional de produção de petróleo *offshore* (sem sistema de captura de carbono) é avaliado e comparado a outras configurações baseadas em um sistema de absorção química através do uso de aminas ou conceitos de oxi-combustão (por exemplo, ciclos S-Graz e Allam) para fins de captura de CO_2. Como os requisitos originais de energia e calor da plataforma de processamento devem ser satisfeitos, uma análise de integração energética é realizada para determinar as oportunidades de recuperação de calor residual. Por outro lado, uma análise exergética ajuda a quantificar os componentes mais críticos que levam a maior irreversibilidade. Como resultado, as plantas com sistema oxi-combustão, com ciclos Allam e S-Graz, apresentam desempenho exergético competitivo, com eficiência exergética de 42,63% e 27,10% em comparação com 25,41% e 23,59% exibidas pelos sistemas de ciclo aberto e pós-combustão, respectivamente. Ademais, esses sistemas avançados permitem reduzir significativamente as emissões atmosféricas de CO_2, mantendo custos de exergia unitários similares e taxas mais altas de recuperação de calor, como mostrado pela análise *pinch* e exergética.

Palavras-chave: plataformas offshore, oxi-combustão, captura de carbono

FIGURES

TABLES

ABREVIATIONS

ASU	Air Separation Unit
BAU	Business As Usual
BioCCS	Biological Carbon Capture and Sequestration/Storage
CC	Composite Curve
CCS	Carbon Capture and Storage
CES	Clean Energy Systems
CHP	Combined Heat and Power
COE	Cost of Electricity
CONAMA	National Environmental Committee
DEA	Diethanolamine
EU ETS	European Union Emissions Trading System
FPSO	Floating Production Storage Offloading
HHV	Higher Heating Value
HPC	High Pressure Column
HPT	High Pressure Turbine
HRSG	Heat Recovery Steam Generator
HTT	High Temperature Turbine
IEA	International Energy Agency
IGCC	Integrated Gasification Combined Cycle
IP	Intermediate Pressure
IPCC	Intergovernmental Panel on Climate Change
ITM	Ion Transport Membrane
LHV	Lower Heating Value
LPC	Low Pressure Column
LPST	Low Pressure Steam Turbine
LPT	Low Pressure Turbine
MEA	Monoethanolamine
MER	Minimum Energy Requirement
MHI	Mitsubishi Heavy Industries
NCS	Norwegian Continental Shelf
NGCC	Natural Gas Combined Cycle
NOx	Nitrogen Oxides

ORC	Organic Rankine Cycle
OTM	Oxygen Transport Membrane
PSA	Pressure Swing Adsorption
SCGT	Simple Cycle Gas Turbine
SCOC-CC	Semi-Closed Oxyfuel Combustion-Combined Cycle
SRC	Steam Rankine Cycle
TIT	Turbine Inlet Temperature
TSA	Temperature Swing Adsorption
TTM	Thermal Turbomachinery and Machine Dynamics
TU	Technology University
TX	Texas
WHRU	Waste Heat Recovery Unit
WOE	World Energy Outlook
ZEP	European Zero Emissions Technology and Innovation Platform

SYMBOLS

Latin Symbols

B	Exergy (kJ)
$\boldsymbol{B}$	Exergy rate/flow rate (kW)
b	Specific exergy (kJ/kg)
$\boldsymbol{b}$	Specific exergy rate (kW/kg)
E	Energy (kJ)
$\boldsymbol{E}$	Energy rate (kW)
h	Specific enthalpy (kJ/kg)
$\boldsymbol{h}$	Specific enthalpy rate (kW/kg)
q	Heat (kJ)
q	Heat rate (kW)
s	Specific entropy (kJ/kg K)
$\boldsymbol{s}$	Specific entropy rate (kW/kg)
R	Universal gas constant (=8.314 J/mol K)
T	Temperature (K) or (ºC)
p	Pressure (kPa), (MPa) or (bar)
x	Molar fraction
c	Unit exergy cost (kJ/kJ), CO_2 emission cost (gCO_2/MJ)
$\boldsymbol{M}$	Direct CO_2 emissions rate (gCO_2/s)
W	Work (kJ)
$\boldsymbol{W}$	Power(kW)

Greek Symbols

γ_i	Coefficient of activity
φ	Chemical exergy to Lower heating value ratio
Δ	Difference
η	Efficiency

Subscript

0	Restricted reference state, Standard value
00	Partial pressure (kPa), (MPa) or (bar)
i	i-th flow, i-th reaction rate
T	Total
P	Products
F	Fuel
CO_2	Carbon Dioxide
O_2	Oxygen
Rxn	Reaction derived CO_2 emissions
power	Power cycle
cogen	Cogeneration
sep	Separation
WHRU	Waste Heat Recovery Unit
ASU	Air Separation Unit
q	Heat

Superscript

T	Total
P	Potential
K	Kinectic
PH	Physical
CH	Chemical
mix	Mixture
j	j-th output
i	i-th input
Q	Recovered heat

TABLE OF CONTENTS

1. Introduction

The last few decades are a particularly unique moment in human history due to the unprecedented challenge posed by climate change and its consequences throughout the globe's systems [1, 2]. The most recent IPCC report [3] revokes the previous widespread consensus on keeping global warming below 2 ºC, urging nations to step up their efforts to limit warming to 1.5 ºC above pre-industrial levels in the next 10 years. Although the situation is alarming and the dire effects of the changing climate are already felt around the world with the prospect of becoming even worse, little has been done to achieve even the most optimistic targets [4]. Despite that, some initiatives launched by governments, private companies, organized individuals and academic institutions intend to search for the best combination of energy technologies that may help eliminate and mitigate emissions from anthropic activities. Special attention is paid to the burning of fossil fuels, particularly in the energy sector, since it is one of the biggest contributors to the global emissions budget [5, 6]. Although a fossil-free future would be ideal, the phase-out of fossil fuels still poses many questions and debates over how the transition towards a decarbonized future should occur. This uncertainty arises in part due to the extensive existing and incoming infrastructure required, economic and political interests, as well as the characteristics of the various techniques and energy sources at hand [7, 8]. Nevertheless, some presence of fossil fuel, coupled with carbon capture and storage techniques, is noted in scenarios such as in the World Energy Outlook 2017 [9] as well as in the IPCC's reports aforementioned. According to the former's Sustainable Scenario, for instance, carbon capture and storage (CCS) as a mitigation tool might account for just under 10% of the total reduction of emissions in 2040, out of which one third would be allocated to the power and industrial sectors. This share of fossil fuels will probably be around due to the intermittent nature of renewables. In fact, the most likely scenario seems to point at a diversified energy matrix in which the solutions are closely integrated and at the same time decentralized [10, 11].

The different CCS techniques reported in the literature are usually grouped in pre-combustion, post-combustion and oxyfuel technology. In his thorough overview of carbon capture and storage technologies, Leung [8] characterizes these three

methods. In pre-combustion equipped systems, as the name suggests, fuel carbon is removed prior to combustion. The fuel is pretreated, undergoing gasification in the case of coal; or reform reaction if the chosen fuel is methane, the predominant component in natural gas.

The gasification process results in syngas which is mostly composed of CO and H_2 through the exposure of coal to a low oxygen level environment. The simplified reaction equation is shown in Equation I.

Analogously, a steam rich environment with methane fuel favors steam reforming also resulting in syngas, as shown in Equation III.

$$\mathrm{Coal} \xrightarrow{\text{gasification}} \mathrm{CO} + H_2 \qquad \text{I}$$

$$\mathrm{CO} + \mathrm{H_2O} \xrightarrow{\text{water-gas shift}} \mathrm{H_2} + \mathrm{CO_2} \qquad \text{II}$$

$$\mathrm{CH_4} + \mathrm{H_2O} \xrightarrow{\text{reform}} \mathrm{CO} + \mathrm{H_2} \qquad \text{III}$$

The water shift reaction follows, Equation II, in which case more H_2 and CO_2 are obtained. Hence, the higher the concentrations of CO_2 achieved through this method, the easier it is to remove the carbon dioxide content before combustion. Consequently, the rich H_2 fuel stream that remains goes on to the combustion chamber to be burnt with air, producing mainly N_2 and water [12]. Although part of the CO_2 content is removed, this type of combustion still produces NOx pollutants, which are highly toxic.

On the other hand, the post combustion process will treat the flue gas derived from air blown combustion with traditional fuels in order to obtain the CO_2 rich stream. The treatment of the flue gas can occur through a wide variety of techniques, since post-combustion technology is the most mature among CCS methods. However, the three most common methods are CO_2 capture by absorption, adsorption and cryogenic separation. In the absorption separation process, a liquid sorbent, the typical ones being monoethanolamine (MEA), diethanolamine (DEA) and potassium carbonate, removes the CO_2 from the flue gas stream by binding to its molecules, a process mainly driven by the concentration gradient. The now CO_2 rich solvent is preheated before entering the

desorber column, where it comes into contact with steam generated in the reboiler. The concentration gradient this time drives the CO_2 back to gaseous phase and the carbon dioxide rich stream eventually leaves the process after it is separated from the steam in the condenser [13].

As for adsorption-based separation, a solid surface is used to bind the CO_2 to it, instead of a liquid sorbent. Typical sorbents include molecular sieves, activated carbon, zeolites, calcium oxides, hydrotalcites and lithium zirconate and its selection is dependent on criteria such as high selectivity and adsorption capacity for CO_2; low energy penalties during regeneration; stable adsorption capacity of CO_2 after repeated adsorption/desorption cycles; and the CO_2 adsorption capacity cannot be inhibited at the presence of gas impurities like SO_2, NOx, O_2, and H_2O [14]. The release of the CO_2 bound and regeneration of the surface can either be done by pressure swing adsorption (PSA) or temperature swing adsorption (TSA) of the system containing the CO_2-saturated sorbent. Decreasing pressure or increasing system temperature releases the CO_2, which becomes available for transport.

Finally, the third post-combustion method is cryogenic distillation. This process is very similar to the cryogenic separation of air, which entails low temperatures and high pressures, which in turn makes it a very energy intensive operation. In it, flue gas is compressed, dried and cooled to temperatures just before the temperature of desublimation of CO_2 contained in the gas. Distillation columns separate the CO_2 from oxygen and nitrogen present in the gas. At last, CO_2 is expanded and another column further purifies the CO_2 stream [15]. Moreover, cryogenic separation may also be achieved through the desumblimation of CO_2. This route would avoid the need for distillation columns and therefore could be less energy intensive than similar techniques [16]. Furthermore, membrane separation is also commonly used to separate CO_2 from natural gas [8].

Oxyfuel combustion is fundamentally different from pre and post-combustion as it does not tweak the fuel composition neither the products of conventional combustion. In this technique, fuel is fired with nearly pure oxygen (above 95% mole), which results in a combustion product composed of mainly CO_2 and water. This particular make up facilitates separation via condensation of the water. The

dry CO_2 rich stream that is left is then ready for commercialization and/or subsequent storage. And since there is no dilution in nitrogen, plants employing oxyfuel are easily low emitters of NOx pollutants [6]. Despite those advantages, obtaining highly pure oxygen is a very costly process energy wise and strains the plant overall performance with its parasitic load [1, 17, 18]. Furthermore, in order to control the turbine inlet temperature and to avoid harmful material overheating, a partial recycling of the flue gases produced is still required. Hot section temperatures could also be controlled by either injecting steam (alongside the gaseous fuel, the oxidizer and the recycled flue gas) into the combustor chamber or directly into the turbine. Such strategy is actually employed in various works [6, 19-21], as long as high temperature resistant gas turbines are not widely commercially available. In order to understand these technical challenges, test and demonstration plants have been built. Most of the demonstration activities of oxyfuel cycles were done for the CES cycle in the Kimberlina test facility in Kern County, California, USA. Moreover, future demonstration is planned for the Semi Closed Oxyfuel Combustion-Combined Cycle (SCOC-CC) in Norway and for the Allam Cycle in its 50 MW demonstration plant commissioned in 2016 [22]. Figure 1 summarises the steps of each of the CCS processes aforementioned.

Figure 1. Modified flowchart indicating the steps of the most common carbon capture techniques

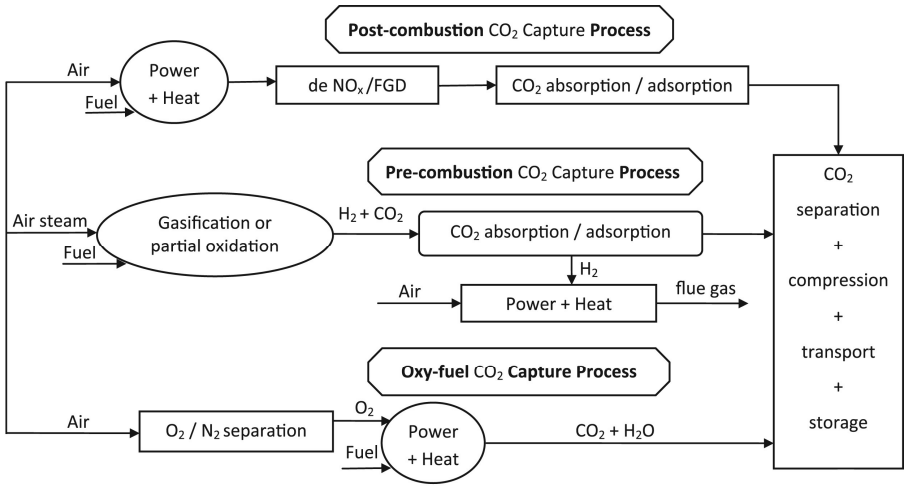

Source: [8]

It is noticeable through the commissioning of oxyfuel based plants and the increasing abundance in the literature of oxyfuel related research that this particular CCS technique is currently seen as a way of decarbonizing highly carbonized sectors. However, despite of the increasing interest and documentation of other CCS technologies in oil and gas offshore activities,[23-27], a technical analysis of the application of oxyfuel technology in a Petroleum Floating Production Storage and Offloading (FPSO) unit has rarely been explored, let alone under the lenses of an exergy analysis. Jordal et al. [28] investigated the cycles based on the simplest oxyfuel cycle (SCOC-CC) and variants there-of compared to a reference case of an amines-based (MEA), post-combustion cycle already extensively studied and monitored since 1996 in the North Sea in Norway [29-32]. In their work, opportunities for size and weight reduction such as decreasing the number of compression trains and membrane equipped air separation units are explored. Yet important to understanding the viability and challenges of integrating oxyfuel cycles and offshore applications, the authors' analysis did not benefit from a combined First and Second Law study of the case. Several other works aiming at efficiency enhancement of offshore platforms and/or CO_2 emissions attenuation through exergy analysis have also been conducted, however, as previously stated, did not include the specific CCS technique of oxyfuel combustion. In [33], Nguyen et al. presents several strategies to improve the platform's performance ranging from integration of steam cycles to Organic Rankine Cycles (ORCs), among others. Furthermore, Carranza et al. [34, 35] investigated the impact of modes of operation and, more to the point, the integration of a post-combustion carbon capture system on a FPSO operating in the Pre-Salt region. Despite reductions in CO_2 emissions and fuel consumption, the mitigation levels accomplished by employing those techniques are still significantly lower when compared to the levels the authors of oxyfuel cycles claim to achieve. In [36], different concepts are assessed in order to satisfy the power and heat supply requirements of an offshore platform. According to the authors, although a remarkable reduction of around 30% in CO_2 emissions can be achieved by connecting the platform to the power grid for instance, in comparison to the Gas Turbine plus Waste Heat Recovery Unit configuration, the oxyfuel driven setups such as the S-Graz and Allam cycle

outperform the environmental mitigation capabilities of the former reported configuration.

Notably, there is a lack of integration between oxyfuel technology and oil and gas offshore activities. Additionally, the current efforts that address emissions attenuation have not been enough [37]. In an attempt to comply with the ever growing stringent regulations and societal demands, Petrobras, has committed to abate CO_2 emissions throughout the enterprise. Brazil's largest oil and gas state company lays out a roadmap to abate carbon dioxide emissions in exploitation, production and refinery activities [38]. Motivated by these factors, the present work applies two selected oxyfuel cycles to a FPSO unit intended to operate at the Brazilian Pre-Salt oilfield conditions. These power cycles are assessed and compared to two other configurations: a conventional and an amines-based equipped platform. The former, also referred to as Business As Usual (BAU) configuration, represents the current state of affairs in Pre-Salt offshore platforms. This means that this layout is not equipped with any sort of CCS system, aside from membranes which separate CO_2 from natural gas incoming from the well [39]. The latter is nearly identical to the conventional configuration aside from the addition of a post-combustion system which utilizes a monoethanolamine loop to remove the CO_2. The four configurations encompass both the processing and utility plants and are analyzed at a specific point in its cycle, instead of the whole platform’s lifetime. Furthermore, the study takes into consideration a platform’s specific mode of operation, of which there are three, and does not dive into the specifics of size and weight budgets of the platform either; however those key points will be the subject of future investigations. The exergy analysis and energy integration method are used to propose suitable exergy efficiency definitions to allow for a fair, level playing field when comparing the four designed setups. The subunit’s exergy destruction breakdown is used to allocate irreversibilities among the main units and streams composing the petroleum platforms. Analogously, unit exergy costs as well as the specific CO_2 emissions costs measure the exergy intensity and environmental impact of said units and streams. Meanwhile, the energy integration analysis is used to calculate the potential heat recovery. Finally, the penalties associated with the introduction of an air separation unit (in the case of the oxyfuel configurations) and an amine absorption carbon capture

system are discussed in the light of the performance of the conventional configuration that spares any CCS system.

2. Objective

The present work seeks to study the application of oxyfuel cycles, taking into account the oxygen production on site, in a FPSO unit, at peak oil production and functioning on a specific mode of operation in the Pre-Salt region in Brazil. The two oxyfuel cycle designs selected, S-Graz and Allam cycles, are compared to the conventional configuration of a FPSO unit and another one equipped with an amines-based (MEA) CCS system, which is regarded as one of the most mature post-combustion technologies. The ability of the advanced cycles to reduce emissions as well as other aspects of their performance are assessed according to indicators and metrics such as exergy efficiency, balanced composite curves, specific exergy destruction, specific CO_2 emissions, exergy breakdown and unit exergy and CO_2 emissions costs. Based on this evaluation, improvement opportunities are identified and discussed.

The steps to develop this work are as follows:

- Simulation models for each configuration are developed according to the control volumes established and scenarios are analyzed through the variation of parameters within admissible intervals for the plants;
- Execution of exergy and energy integration analysis;
- Comparison between designs based on the metrics, identification of irreversibility sources, integration opportunities and improvement discussions.

2.1 Index

In the following chapter the work is properly presented. Chapter 3 shows the background information on the systems that compose a regular FPSO unit. On topic 3.2, general information on oxyfuel cycles is introduced and how the different cycles are categorized. The oxyfuel cycles chosen for the present work are further detailed in subtopics 3.2.1 (The S-Graz cycle) and 3.2.2 (The Allam cycle). Then air separation techniques are explained on topic 3.3. The chapter closes with topics 3.4 on CO_2 purification and 3.5 showing a literature background on exergy analysis applied to the context of offshore activity and CO_2 mitigation.

On chapter 4, the methodology applied to the study is presented and its steps detailed. Chapter 5 gives an overall look at the exergy concept, types of exergy and exergy balance for a control volume. Topic 5.1 details the difference and meaning of the restricted reference state and dead state. Meanwhile, topic 5.2 displays the theory necessary for the accomplishment of an energy integration analysis. Analogously, topic 5.3 dives into the background of unit exergy costs and CO_2 emissions costs. Finally, on topic 5.4 exergy efficiencies are defined as performance indicators along with an explanation of the modeling process.

Chapter 6 goes into the specifics of the layout of each power cycle considered and how they function. Moreover, topic 6.1 details how the cryogenic air separation unit of the oxyfuel cycles operates and its parameters. On chapter 7, results are presented followed by a discussion of their meaning. Topic 7.1 contains tabled relevant parameters for the FPSO units operation as well as the discretion of the setups' subunits into power producers and consumers. On 7.2, the energy integration analysis is presented where waste heat recovery opportunities are put forth. On 7.3, the performance of each layout is measured using exergy definitions established on 5.4 along with metrics of exergy destruction rates and CO_2 emissions. On 7.4, the theory and methods layed out on 5.3 are applied to the four platforms and the most relavant costs are displayed in a bar plot. At last, the results presented previously are recapitulated and discussed in light of the larger context the work is immersed in.

3. Background

In this chapter, bibliography surrounding FPSO functioning and evaluation in light of an exergy analysis perspective, carbon capture technology and oxyfuel cycles is presented.

3.1 FPSO

A FPSO unit is one of the facilities through which petroleum can be exploited in deep and ultra-deep waters. Its initials stand for Floating, Production, Storage and Offloading, which characterize the main attributes and functions of this ship. These floating units are employed in offshore sites above 2000 meters of water and can be kept in place thanks to modern anchorage systems or dynamic positioning systems. They are usually repurposed oil tankers although some can be fabricated for that end. The production function of these ships begins at the *risers*, flexible tubes that take petroleum from the reservoirs to the platform's *manifold* or *production header*. In the manifold the pressure of income fluid from multiple wells is equalized and reduced until it reaches the appropriate pressure of primary separation [40, 41].

In the primary separation, the petroleum is heated by hot pressurized water and goes on to a three-phase separator where oil, water and gas are obtained. Each individual stream follows different paths in order to receive adequate treatment and be referred to its proper destination. In the case of the main product, namely oil, it is stored in tanks until it is offloaded into oil tankers which in turn take it to shore. The water, when it reaches acceptable levels of contamination, is discharged to the sea, and the gas is treated to be either exported or re-injected back into the reservoir [42]. The FPSO unit scheme described is displayed in Figure 2 as follows.

Figure 2. FPSO unit scheme

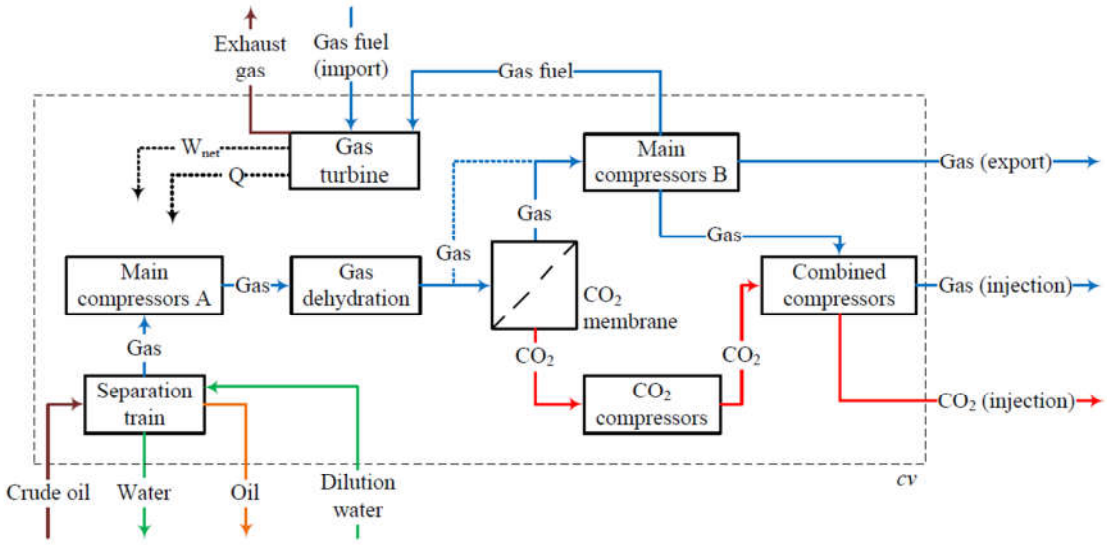

Source: [43]

In his dissertation, D'Aloia presents a thorough description of the multiple systems that compose a FPSO unit operating in the Pre-Salt region in Brazil. Therefore, the subsequent sections are based on D'Aloia's work and present the subsystems and its processes which compose the FPSO operation [44].

3.1.1 Primary separation of petroleum

A chain of vessels allow the separation of the petroleum mixture into its three main components: oil, water and gas. The first vessel is the three-phase vessel (Figure 3) which, by keeping the fluid for an interval of time known as *residence time*, achieves rudimentary separation due to differences in specific mass. Gas, which is the lightest fraction, is collected from the upper part of the vessel and routed to the platform's compression system. The produced water stream goes on to the water treatment system, and the oil goes to other vessels so separation may be refined.

Figure 3. Three-phase vessel/gravitational tank

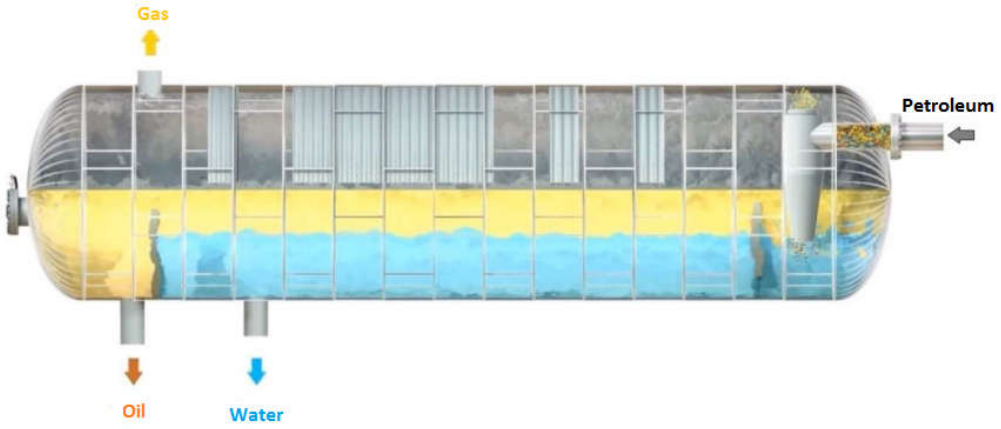

Source: [42]

The oil stream, as it goes through its purification process, flows through two heat exchangers. The first heat exchanger pre-heats the oil while the second one complements heating by utilizing pressurized hot water. The water used for primary separation usually is heated through the recovery of heat of the turbine exhaust gases in a *Waste Heat Recovery Unit* (WRHU). Downstream from the heating process, two degasser and two electrostatic coalescer vessels are alternated to further separate oil from light hydrocarbons and water. The first degasser (called pre-degasser) will separate light hydrocarbons that remain in the oil at milder pressures than the pressure in the three-phase vessel (around 8 bar). Subsequently, oil is separated from residual water in the pre-electrostatic coalescer vessel where parallel plates are polarized by an alternate current and demulsify water from oil (see Figure 4). The electric field generated elongates the water particles causing them to agglutinate. The bigger water droplets decant and the water is removed from the bottom part of the vessel while the oil continues towards the second pair of degasser/electrostatic vessels. That second step functions the same way as the first described above however at even lower pressures (4 bar). After industry standards for oil purification are met, the oil goes to storage tanks in the FPSO until it is offloaded into oil tankers.

Figure 4. Electrostatic vessels

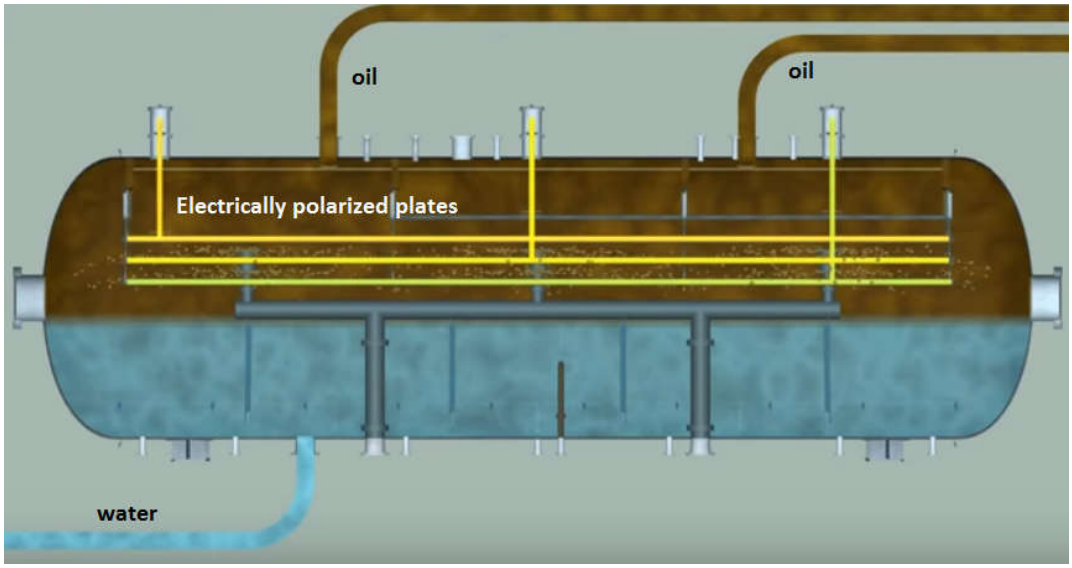

Source: [45]

3.1.2 Produced water treatment system

The water obtained from the three-phase vessel still contains a high amount of oils present in its composition, which prevents its discharge into the sea. According to Brazilian legislation CONAMA 393/07 [46], the maximum limit of oils allowed in discharged water is 29 mg/L. Therefore, further treatment of produced water (water resulting from oil production) is necessary and is described as follows.

The first stage of water treatment consists of the employment of hydrociclones (see Figure 5). These devices are equipped with cylindrical and conic parts, the former with an opening known as *vortex finder*, the latter with an opening known as *apex.* The water is fed through an orifice tangentialy into the cylindrical section. The potential energy of water flux due to pumping transforms into kinetic energy as it rotates inside the hydrociclone. The heavier components, namely water and solid particles, occupy the periphery of the cylinder, whereas the lighter components tend to stay in the central region. The fluid is accelerated as the diameter decreases in the conic section of the equipment which cause a counter flow of the lighter components to form due to pressure diferential between center and wall. The heavier components flow is discharged through the apex and the

lighter components flow, through the vortex finder orifice, effectivily separating water and oil streams [47]. The oil returns to the three-phase vessel inlet and the water undergoes further treatment.

Figure 5. Hydrociclone

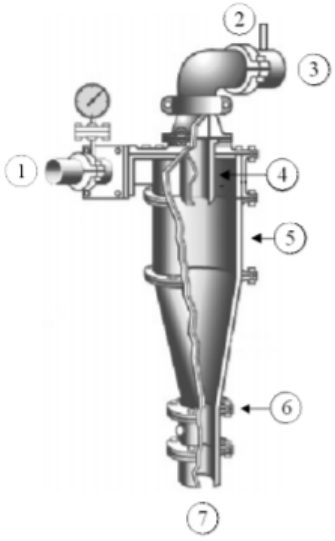

Source: [47]

In the next step, the remaining oil is separated from water through the use of an ascending stream of air. In a skim vessel, the air, in the form of bubbles, ascend in the tank going through the water encasing oil droplets in their way counter to the water flow, as being the heaviest component, tends to go towards the bottom of the vessel. The oil that was brought to the upper section of the vessel is then skimmed off the surface. The water is collected from the bottom of the vessel and analyzed to check whether or not it exhibits the proper conditions to be discharged into the sea. If that is not the case, it is stored in tanks specifically set apart to receive water out of specification. Depending on the platform, the produced water can be treated to the specific purpose of being re-injected so well pressure is maintained and oil production does not decline.

3.1.3 Gas compression and treatment systems

The systems encompassed in gas treatment and compression are considerably more complex than the processes of water and oil treatment. This is especially true for the platforms in the oilfields considered in this work. Moreover, the gas

may have more than one destination at once and varied allocation modes over time. The gas may be exported through pipelines in which case it must comply with more rigorous standards when compared to other ends. Another portion might be re-injected into the well. In that case, the volume of gas re-injected will depend on how much gas needs to be exported. The gas stream then needs to have its pressure elevated to higher values than the ones of the reservoir since the pressure level ascertained in Brazilian Pre-Salt are quite high (around 550 bar). At last, gas might also be directed to the flare system of the platform. It is noteworthy that this destination is only used as a last resort or in case the platform is not equipped with proper gas treatment systems. If treatment options for gas are not readily available in a few hours, production restrictions and operation shut down of the platform may occur. Figure 6 shows a flowchart that illustrates ways the gas may move through the FPSO unit.

Based on D'Aloia's work and operation requirements of Petrobras' FPSOs in Pre-Salt, the flow chart presented below gives an overview of the gas compression and treatment subsystems.

Figure 6. Processes' Flowchart

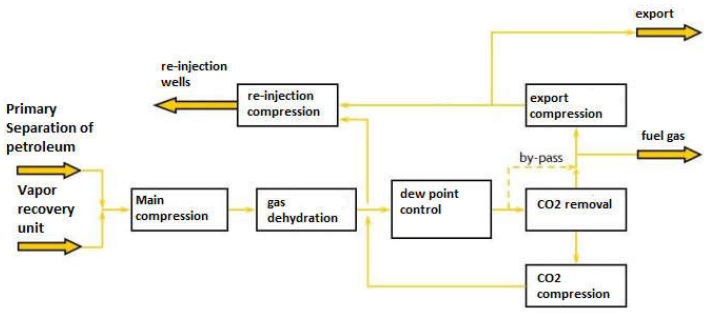

Source: adapted from [44]

3.1.3.1 Main gas compression system

In this subsystem, gas both coming from the three-phase vessel separation and oil treatment recovered by the vapor recovery unit is compressed to the first pressure step (50-55 bar). Before actual compression though, in fact before each compression step, the gas goes through a scrubber vessel (see Figure 7) in which water and heavier hydrocarbons that may still be present in it are separated from the gas. The dry gas leaves the scrubber, is compressed and is

subsequently cooled, which in turn condenses heavier fractions that are returned to the three-phase vessel separation stage to be processed again. The light and dry gas goes on to the dehydration step.

Figure 7. Scrubber vessel in yellow

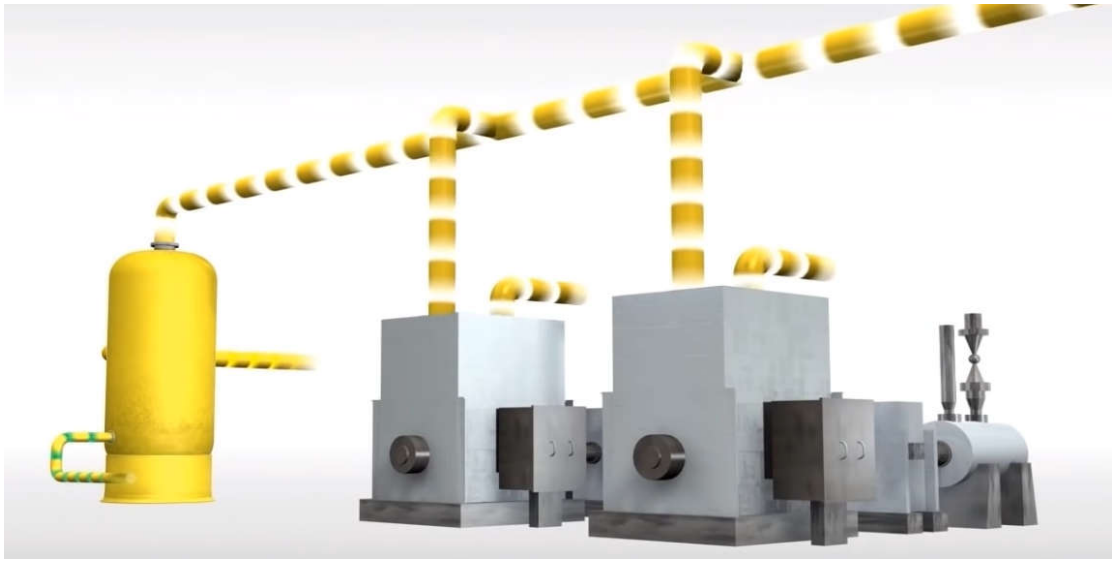

Source: [42]

3.1.3.2 Gas dehydration system

Although the gas leaving the scrubber is referred to as dry gas, as opposed to the “wet” gas at the inlet, it still is not exempt of water. The presence of natural gas and water at low temperatures and high pressures, often present in oil and gas well and pipeline equipment, offers the proper conditions needed in order to form gas hydrates. These hydrates can cause plugs which damage the gas transport system by such an extent that the petroleum industry spends around one billion US dolars a year trying to prevent its formation [48]. Therefore, in FPSO units, vertical vessels filled with zeolite sieves are used to remove the remaining water from the gas. The gas stream is forced from the bottom up and while it goes through the sieves, the water is left behind adsorbed by the zeolites due to its hydro affinity. When the sieves are saturated with water and can no longer adsorb, high temperature gas is forced on the opposite direction of operation capturing the water from the sieves actively regenerating them. There are usually three molecular sieves and while two of them dehydrate gas, the other one is regenerated.

3.1.3.3 Dew point control system

With practically no water content left in the gas, it now undergoes a process to further extract whatever heavy hydrocarbon molecules that may still be present in it. If left in the gas mixtures, the heavier hydrocarbons could condense in the pipelines, over pressuring the pipe and over powering liquid handling facilities, flow into compressors and end user sales points and even cause explosions at certain points. In order to avoid such consequences, after dehydration there is a dew point control system. Here the gas is cooled to temperatures below zero as to condense the heavier, denser hydrocarbon molecules. The cold fluid utilized to ensure cooling can either be a fraction of the gas that has been throttled as to have its temperature dropped through the Joule-Thompson effect, or refrigerant fluid such as R-134.

3.1.3.4 CO_2 removal system

This system removes the main contaminant of natural gas in the Santos basin, carbon dioxide. In order to achieve this, the gas goes through a set of membranes that allow the passage of smaller molecules, such as light hydrocarbon like methane, and halt bigger molecules such as CO_2. Depending on the composition of the incoming gas, it might carry 8-40% mol of CO_2. After undergoing the CO_2 removal process however, it leaves the membrane containing only 2-5% CO_2. The CO_2-rich stream, on the other hand, contains 30-50% CO_2 in its composition, although newer membranes can accomplish a 70% rate. There is also the option to bypass the membrane system partially or altogether which gives rise to the other modes of operation of the FPSO unit, which will be presented later on. Figure 7 (a) and (b) show the streams and its components before and after CO_2 removal and subsequent injection.

Figure 8. (a) petroleum from the well at approximately 2220 m under water before CO_2 removal (b) CO_2-rich stream injected into the well after the CO_2 removal process

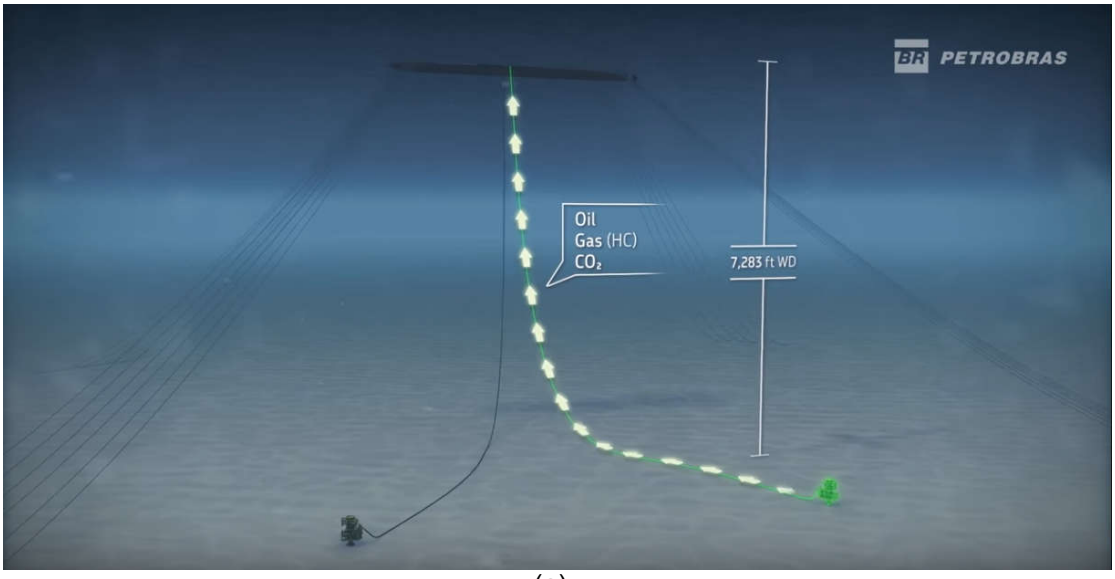

(a)

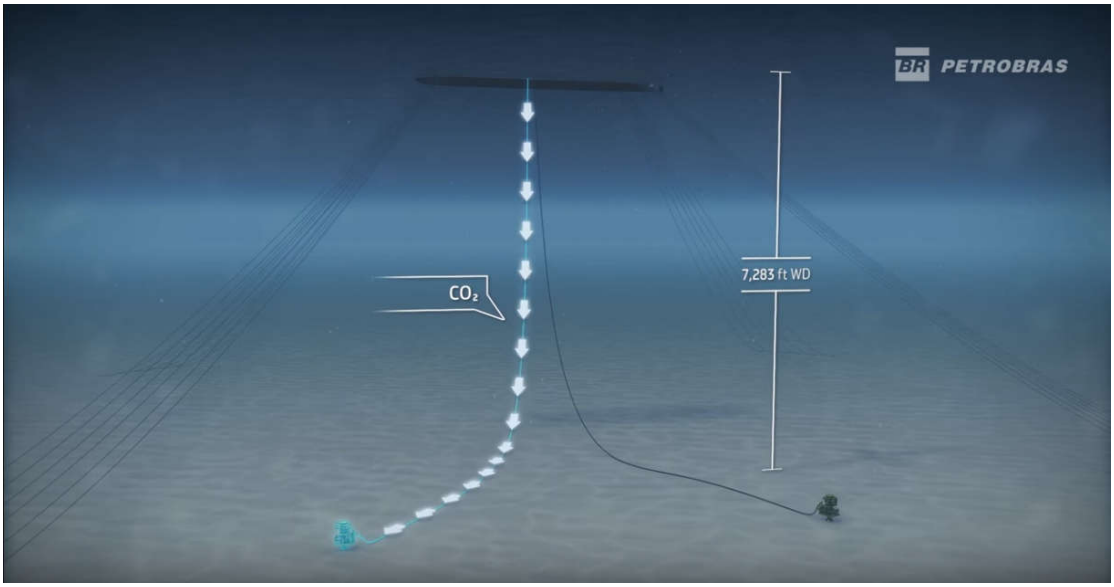

(b)

Source: [39]

3.1.3.5 CO_2 compression system

In this system, CO_2-rich stream has its pressure elevated after leaving the membrane from 3-4 bar to around 250 bar in order to allow suction by the injection compressors, which in turn will further compress it to 450-550 bar.

3.1.3.6 Export compression system

The hydrocarbon rich stream at this point is considered treated therefore it can be compressed to export. In this system, the pressure of said stream is elevated to around 250 bar, appropriate for transportation. After discounting the export portion of the gas, the remainder may be referred to the injection compression system. Furthermore, after membrane treatment and before export compression, part of the gas stream may be diverted in to the power generation system which is responsible for supplying the platform with electricity, as shown in the Process' Flowchart in Figure 6. Currently, the common configuration entails 4 gas turbines, out of which one is in stand-by while the others work. In case of unavailability of natural gas, the turbine operates utilizing diesel as fuel. Downstream of the turbines, the WHRU harvests exhaust gas exergy in order to heat water for petroleum primary separation.

3.1.3.7 Injection compression system

This system receives the CO_2-rich stream from the carbon dioxide compression system and/or the treated, compressed gas and elevates its pressure to 450-550 bar so it can be injected into the reservoir.

3.1.4 Water injection system

This system's function is to pump water into reservoirs as to avoid the decrease in pressure in the oil wells throughout the years. Recently, sea water has been used as injection fluid in Brazilian platforms, although produced water was the fluid of choice in older projects.

3.1.5 Utility and auxiliary systems

Utility systems are all of those which provide needed input to the operations related to the production and treatment of oil, gas and water. Some of which are:

cooling water system, vapor generation system, compressed air and water prospection.

Auxiliary systems are all of those that ensure inhabitability of the plant such as sewage treatment system, firefighting and drinkable water system.

3.1.6 Gas processing operational modes

As previously mentioned, the decision to bypass CO_2 removal via membranes allow for the possibility of the plant having different modes of operation. The three possible modes are as follows:

Operation Mode A – this mode entails complete deviation from the CO_2 removing membranes. Therefore, the gas is not treated and its only destination possible is reinjection into the reservoir.

Operation Mode B – in this mode, the CO_2 removal system is used to its full extent. This is the standard operation mode in which the plant functions 90% of the time. This mode allows for the export of treated gas and re-injects the CO_2-rich stream along with treated gas that has not been exported.

Operation Mode C – this mode represents the partial utilization of the CO_2 removal system. A portion of the gas is indeed treated while the rest bypasses the membranes, either by a change in the membrane system or low levels of carbon dioxide that do not justify the full use of the removal system. Some of the treated gas may be exported while the remainder might be injected back into the well along with the untreated gas and CO_2-rich stream.

Next section will present an overview of oxyfuel cycles and their exploration in the context of FPSO operation.

3.2 Oxyfuel cycles

Oxyfuel cycles are thermodynamic cycles which have as main characteristics the use of a nearly pure O_2 stream as oxidant. The main purpose of employing highly pure oxidant instead of air in the combustion process is to have the products of combustion present higher concentrations of CO_2 and water. In that way, purification towards achieving a concentrated CO_2 stream would be facilitated

given that water could be easily separated from it via condensation. However, this change in oxidant composition gives rise to other sets of factors in oxyfuel combustion that need to be addressed. Figures 9 (a) and (b) represent reactions IV and V, respectively, showing the key difference in combustion products in air blown and oxygen blown fuel oxidation (the fuel here assumed to be methane).

$$CH_4 + 2(O_2 + 3.76N_2) \rightarrow CO_2 + 2H_2O + 7.52N_2 \quad \text{IV}$$

$$CH_4 + 2O_2 \rightarrow CO_2 + 2H_2O \quad \text{V}$$

Figure 9. (a) Air-blown combustion (b) Oxyfuel combustion

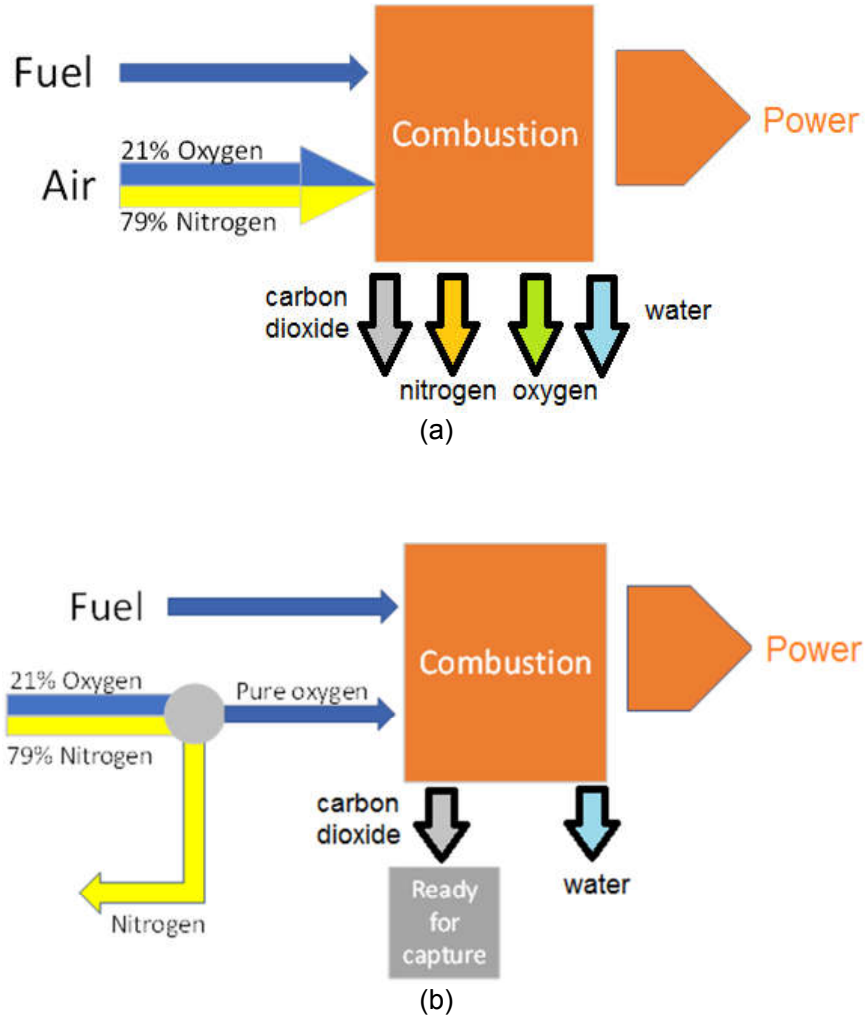

Source: author

Since the oxidant composition is different for oxyfuel cycles, the first issues arise from the air separation process which will supply the pure oxygen stream needed for combustion. The first question to be raised is regarding which process of air separation should be chosen and, unfortunately, various constraints relating to application, mass flow magnitude and purification requirements limit substantially the options at hand. For the specific situation approached in this work, the cryogenic distillation method is the most, if not the only one, suited technique for air separation. More detail on how the application requirements determine which separation technique is to be used will be shown in section 3.3.

Being cryogenic distillation the method of choice for applications such as the one presented in this work, issues inherent to this technique need to be considered in design, operation and analysis. First and foremost, the cryogenic distillation method is highly energy intensive. This is due to the need of compression of air to pressures to 5 bar or higher so it can be liquefied for distillation. Besides, the process destroys a significant amount of exergy, especially in the portions involving phase change such as the passage through the main heat exchanger and distillation columns due to intense heat exchange.

Another issue arises as a result of the change in the oxidant stream. Oxygen is no longer diluted in nitrogen, which makes oxyfuel cycles usually low in NOx emissions, with fuel being the only source of nitrogen. Nevertheless, dilution is still necessary due to the need to control the turbine inlet temperature, typically higher in oxyfuel cycles. Oxyfuel turbines are not yet widely available and even these equipment withstand, at best, a temperature of 1400 ºC maximum at their inlet, which is easily achievable and surpassed in oxyfuel combustion. Thus, dilution becomes a necessary step to lower turbine inlet temperatures which in turn alters the composition of the working fluid. Generally, CO_2 or H_2O will be the predominant component of the working fluid after dilution. The oxyfuel cycles are then categorized according to the working fluid's composition and it greatly influences the cycle's layout and operation parameters.

In the International Energy Agency's *Oxy-Combustion Turbine Power Plant* 2015 report [49], a comprehensive review and simulation comprised of over six hundred pages, along with commentary by companies and researchers, of the

main oxyfuel cycles found in the literature was conducted. As previously mentioned, the cycles are divided between two categories according to the composition of the working fluid. The CO_2-based cycles investigated, which are the ones whose main component of the working fluid is carbon dioxide, were the Semi-Closed Oxy-Combustion Combined Cycle (SCOC-CC) and the NET Power or Allam Cycle. On the other oxyfuel category, the water-based cycles, the cycles selected were the S-Graz and the CES cycles. The first cycle to be investigated in the report is the oxyfuel combined cycle (SCOC-CC) which exhibits a concept quite similar to common air-based combined cycles, however with near stoichiometric combustion with oxygen. The bottoming cycle to the main oxyfuel one is fed with steam raised in the Waste Heat Recovery Unit (WHRU) using high temperature exhaust gas, which will, downstream, go through a condensation process in order to separate the carbon dioxide stream from the water. Around 90% of the resultant stream (mainly CO_2 by this point) is recycled back to the combustor and the rest goes on to CO_2 compression [50], as shown in Figure 10.

Figure 10. Semi-Closed Oxyfuel Combined Cycle (SCOC-CC)

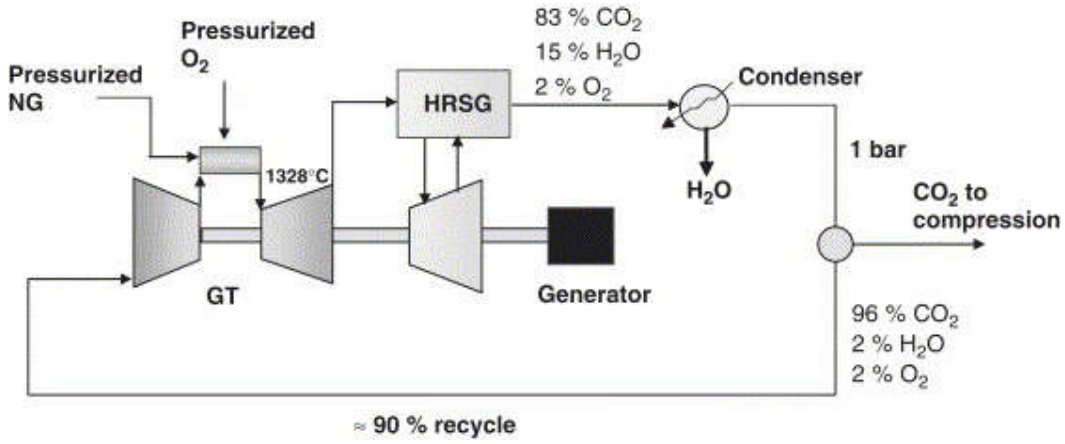

Source: [50]

Differently from SCOC-CC but still in the same CO_2-based category, the exhaust gas in the Allam cycle (or NET Power cycle), Figure 11, is not used to raise steam but to heat up recycled CO_2 and the oxidant stream. Furthermore, pressure ratios and inlet pressures are very different between these cycles. While the Allam cycle operates with pressures in the range of 200-400 bar at turbine inlet, but pressure ratios are around 10 [51], the oxyfuel combined cycle, on the other hand,

operates with pressures of 45-50 bar at turbine inlet and an approximate pressure ratio of 30. [52].

Figure 11. Allam cycle configuration

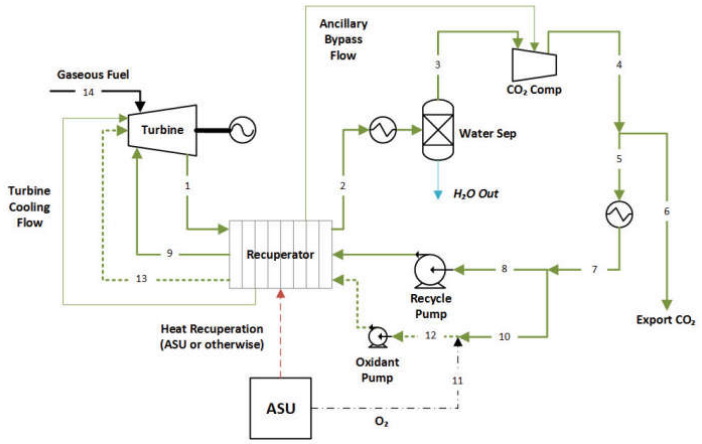

Source: [53]

On the water-based oxyfuel cycles front, the CES cycle uses water in vapor and liquid phases as temperature moderators. In the high pressure combustor, the “gas generator”, fuel conversion happens in the presence of preheated liquid water. The combustor operates at pressures around 80-100 bar and provides exhaust gas at outlet temperature of 760 ºC. The hot gas produced is expanded in a high pressure steam turbine (HP) and a fraction of it is reheated through the use of extra oxyfuel combustion in a re-heater to around 1760 ºC and is now at 40 bar. The gas that bypasses the re-heater is used to cool the intermediate pressure turbine (IP), which is the second expansion step. The final expansion takes place at the low pressure turbine (LP) which takes the gas from roughly 1 bar and 760 ºC to condensing pressure around 0.15 bar and 433 ºC [21]. The exergy in this stream is recovered by preheating the high pressure recycled water to the gas generator. Then, CO_2 is separated from water in a vacuum condenser and compressed to pipeline pressure. Figure 12 shows the cycle’s scheme described above.

Figure 12. CES cycle

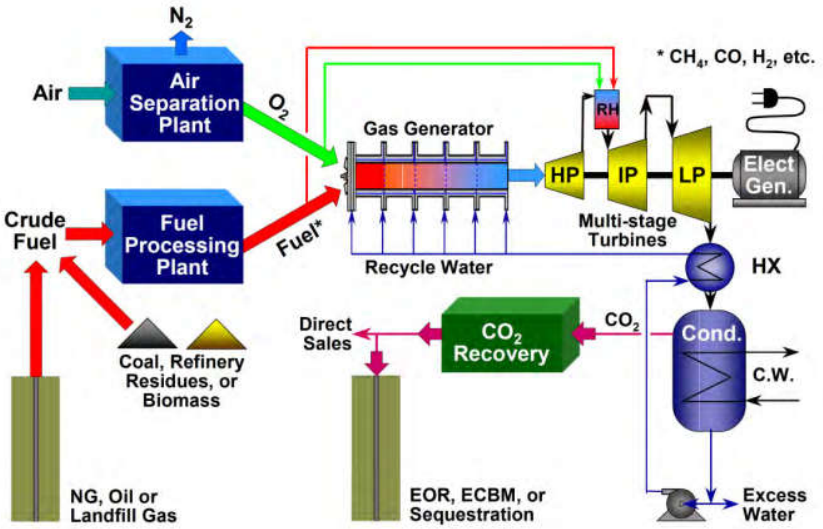

Source: [21]

Finally, the water-based cycle S-Graz is also analyzed in the report. Similarly to the oxyfuel combined cycle (SCOC-CC), exhaust gas is used to raise steam for a bottoming steam cycle which uses part of the water generated in the combustion process. After expansion, the steam cools both the combustor and the High Temperature Gas Turbine (HTT), as shown by the blue lines labeled “steam” leaving the High Pressure Turbine (HPT) in Figure 13. Exhaust gas from the High Temperature Turbine’s (HTT) outlet heats up the water for steam generation; a fraction of it is then further expanded to vacuum pressures at the Low Pressure Turbine (LPT), and condensed as to separate CO_2 from water. The resultant purified CO_2 goes on to the compression stage to be sold, used for enhanced oil recovery (EOR) or geological storage. The fraction of CO_2 that was not destined to the pipeline is recycled and along with steam acts as temperature control. Figure 13 shows the overall functioning of the S-Graz cycle described above.

Figure 13. S-Graz cycle

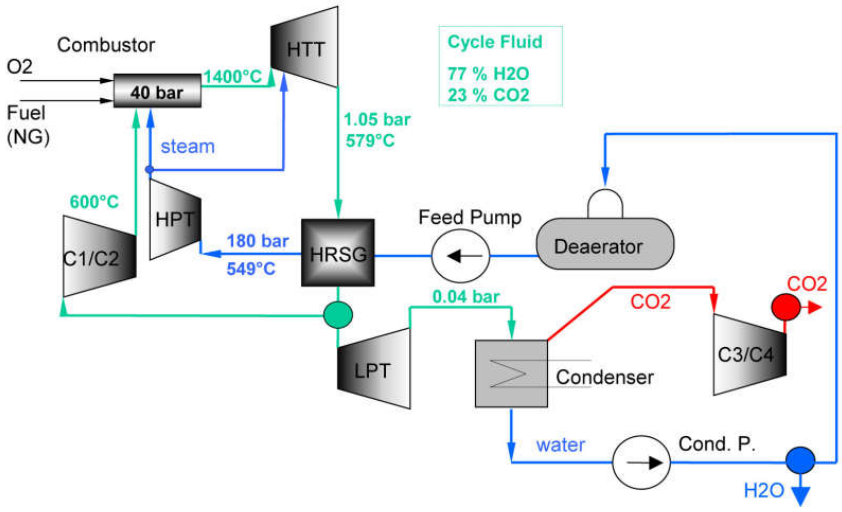

Source: [54]

Taking these cycles and variations there-of, metrics to carry out a technical evaluation, potential future improvements and application evaluation were defined and compared. As shown in Table 1 from the IEA's report, the Allam cycle, followed by the SCOC-CC and the S-Graz cycle, is the most efficient oxyfuel cycle (LHV and HHV) and the one with the lowest specific CO_2 emissions value. Interestingly, the IEA carried out another study on post-combustion capture technology in 2012 [55] and compared the results of these two reports, as shown in Table 2. The Allam cycle remains superior in terms of efficiency, levelised cost of electricity and CO_2 avoidance cost, which further enriches the argument pro implementation of oxyfuel cycles instead of other CCS technologies. However, total plant cost still favors deployment of post combustion capture technology, given its maturity and availability.

Table 1. Comparison between oxyfuel combustion powered plants and a reference NGCC plant in terms of CO_2 emissions, CO_2 captured and efficiency

	Net power output	CO_2 captured	CO_2 emissions	Efficiency		Efficiency penalty for capture (LHV)
				LHV	HHV	
	MW	kg/MWh	kg/MWh	%	%	% points
Reference NGCC plant	904	-	348	58.8	53.2	–
SCOC-CC	757	377	39	49.3	44.6	9.5
Allam cycle	846	336	37	55.1	49.9	3.7
Modified S-Graz	756	375	41	49.2	44.6	9.6
CES	751	379	41	48.9	44.3	9.9

Table 2. Comparison between post combustion and oxyfuel combustion performance with a reference NGCC as standard

	Efficiency (LHV)	Total Plant Cost	Levelised Cost of Electricity	CO_2 Avoidance Cost
	%	€/kW	€/MWh	€/tonne
Reference NGCC	58.8	655	62.5	–
SCOC-CC	49.3	1470	92.8	98
Allam cycle	55.1	1320	83.6	68
NGCC post combustion capture	52.0	1170	84.7	72

Source: adapted from [49]

Stanger et al. [22] also performed a multilayered and thorough evaluation of CO_2, water-based and second generation oxyfuel technology. In regards to turbo machinery and how its relation to the working fluid affects performance, efficiency may be largely penalized depending on working fluid composition when using conventional machinery, which is what IEA's 2015 report seeks to do as much as possible. New machinery for the SCOC-CC for instance would require reduced speed that also is appropriate to endure the high pressure ratios. As for the CES cycle, most of the challenges are related to the development of the intermediate pressure turbine (IP) which, in its third generation, requires its materials to withstand a 40 bar drop in 7 stages and 1760 ºC inlet turbine temperature; an incredibly high temperature even for oxyfuel turbines. In order to verify the feasibility of such technology, larger scale plants are needed to test Oxy-gas turbine concepts. So far, the only experience to date is the Kimberlina plant, in Kern County, California, where the CES cycle has had some developments, but

according to [56] the project has been either cancelled or put on hold. The latest developments of the CES cycle have been presented in [57], which point to CES's plans to use it as BioCCS technology in the following years. Furthermore, a testing plant in Norway is expected to test the oxyfuel combined cycle and a 50 MW Allam cycle demonstration plant was being developed and some success has been achieved [58], however little information has been reported on its progress since the start of the COVID-19 pandemic outbreak.

Although the cycles shown so far represent the most mature technology when it comes to oxyfuel combustion, second generation oxyfuel technology,such as air separation membranes instead of cryogenic distillation, does exhibit some promising performance results aligned with much less environmental impact. In his dissertation, Soundararajan [59] carried out an energy and exergy analysis to ascertain the efficiency loss incurred by the integration of cryogenic air separation and Oxygen Transport Membrane (OTM) in an oxyfuel combined cycle. When using conventional technology, by increasing the gas turbine pressure ratio (doubling it), the exergy and thermal efficiency of the cycle increase by 2 percentage points. When the OTM is integrated, exergy and thermal efficiency show even more potential, reaching a four to six percentage point increase when compared to the reference oxyfuel cycle used by the author.

Simpson and Simon [25] demonstrated which fuels and conditions would make oxyfuel technology attractive by comparing a base case (without carbon capture), an oxyfuel combined cycle and a generic post-combustion cycle. The authors concluded that oxygenated, high carbon content fuel such as biomass benefits oxyfuel cycles making it more efficient. The authors also correctly pointed out that a carbon purification step could be removed from the oxyfuel plant, therefore making it more competitive, if oxygen over 99% purity could be produced and burned in a combustor that operates very close to stoichiometry. Indeed, multiple authors and developers stress the need for combustors that operate with little oxygen excess [6, 51, 60] and some successful firings of such combustors have been documented [61].

Now that some background on some of the most important oxyfuel cycles has been laid out, the two oxyfuel cycles chosen to be approached in the present

work will be further detailed in the next subsections regarding their history of development and technical characteristics. The water-based cycle selected was the S-Graz cycle since its developers have been working on multiple aspects of the cycle for decades, from turbo machinery design to cycle lay out, as well as its flexibility to allow not only multiple kinds of fossil fuels but also use of hydrogen; an interesting characteristic given that the overarching goal is to assess technologies that allow greenhouse gas emissions attenuation. As for a representative of the CO_2 based cycles, the Allam or NET Power cycle has been selected. Among the oxyfuel cycles, this is the one that present the most promising results and the compact nature of the equipment involved makes it more suited for offshore applications.

3.2.1 The S-Graz cycle

The Graz Cycle was first proposed by H. Jericha in 1985 [62]. The original cycle seeks to be a carbon free cycle through which hydrogen and oxygen, products of electrolysis and/or thermochemical dissociation for load equalization, storage or simply avoiding high voltage transfer lines, could be burnt at higher efficiencies. This higher performance would be achieved through the transfer of the heat input by internal combustion of hydrogen and stoichiometric oxygen to the working fluid, steam, in the combustion chamber. Resorting to a Rankine cycle operating at pressures of 100 to 200 bar and temperatures of 1100 ºC, the author claims to achieve thermal efficiencies of 50 to 57%.

Figure 14 presents the plant's layout for an internal combustion steam cycle. Hydrogen and oxygen in stoichiometric proportions are supplied to the combustion chamber together with the working fluid, in this case, recirculated steam. Besides the heat recovery by direct contact that occurs here which, in turn, helps increasing efficiency, the presence of cooler steam also regulates the fluid's turbine inlet temperature. Hot steam as a result of hydrogen combustion is expanded following the combustion reaction. At this point, part of the exhaust steam enters a heat exchanger in order to heat up recirculated working fluid for combustion, as previously mentioned. The other fraction is further expanded to pressures below environmental conditions, condensed, degassed and water is purged from the system so it does not accumulate in the cycle as more water is

generated through combustion. The fraction that is not purged then joins the exhaust steam, before and after compression, and the resultant stream is heated in the heat exchanger before going into the combustion chamber.

Figure 14. Original Graz cycle with hydrogen as fuel

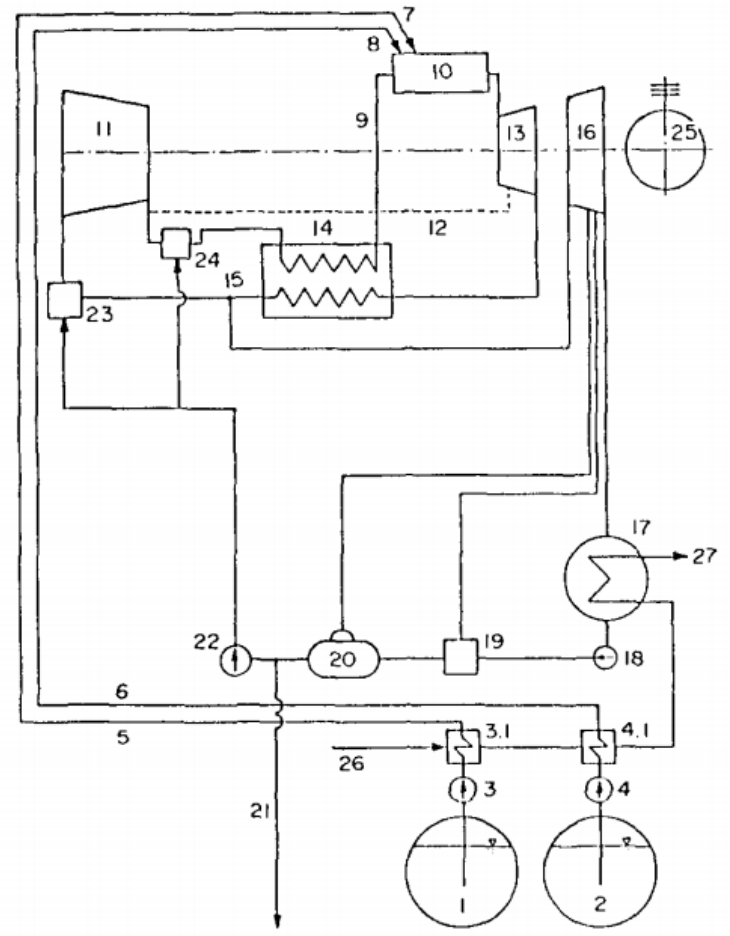

Source: [62]

Turbo machinery adequate for fuel hydrogen burnt in stoichiometric conditions would require development of hydrogen-oxygen burners, combustion chambers that operate near stoichiometry, steam cooled turbine blades to withstand high temperatures together with internal casing insulation and steam heat exchangers and injection coolers. Therefore, in subsequent years, researchers at Graz University presented improvements in cycle efficiency (1989) and detailed design of said combustion chamber (1991). In 1998, discussions with Japanese researchers resulted in a cooperative proposal for a 500 MW plant by Mitsubishi

(MHI) [60, 63]. Despite these efforts, high output solar plants producing H_2 and O_2 via electrolysis would not be available in time, so the cycle was adapted to fire fossil fuels and retaining the CO_2 generated. As of 2002, a Graz cycle was presented as "*prototype design for an industrial size plant, suited for natural gas-fuel and coal and heavy fuel oil gasification products, capable to retain the CO_2 from combustion and at the same time able to achieve maximum thermal efficiency*" [60].

The proposed prototype, when accounting for the air separation unit and oxygen compression, reaches a thermal efficiency of 57.51%, in line with optimum conventional combined cycle plants. The authors also detail the design of the most critical cycle equipment. The combustion chamber required to operate close to stoichiometry is arguably one of the most critical equipment in oxyfuel cycles. The combustor should entail a good mixing system since excess oxygen results in greater power for the air separation process and therefore penalizes overall efficiency. Cooling process of these structures should also be stressed since high flame temperatures compromise the integrity of reaction products causing their dissociation besides causing material degradation of the equipment. In order to address these problems, the authors propose a solution that consists of 4 burner tubes in parallel working in such a way that fuel and oxidant are injected in close proximity and steam is fed tangentially. As a result strong vortexes provide the cooling and mixing necessary for efficient combustion.

High inlet turbine temperatures also pose a significant challenge for the expanders operating in the high temperature region of the cycle. Material able to withstand such temperatures count on a cooling system patented for TU Graz in 1997 and is said to provide minimum heat loss, minimum cooling effort and minimum pressure loss in the flow from stage to stage. As for the CO_2 compressors, their connection relative to the expanders is laid down by the authors as well as specific speeds, such as inlet tip Mach number of 1.3 to 1.4 at the highest possible stage diameter ratio for the second and third CO_2 compressors, rotor and blade dimensions. In regards to waste heat recovery unit and feed system, high temperature differences are allowed in the top temperature region which saves costs in high temperature tube alloy, although solubility of CO_2 in feed water will require higher quality material in the low temperature

region. Finally, the remaining equipment necessary is commercially available and technology is mature [49, 64].

In 2003, TTM Institute of Graz University of Technology carries on the ongoing research in a design optimization for a prototype, much like that of 2002, based on current technology and cutting edge turbo machinery along with outlines for the next step which the authors describe as demonstration of the operational capabilities of a prototype power plant. In addition to equipment development, a business case investigation of such a zero emission configuration would follow which depends heavily on the future of carbon taxation [65] and, as of 2005, the Norwegian oil and gas company Statoil ASA ordered a techno-economic evaluation study of a natural gas fired Graz Cycle. In said study, new assumptions of component efficiency and losses were adopted and agreed upon by both parties in order to benchmark the Graz Cycle as well as compare it to other CO_2 capture technologies.

Variants of the plant under these new premises are also discussed in [54] along with an economic analysis. The cycle configuration remained the same as previous works but under new parameters the thermal efficiency considering efforts of O_2 generation goes from 56.8% to 54.8%. When CO_2 compression to 100 bar is also taken into account, net efficiency of the cycle further reduces to 52.6%. The new data adopted shows that key parameters such as High Temperature Turbine (HTT) efficiency and cooling mass flow are quite influential. It has been observed that one percentage point increase in cooling mass flow causes a decrease in net efficiency as far as 0.22% point due to the high output of this turbine. Thus, besides its technical development challenges, operation parameters also need to be carefully looked into. Modifications to the cycle and equipment layout were then discussed by the authors in hopes of further enhancing cycle performance. At this point in development, three modifications were pinpointed for further investigation: possible replacement of single-pressure Waste Heat Recovery Unit (WHRU) by a dual-pressure one; condensation of working fluid at 1 bar and re-vaporization of the separated water and use of CO_2 compression heat as supply to deaerator. The results obtained by the authors on the dual-pressure WHRU employment show that the smaller temperature difference is counteracted by both a reduction in cooling mass flow in the High

Pressure Turbine (HPT) and an increased Low Pressure Turbine (LPT) inlet temperature which cannot be exploited. So the scenarios emerging from the multiple pressure levels WHRU result in a slight drop in efficiency. As for condensation of working fluid at 1 bar and subsequent water re-vaporization, it is proposed as means to save CO_2 compression effort from vacuum to atmospheric conditions. It is then proposed that CO_2 and water be separated at 1 bar via condensation; the water is throttled and goes on to the evaporator. Here three alternatives are investigated: re-vaporization at 0.5 bar, at 0.3 bar or dual-pressure re-vaporization at 0.5/0.3 bar. The dual-pressure re-vaporization presents the best results in regards to LPT net power. In the case of a single-pressure re-vaporization, 0.3 bar is the optimum pressure which allows higher superheating. Finally, a layout that grants usage of CO_2 compression heat as supply for the deaerator is envisaged. Such disposition can completely replace the extraction from LPT mass flow previously used with the purpose of removing inert gases from recycled water. Consequently, power output by the LPT increases by 8.5% which in turn results in a 0.8% point up in net cycle efficiency. Moreover, the challenges posed by the critical machinery, namely HTT and combustion chamber, outlined from 2002 to 2004 Graz Cycle University studies, remain the same in the 2005 study for Statoil. Combustion chambers that operate close to stoichiometry have been investigated by that point with tests showing that oxyfuel combustion with steam dilution is viable. In May of 2018, 8 Rivers, one of the responsible parties for the evaluation of another oxyfuel cycle (NET Power or Allam cycle), would also successfully test such a combustion chamber for a future Allam cycle demonstration plant [61].

Even though the Graz cycle and oxyfuel cycles alike may present a positive impact on power generation footprint at a first glance, the implementation of such technologies depend mainly on their economic viability. Through a series of assumptions about capital charge rate, cost of fuel, investment costs and others, the authors have pinpointed mitigation costs around \$19.7 to \$20.7 per ton of CO_2 avoided and an increase in cost of electricity (COE) of 19%. It is noteworthy the EU ETS, also known as the cap and trade European system for carbon emissions, went into effect that same year (2005) and that these calculated mitigation costs are below the threshold of \$30/t CO_2 assumed for future CO_2

emission trading at that point. The price per ton of CO_2 was in fact lower that year [66]. As for investment costs, main factor in the economic study, a sensitivity analysis shows additional investment costs that could range from 50 to 100%. The variation in capital costs is also broad going from same investment cost as the reference plant utilized in the study to three times higher since it is difficult to foresee new turbo machinery capital costs. Therefore, a more detailed study is needed.

Despite the great uncertainty that still surrounds the actual deployment of carbon capture technologies [37, 67], over the years, Graz Cycle research grew in ambition and larger net output plants have been conceived with higher operating pressures, temperatures and advanced equipment design. In 2006, the plant grew to industrial size reaching 400 MW net output power generation [68]. The steam cycle is modified to address the impairing effects of water films and CO_2 concentration in heat exchanger cooling tubes for heat transfer, which results in excessively large condenser heat transfer surface and consequently in high costs. So instead of condensing flue gas water at vacuum conditions, it is now condensed at close to atmosphere pressure to separate CO_2 from water; as the authors had begun investigating the year before. A fraction of the water obtained is recycled, expanded and then used as means of temperature control, same as before; whereas the water used for cooling of the working fluid is expanded in a low pressure steam turbine (LPST), condensed and pumped in a cycle of its own, as show in Figure 15. And this is the main modification in cycle layout from previous studies on the Graz Cycle.

Figure 15. S-Graz modified configuration

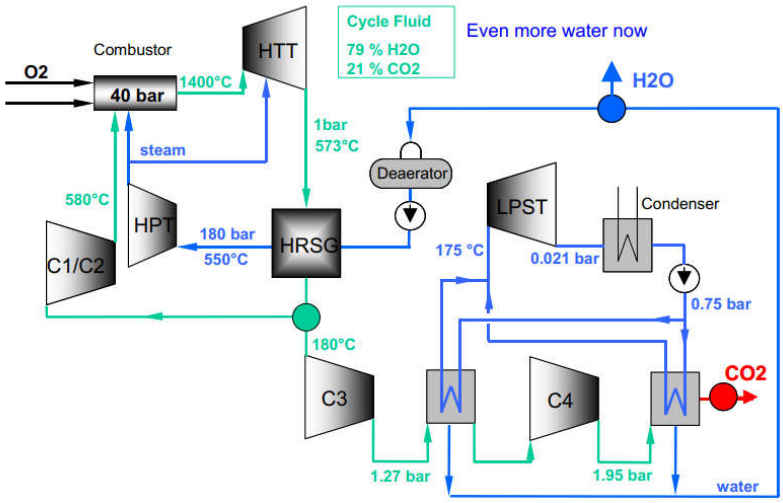

Source: [68]

By 2008, the same basic design is maintained, but for a Graz cycle based power plant with a net output of 600 MW. In this plant design, the combustion chamber operates at 50 bar with peak temperature of 1500 ºC and the authors claim to achieve 54.1% plant efficiency. Equipment wise, compressors 1 and 2 shown in Figure 15 are kept the same as long as there is an additional stage before C1. Moreover, equipment development details are laid out by the authors in their 2008 study in an attempt to respond to the short time limits shown by The European Zero Emissions Technology and Innovation Platform (ZEP) and Princeton University warnings [69].

In 2010, Graz cycle developers and researchers branch out to comparing the 400 MW output design to pre-combustion capture based on an absorption loop with monoethanolamine (MEA) and an Integrated Gas Combined Cycle (IGCC) without any CO_2 capture, all of which use syngas as fuel. The authors found that between the two carbon capture configurations, the Graz cycle-based plant far outperforms the MEA based setup and in fact starts falling behind on efficiency compared to the reference IGCC plant when oxygen and CO_2 compression power demand are discounted. According to the authors estimates, the Graz cycle would also result in cheaper electricity than the MEA scenario would [70]. Despite of the positive results yielded by the Graz cycle and the decades long research carried out about the cycle and its components, no demonstration or pilot plant featuring

the Graz cycle, in any of its variations, has been built. In order to facilitate near term employment of the Graz cycle, in 2011, Graz University researchers adapted the 2005 cycle design to use technology developed and somewhat tested by CES in their oxyfuel cycle at the Kimberlina plant. The new cycle makes use of the CES cycle gas generator, capable of near stoichiometric burning, and GEJ79 turbines. For the recycle CO_2 compressors, the authors present their own design developed in previous works. Ultimately, the use of less specific equipment, change in working fluid composition and maintenance of CES's parameters lead to a net cycle efficiency of 20.2% (HHV). If turbine inlet temperature (TIT) increase is allowed, net efficiency 23.2% (HHV) may be achieved [64].

Finally, after being evaluated in the 2015 IEA's report on oxyfuel cycles, as mentioned before, also achieving good results, the latest paper by the Graz cycle developers is published in 2018 and it assesses the cycle for hydrogen combustion – much like as it has been initially proposed in 1985 – and investigates its part load behavior. The authors assume hydrogen and oxygen are provided to the Graz cycle based plant through electrolysis powered by renewable energy. Given these conditions along with 1500 ºC and 40 bar at combustor chamber outlet, the cycle is supposedly able to reach net cycle efficiency of 68.5%; 61.89% if an on-site ASU is required for the production of O_2. The cycle remains an attractive option for energy conversion of surplus renewable energy even at part load. At 70% of the base load, efficiency is still high, 62.4%, and at 30% load it is 42.8% [71].

3.2.2 The Allam cycle

A fairly recent oxyfuel cycle that has come into the scene is the Allam or NET Power cycle. Patented in 2011 [51] and then amended to include a partial oxidation version of the cycle in 2013 [72], this oxyfuel cycle and the ensuing equipment have been developed through a partnership of multiple utility companies and manufacturers, namely NET Power, Toshiba Corporation, Exelon Corporation and the Shaw Power Group [20]. In 2015, the aforementioned IEA's oxyfuel report had the Allam cycle outperforming other oxyfuel cycles across the board and an exergy analysis by Pekuhn [73] reaffirmed the potential of the cycle to indeed achieve close to 60% efficiency. As of November 2016, "*a 50 MWth*

demonstration-scale natural gas version of the plant is currently in construction by NET Power to prove out operation of the cycle and validate performance, control methodology, operational targets, and component durability" [74]. A commercial scale 300 MWe Allam Cycle plant is also underway and expected to be operational by 2020. In May 2018, NET Power announced to have successfully achieved "*first fire of its supercritical carbon dioxide (CO_2) demonstration power plant and test facility located in La Porte, TX, including the firing of the 50MWth Toshiba Energy Systems & Solutions Corporation ("Toshiba") commercial-scale combustor*" [61]. Since then, however, little information has been reported on its progress afterwards, especially since the start of the COVID-19 pandemic outbreak.

In the Allam cycle, involved pressures are much higher than in most oxyfuel cycles, certainly many times higher than in the Graz cycle. Oxidant stream is formed by mixing a highly pure O_2 stream with a fraction of the recycled CO_2 flow. It enters the combustor chamber at 200-400 bar along with pressurized fuel and some more recycled carbon dioxide. The flue gas resultant from the combustion flows towards the gas turbine inlet at a temperature between 1100-1200 °C where it is joined by the remaining recycled flue gas and is expanded considering a pressure ratio of 6-12. After expansion, the flue gas rich in CO_2 goes through a multiple stream heat exchanger in which heat is recovered by heating up the recycled and oxidant flows. Due to differences in specific heat of carbon dioxide at radically different pressures and temperatures, as shown in Table 3, which flows through the heat exchanger, heat from an external source, may it be from oxygen/air compressors or from an external source ranging from 100-400ºC, must be supplied to balance the heat requirements [73, 74]. Figure 16, shows a Pressure vs Enthalpy diagram considering a CO_2 stream, which is a good approximation of the working fluid composition in the Allam cycle. The clear imbalance between the low pressure turbine exhaust enthalpy availability (B-C) and the heat necessary to heat the high pressure recycled stream can be observed (G-I). The additional heat input in order to close that gap is highlighted in the G-H portion of the diagram.

Figure 16. Pressure vs Specific Enthalpy diagram showing a CO_2 mass flow in a Allam power cycle

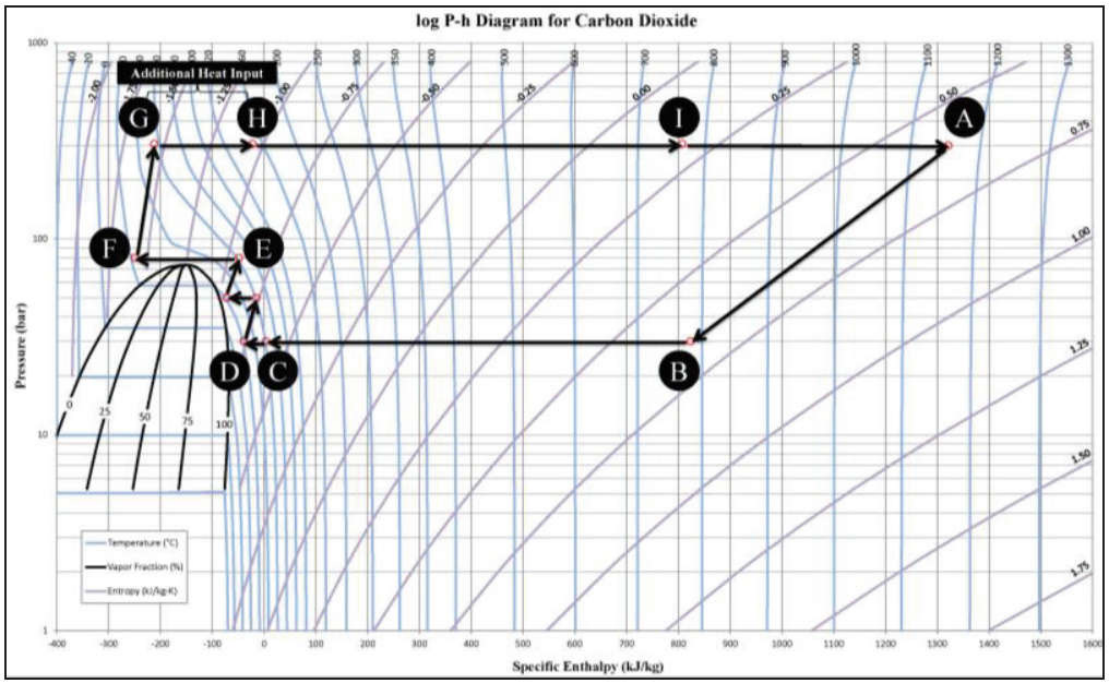

Source: [20]

Table 3. CO_2 Specific heat at 30 and 300 bar at various temperatures

Temperature (K)	CO_2 at 30 bar (kJ/kg K)	CO_2 at 300 bar (kJ/kg K)
300	1.18	1.95
350	1.05	2.00
400	1.02	1.90
450	1.03	1.63
500	1.06	1.47
600	1.10	1.31
750	1.17	1.23
1000	1.24	1.28

Source: adapted from [20]

Finally, in order to separate the water present in the combustion products, further cooling to 40-70°C must be performed. The highly pure CO_2 is thus initially compressed up to pressures above the critical pressure of the CO_2 rich stream, and then around 95% of the compressed stream is recycled back to the combustion chamber and turbine, to compose the aforementioned oxidant stream

and recycled flows. The remainder is further compressed to re-injection pressures, if needed.

3.3 Air separation unit

More often than not, air separation for production of oxygen is required on site as to ensure the operation of oxyfuel cycles. This is especially true in the context of offshore production since bringing in oxygen from stand-alone plants might escalate complications or be right out unfeasible. Therefore, various air separation techniques available may be evaluated when designing the plant. In order to decide between them, requirements such as specific rate, purity, pressure, use pattern, and in a FPSO application, weight, size and stability, need to be considered. Such factors as well as integration opportunities between the air separation unit and other processes has been carried out by Smith and Klosek [75]. Fan Wu [76] recently presented the newest techniques for air separation, its challenges and opportunities. Jordal et al. [28], in IEA's oxyfuel conference (2015), explored the potential of some of these technologies in offshore applications, whereas Lee van der Ham [77] and other authors [78-82] seek to understand and improve on the most popular and employed technique of air separation. Thus the most widely investigated methods of air separation in the literature and its characteristics are presented in the following subsections.

3.3.1 Adsorption

Adsorption separation is based on the capacity of some surfaces to allow the passage of some gas molecules, ions, atoms, liquid molecules or dissolved solids while retaining others in its surface due to their specific characteristics. For instance, in zeolite beds, nitrogen is retained in the surface's cavities due to non-uniform electric fields and its greater electrostatic quadrapolar moments, allowing an oxygen rich stream to come out the other way. This process can be repeated in cycles and to do so, the adsorbent material must be regenerated after it reaches its saturation point. Depending on how regeneration occurs, the adsorption process can be classified as temperature swing adsorption (TSA) or pressure swing adsorption (PSA). The former desorbs the substance retained by exposing the adsorbent to temperature differences with adsorption generally

taking place at close to ambient temperatures and desorption at elevated temperatures. Similarly, an analogous mechanism is used in PSA: higher pressures must increase adsorption while lower pressures must decrease it. Although adsorption methods are very promising and can achieve purity levels of 93-95% vol., so far they are only suited for small and medium-sized applications due to the flow rates current technology is able to produce.

3.3.2 Membranes

- Polymeric membranes

These membranes made of polymeric materials produce two purified streams, the low pressure permeate and the high pressure retentate. The permeate stream, which penetrates the membrane, do it based either on the difference in the mean free path of molecules, size exclusion or diffusion rate. The latter being the typical mechanism used in air separation through polymeric membrane utilization.

- Mixed matrix membranes

These kinds of membranes are typically polymeric membranes with an inorganic filling, such as zeolite. The mixture is intended to combine the selectivity of the filler material and the simplicity of polymeric membranes. The success of this combination highly depends on the material selection and their interaction.

- Ceramic ion transport membranes (ITM)

ITMs are solid inorganic oxide ceramic materials which allow the passage of oxygen ions through its matrix. Oxygen is firstly adsorbed on a porous electrically conductive coating that is applied to the surface of the membrane. Once oxygen dissociates and form ions, they are able to be transported through the non-porous ceramic electrolyte. On the other side, the oxygen ions lose electrons and form molecular oxygen that desorbs from the surface. Oxygen flux can be obtained by applying a driving force of either electric nature or partial pressure difference.

Although membrane air separation is simpler and a much cheaper method of obtaining air components, their reliability in regards to material and mechanical integrity is still an issue whereas ITMs still operate at very high temperatures.

3.3.3 Chemical looping

Chemical looping is based not on the production of free oxygen per se, but on the delivery of it through metal oxides. The process entails two interconnected fluidized bed reactors, one being an air reactor and the other, a fuel reactor. The oxygen carrier, which is usually a metal, is oxidized in the air reactor and then transferred to the fuel reactor, where it is reduced and fuel reacts with the oxygen. The carrier then circles back to the air reactor to be oxidized again and repeat the cycle. Although chemical looping is under rapid development, it still remains at laboratory testing stages.

3.3.4 Cryogenic distillation

Cryogenic distillation is the process of separation through which the components of the mixture are separated based on their different boiling points. Since air components hold very low boiling point temperatures, the distillation process happens in the realm of cryogenic temperatures [83]. The double column cryogenic distillation process, as it is mostly common today, first came about in 1910 pioneered by Carl von Linde and produced pure nitrogen and oxygen simultaneously [84]. The process begins with the removal of water, CO_2 and hydrocarbons from air utilizing molecular sieves. Then the treated air is compressed to pressure levels around six times atmospheric pressure. The compressed air is liquefied at the main heat exchanger by the product streams and fed to the distillation columns, mainly the high pressure column. In the columns' trays, see Figure 17, the equilibrium between liquid and vapor mixture dictates that the most volatile component is in greater proportion in the vapor phase than in the liquid phase. In order to achieve said equilibrium, the most volatile component, namely nitrogen, increases its concentration in the gas phase going upwards and forms most of the overhead gas product. Meanwhile, more oxygen is condensed each tray going down the column and so it constitutes the better part of the liquid product stream from the bottom of the column.

Figure 17. Illustration of liquid-vapor equilibrium in cryogenic air separation column trays

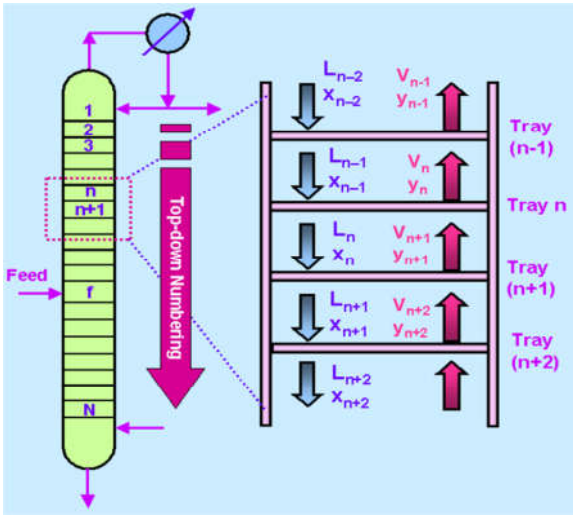

Source: [85]

The boiler at the bottom and the condenser at the top of the distillation column provide means of countercurrent contact between rising vapor and descending liquid, such that at all levels nitrogen moves from liquid to vapor and oxygen moves from vapor to liquid, thus ensuring continuity of the distillation process. Nitrogen and oxygen rich liquid streams are throttled to the lower pressure column where this process is repeated and highly pure oxygen is yielded as bottom product and nitrogen as overhead product. Moreover, the streams transfer heat in heat exchangers that connect the columns thermally and main heat exchanger previously mentioned to liquefy the compressed air. The process of cryogenic air separation is at the moment the most mature technology for air separation and the one that yields the highest product purity and flow rates, which makes it the technique of choice if high values of those requirements are to be met.

3.4 CO_2 purification

The CO_2 generated from combustion is often mixed with other gases and water vapor. Even in the case of an oxyfuel cycle, a significant amount of water vapor is present as well as some excess O_2 from combustion. Such impurities can cause damages to the pipeline in CO_2 transportation such as corrosion and two-phase flow. Therefore, depending on the specific requirements, a CO_2 purification unit may be necessary. In the specific case of the of oxyfuel cycles, water can be

separated from CO_2 via condensation, as previously mentioned. As for the oxygen, having combustion happen in a combustor chamber able to operate close to stoichiometry and utilizing highly pure oxygen goes a long way to decrease efforts to purify CO_2 streams from O_2. Dugstad [86] compared impurity levels of CO_2 streams in some pipelines to the acceptable impurity levels intervals published in the literature and according to some general guidelines such as [87]. A certain composition and levels of impurity were set and its effects tested in slim autoclaves rotated on a shaft inside a temperature controlled chamber. The study found that, in general, the published recommendations are very high as elemental sulfur and sulfuric and nitric acids were formed and had a corrosive effect on the simulated pipeline. On the other hand, the impurity levels in existing pipelines did not report having all the impurities taken into account by the study (water, H_2S, O_2, NOx, SOx), disclosing only the amounts of water, H_2S and some, O_2. Nevertheless, the results seem to suggest that reducing the amount of water and oxygen might decrease acid formation. Abbas [88] investigated and ranked numerous methods of water and oxygen removal for deep CO_2 purification for pipeline transport, enhanced oil recovery (EOR) and/or geological storage. The author found that catalytic oxidation of H_2 was the best technology for O_2 removal according to the following set of criteria: removal efficiency, operating conditions, energy requirement, estimated cost and safety; although it increases humidity. The second best method according to the author would be cryogenic distillation, which rids CO_2 of all impurities but water. As for dehydration of the stream, refrigeration and condensation ranked as the best methods for water removal.

3.5 Exergy analysis applied to FPSO units and CO_2 mitigation background

The application of exergy analysis can produce insights about a system's functioning and potentialities that a purely First Law approach wouldn't otherwise provide. By combining First and Second Law in an exergy approach, the magnitude as well as location of irreversibilities can be pinpointed and the reasons for theses bottlenecks may be addressed. For this reason, exergy analysis becomes a powerful tool in analyzing and optimizing multiple systems of interest, from the metabolism of living beings to industrial and power generation

plants of various kinds. Nevertheless, its application to offshore systems is not yet as widespread as it is in other areas. Although current circumstances such as emissions mitigation are causing this scenario to change.

One of the first works to apply exergy analysis to an offshore platform system was by Oliveira Jr. e Hombeeck [89] which identify petroleum heating as one of the major contributors to the low exergy performance of the platform. Efforts towards emissions reduction are presented in the work by Kloster [90] through energy optimization in the platforms Osenberg, Eldfisk and Snorre B in Norway. Combined cycle was shown to improve energy efficiency from 37% to 50% and achieve emission abatement levels of 25%. From then on, the usage of exergy analysis applied to platforms and observation of emission levels became more prevalent in the literature and likely to be cited or recommended to be used in conjunction. Voldsund et al. [91] applied exergy analysis to an offshore platform process plant in the North Sea using data from a real production day. Compression processes and subsequent cooling were found to be responsible for the biggest exergy destruction, similar to the findings of Oliveira Jr. and Hombeek, although Voldsund et al. does not include in their analysis pre-heating of petroleum, a large source of exergy destruction. In 2014, Voldsund et al. [92] assessed this and other three platforms processing plants in the North Sea. Although the processes are similar across platforms, the fluid and reservoir characteristics are widely varied, which impact significantly the rates of exergy destruction. It varies from 27%-57% in the gas treatment sections, 13%-29% takes place in gas recompression sections and 10%-24% in production manifolds. The authors identified the gas compression systems, production manifolds and flared gas recovery as the main sources of improvement and that the older platforms tend to exhibit higher rates of exergy destruction due to higher recirculation rates associated with lower hydrocarbon production. Measures such as larger number of compression trains so they operate longer in the ideal range could improve the performance of one of the largest focuses of exergy destruction. Moreover, it is clear that although multiple studies point to similarities between case studies, platform operation and reservoir characteristics have a relevant impact in the results of the exergy analysis so each case should be carefully analyzed and specificities taken into consideration.

Dias [93] conducted an exergoeconomic analysis of an FPSO in the Pre-Salt. The utility plant considered and analyzed in the study is a cogeneration plant composed of four gas turbines and heat exchangers fed by exhaust gas that heats up process water. Two very different fuel compositions in CO_2 content were ran by the power plant and the author found the fuel with lower CO_2 content provided an exergy efficiency 1.5% higher and lower emissions than the fuel containing 60% mol CO_2 (fuel 2). Fuel 2, however, proved to be more economically attractive, factor that could also be shifted in fuel 1's favor if penalties were to be applied according to emission levels. Mazzetti's work [94] further expanded on the idea to curb CO_2 emissions by increasing energy efficiency. In their paper, Mazzetti et al. investigates three case studies: three platforms in the Norwegian Continental Shelf (NCS) and one in the Brazilian basin with bottoming cycles for recovery of waste heat using steam and alternative working fluids. The steam and CO_2 bottoming cycles displayed similar efficiencies, increasing net output by more than 30% compared to simple-cycle gas turbine. They also result in similar CO_2 emissions reduction; steam cycle achieves reduction of 25% and dual stage combined CO_2 cycle, 24%. On one hand, CO_2 cycles have the advantage of being much less space demanding since they operate at higher pressures, while steam bottoming cycles require a water treatment system. On the other hand, CO_2 cycles also require extra recuperators to be efficient, so such trade-off needs to be evaluated.

Pierobon et al. [95] set out to find the most suitable waste heat recovery technology for existing and future offshore facilities according to the metrics of daily CO_2 emissions, weight and economic revenue. Technologies accessed were steam Rankine cycle (SRC), air bottoming cycle and organic Rankine cycle (ORC) and guidelines for design of offshore installations are also provided. The organic Rankine cycle had the best yearly performance therefore enabling the highest abatement of CO_2 emissions and other pollutants while the steam Rankine cycle is more favorable economically as it presents the highest net present value as well as the lowest weight. For all the cycles the heat exchanger is the heaviest component whereas the gas turbine is the most costly. Nguyen et al. [96] also investigated solutions targeting CO_2 mitigation, some of which relied on increasing cycle performance by recovering heat. The scenarios run on

platform at the North Sea were the implementation of waste heat recovery, installation of CO_2 capture unit and platform electrification. All of these options result in more than 15% reduction, although costs vary widely and they are very sensitive to swings in natural gas prices and CO_2 taxes. Just as Mazzetti proposed, the authors suggest replacing one of the gas turbines with a waste heat recovery unit so no extra space is required, however, the lack of redundant equipment could place risks in case of system failure. This alternative boosts natural gas export by 14% and curbs emissions by 16-20%. The post-combustion achieves 70% reduction, out of which 10-20% relates to the steam network and 50-60% to the carbon capture unit. Electrification seemingly presents the highest efficiency but as for CO_2 mitigation it is highly dependent on how the grid generates electricity.

Nguyen et al. [97] reviewed several literature definitions of exergy efficiency, arguably one of the most relevant metrics in exergy analysis, and applied them to four offshore platforms. The definitions registered by the authors fall into one of either two types of efficiency: total, which is defined as the ratio of outgoing to ingoing flows; or task, which is defined as the exergy terms associated with the products to the exergy terms associated with the resources expended to produce them. Each efficiency definition employed showed a different result, favoring certain boundary and operating conditions, displayed low sensitivity to improvements and calculation inconsistencies. As a way to offer a more robust definition as alternatives, the authors propose what they called component-by-component efficiency which, instead of following streams through the system, it follows the components that form the streams as they may or may not be scattered throughout several streams. This definition is sensitive to improvements and gives consistent results; however, it requires high computational power.

Analyzing a system close to the one in the present work, D'Aloia [44] studied the influence of the different FPSO operation modes on the exergy efficiency, specific exergy consumption, CO_2 emissions and emissions per unit of produced exergy. The author concluded that the operation mode A, which bypasses the membrane that separates natural gas from CO_2 and re-injects this mixture back into the well, is the most efficient mode as well as the most favorable regarding specific exergy consumption and specific CO_2 emissions. It is also pointed out the importance of

metrics such as the specific CO_2 emissions due to the relationship established between an environmental and an exergy based parameter. That way it relates the negative impacts of the activity with the benefits it produces. And just as variability is introduced to the platform such as operation modes, changes to the oilfield over time also influence several aspects, including design steps. Riboldi et al. [98] designed and optimized scenarios employing a combined cycle with either a backpressure steam turbine or an extraction steam turbine. Then the optimized scenarios for maximizing energy efficiency and minimizing weight were compared. For high heat to power ratios, the backpressure turbine was able to provide a cut from 9.3% to 12.1% in CO_2 emissions, while low extraction steam turbine achieves a 22.2% cut with lower heat to power ratios. Moreover, the design for peak production, despite reaching high efficiencies, requires quite heavy equipment; whereas design for end-life years generally returned overall better performances throughout the plant's lifetime for bottoming cycles of the same weight.

Riboldi et al. [36] also verified several other concepts for heat and power supply of offshore installations targeting increase in efficiency and decrease in CO_2 emissions. The concept involving electrification for power supply and a gas burner for heat supply returns the best performance, cutting by 35.5% CO_2 emissions in comparison to the base case (gas turbine + waste heat recovery unit). It is followed by the combined cycle concept (gas turbine + waste heat recovery unit + steam cycle) which cuts emissions by 32.2%. The hybrid concept that involves gas turbine and heat recovery with electrification although reducing emissions by 24.2% and offering flexibility could entail double investment that might make it unfeasible. Furthermore, as also stated by Nguyen [96], the CO_2 associated with electrification strongly depends on how power is generated and although it is generally lowest cumulative CO_2 emitter, it starts being increasingly penalized when higher amounts of heat are required.

Nguyen et al. [99] assessed three representative stages of an oilfield, namely early-life, plateau and end-life. Most inefficiencies turned out to take place where chemical exergy is consumed, ranging from 50-55%; followed by thermal exergy transfer, 15-20%; and mechanical exergy, 10-15%. These findings are true for all production periods. Additionally, optimization of the integration of steam and

organic Rankine cycles were evaluated. The most exergy was destroyed in the gas turbines, which is mostly unavoidable, and as for the fraction destroyed in heat exchangers it shows the mismatch between the temperature levels in process and utility plants and there is where a bottoming cycle can immensely benefit the integration between these two units. To that end, the authors concluded that a steam Rankine cycle best attend to the synergy between the utility and processing plants while also being mature technology and cost-competitive. Merits of three different cogeneration plants and two process plants but in terms of unit exergy and CO_2 emissions costs over the well's lifespan and different operating modes were assessed by Silva et al. [100]. The case study found that water produced along the lifespan, which can vary quite drastically, has a strong impact on the unit exergy cost of oil and gas of up to 175% and that the choice of cogeneration plant has only a mild influence but that during the lifespan could mean a difference in 308300 t of natural gas produced. Furthermore, the cogeneration plant which presents the highest efficiency, lowest unit exergy cost and CO_2 emissions is the one equipped with the reciprocating engine, although reliability, weight, size and monetary costs need further evaluation to verify its feasibility.

As can be observed by a literature review, many works over several years have been successfully applying exergy analysis to offshore platforms which in turn produces helpful insights as to where and by how much processes can be improved. Noticeably, preoccupation to enhance performance while curbing CO_2 emissions as much as possible has become the norm as stricter legislation is enforced. And although efficiency improvement has a significant impact on reducing emissions, around 25-35% as seen in the studies presented, it is still far from the level of mitigation required to meet the CO_2 mitigation goals needed to attenuate the effects of climate change caused by this sector. As will be shown later on, the present work attempts to apply and compare carbon capture techniques that strive for near zero emissions to try and reach that goal.

4. Methodology

The research has been carried out through survey, synthesis and systematization of information, definition of design, elaboration of mathematical models, calculation of indicators, simulation, evaluation of results and proposition of improvements. In order to achieve the proposed objective, the methodology to be used can be divided into the following steps:

1. Study of current and pertinent literature on the subject in order to raise possible designs for the air separation unit and oxyfuel cycles, characterize them in terms of their processes, materials and integration to the other units of the plant. Collection and selection of costs and exergy performance indicators registered in the researched literature were also executed in order to assist in the work's crafting of its own indicators.

2. Selection of the design of the air separation unit and power cycles according to the boundary conditions inherent of the scenario in which the FPSO is located.

3. Thermodynamic and energy integration analysis of the overall system as well as unit exergy and CO_2 emissions accounting and allocation through the use of mathematic models, mass, energy and exergy balances (modeling and simulation).

4. Use of diagrams, graphs, exergy indicators such as efficiency definitions, unit exergy costs, and allocation of CO_2 produced to process streams expressed through CO_2 emissions costs in order to quantify and locate the rates of exergy destruction, exergy performance, energy integration potential, exergy and CO_2 cost of products and overall behavior of the units and the system as a whole.

5. Comparison between the designs selected and analysis of calculated performances in light of the objective to be reached. Finally, discussion of the results and overarching scope which encompasses this wok and proposition of changes as to move toward the goals set.

In order to complete the steps described in the proposed methodology, two main softwares were used for the following purposes:

a. ASPEN HYSYS ®: modeling and simulation of processes related to air separation and oxyfuel cycles;

b. MS-EXCEL ®: integration, organization and analysis of the numerical results obtained as well as plotting tool.

Furthermore, the fundamentals of a combined energy integration analysis and exergy assessment of step 3 are laid out in subsequent sections. The equations for the allocation of the unit exergy costs and specific CO_2 emission among the representative streams of the studied platforms is also described, along with the proposed exergy efficiency definitions used to rank the performances.

In section 5, the concept of exergy is presented. The next item, 5.1, introduces the definition of restricted reference and dead state, which allows the calculation of the two most relevant types of exergy. In 5.2, the method for plotting both hot and cold composite curves is described as well as which valuable information can be extracted from it. In 5.3, the equations that allow the allocation of input exergy and produced CO_2 to the plant's streams are shown. Their usage in pertinent literature and how they have been applied is also briefly described. Finally, in section 5.4, process modeling is described and efficiency metrics for evaluation of the case study are shown in Table 4.

5. Exergy concept

Many systems of interest in Engineering are such that they are not in equilibrium relative to the surrounding environment which encompasses them. This difference in relation to the system's neighborhood, whether it is a temperature, pressure or chemical composition difference, may be used for generating work. Its maximum value, which is achieved via interactions with the environment through reversible processes, is defined as exergy [101].

The calculation of this theoretical limit is made possible through the combination of the First and Second Law of Thermodynamics. The First Law deals with the conservation of energy through its various forms, but nothing says of the difference in quality between them, if there is even a difference. This distinction is in the realm of the Second Law of Thermodynamics, which accounts for the generation of entropy that takes place in energy conversion processes. The entropy generated, in turn, means that the energy's ability to produce work is degraded even though energy itself is conserved. This thermodynamic property of the system can be thought of in many ways, including as measure of the vestiges processes leave either on systems and/or their surroundings; even if the process is reversed. These vestiges (entropy generation) are present in all real processes and due to this inalienable feature they are called irreversible processes.

Therefore, with the aforementioned combinations of the First and Second Laws of Thermodynamics, one can reach an equation which takes into account both energy conservation and degradation at the same time. A "new property" is then defined which requires the system to be looked at in relation to its surroundings: exergy. The following Equations (1), (2) and (3) represents the First, the Second Law and the Exergy balance, respectively. Note that the exergy balance for a generic control volume is obtained by multiplying the Second Law of Thermodynamics (Equation 2) by $-T_0$, where T_0 is the environmental temperature, and adding the result to the First Law (Equation 1). And that is how Equation (3) is obtained.

$$\frac{dE}{dt} = \sum \boldsymbol{Q}_j - \boldsymbol{W} + \sum_i \boldsymbol{m}h - \sum_o \boldsymbol{m}h \quad (1)$$

$$\frac{dS}{dt} + \sum_o \boldsymbol{m}s - \sum_i \boldsymbol{m}s = \sum \frac{\boldsymbol{Q}_j}{T_j} + \boldsymbol{S}_{ger} \quad (2)$$

$$\boldsymbol{W} = -\frac{d(E - T_0 S)}{dt} + \sum \left(1 - \frac{T_0}{T_j}\right) \boldsymbol{Q}_j + \sum_i \boldsymbol{m}(h - T_0 s) - \sum_o \boldsymbol{m}(h - T_0 s) - T_0 \boldsymbol{S}_{ger} \quad (3)$$

The liquid amount of work interaction, or in a rate based description, power done upon or by the boundaries of the control volume can be written as $\boldsymbol{W}_{liq} = \boldsymbol{W} - P_0 \frac{dV}{dt}$, in which P_0 is the pressure of the environment the control volume is in. When isolating $\dot{W}$ as in $\boldsymbol{W} = \boldsymbol{W}_{liq} + P_0 \frac{dV}{dt}$, replacing it in Equation (3) and rearranging so the derivative is on the left side of the equation, Equation (4) emerges.

$$\frac{dB}{dt} = \frac{d(E + P_0 V - T_0 S)}{dt} = \sum \left(1 - \frac{T_0}{T_j}\right) \boldsymbol{Q}_j - \boldsymbol{W}_{liq} + \sum_i \boldsymbol{m}(h - T_0 s) - \sum_o \boldsymbol{m}(h - T_0 s) - T_0 \boldsymbol{S}_{ger} \quad (4)$$

Equation (4) is an exergy balance equation for a generic control volume that interacts with its surroundings through work and heat interactions and has multiple streams of mass crossing its boundaries. As a result, the control volume's exergy change over time $\left({}^{dB}/_{dt}\right)$ is affected and accounted for. Just as types of energies, exergy can be expressed in terms of its components. Considering the radioactive, magnetic, electric and superficial tension effects to be negligible, total exergy can be understood as:

$$B^T = B^P + B^K + B^{PH} + B^{CH} \quad (5)$$

The terms B^P and B^K represent potential exergy and kinetic exergy, respectively, and are associated with potential and kinetic energy. The terms B^{PH} and B^{CH} correspond to physical and chemical exergy, respectively. This means that they are associated with the temperature and pressure differences (physical) and chemical composition differences (chemical) between the system and the

environment surrounding it. More often than not, these last two components of exergy are more significant to the types of systems analyzed in Thermal Engineering, as show in Figure 18; and so are the ones calculated in this work.

Figure 18. Illustration of the proportion of types of exergy most relevant in Thermal Engineering

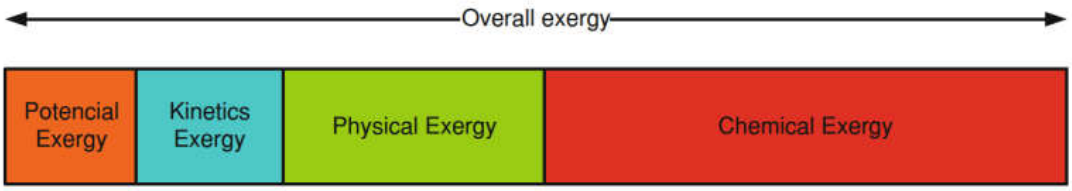

Source: [102]

Physical exergy is then equal to the maximum possible work achieved when mass is taken from its initial temperature and pressure to the reference state. The reference state is, in short, the state defined by the temperature and pressure parameters of the surroundings of the system, and will be more detailed later on along with the dead state. The specific physical exergy for a given mass flow rate is given by the following equation.

$$b^{PH} = \left[h - h_0 - T_0 \left(s - s_0 \right) \right] \tag{6}$$

Chemical exergy, on the other hand, is the maximum possible work to be done when mass is taken from the restricted reference state to the dead state, i.e, the state defined not only by the temperature and pressure of the environment but also by its chemical composition at these physical conditions. Specific chemical exergy is calculated by the following equation.

$$b^{CH} = h_0 - T_0 s_0 - \sum_i \mu_i^* x_i \tag{7}$$

Where μ_i^* is the chemical potential of the i-th substance at the dead state and x_i is the molar fraction of the i-th substance. Just as the physical exergy can be interpreted as measuring how distant a system is to the restricted reference state,

chemical exergy measures the distance between the restricted reference state and the dead state. Such understanding is well illustrated in Figure 19.

Figure 19. Graphical representation of physical and chemical exergy

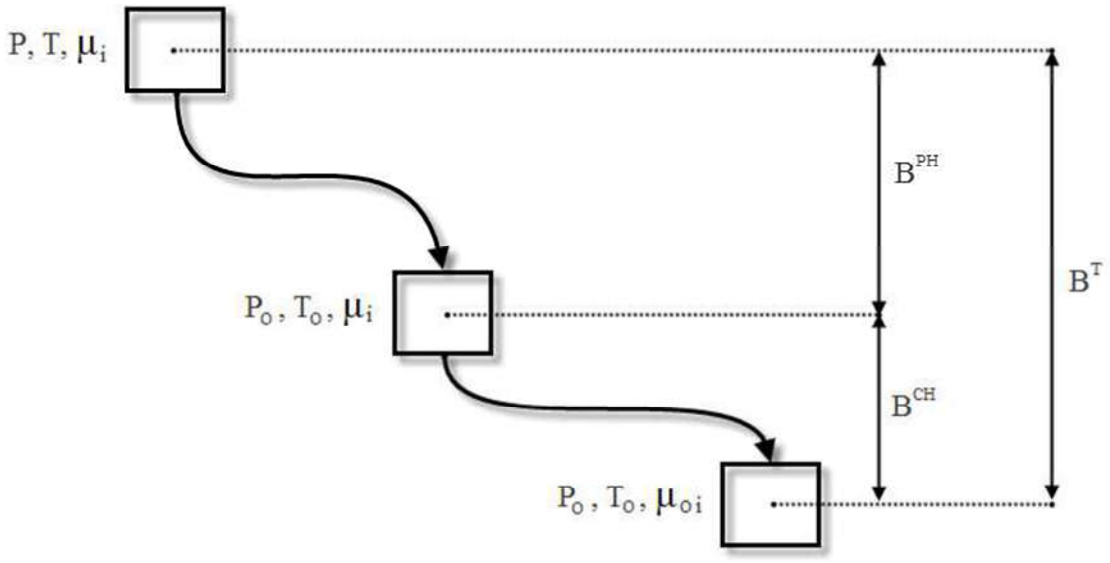

Source: Adapted from [103]

Figure 20 illustrates how the chemical exergy of any substance can be calculated. In it, a scheme allows one to ascertain the Gibbs free energy, which relates to chemical potential, and the isothermal work theoretically necessary to change the concentration of the products formed in the first box (reactor), as to match the concentration in which they are found in the environment. Substance's standard chemical exergy is tabled and its value depends on how the environment of reference and its components have been modeled. In this work, the tables developed in by the work of Szargut, Morris and Steward [104] are used to obtain the standard chemical exergies of the pertinent substances.

Figure 20. Ideal scheme for calculation of chemical exergy

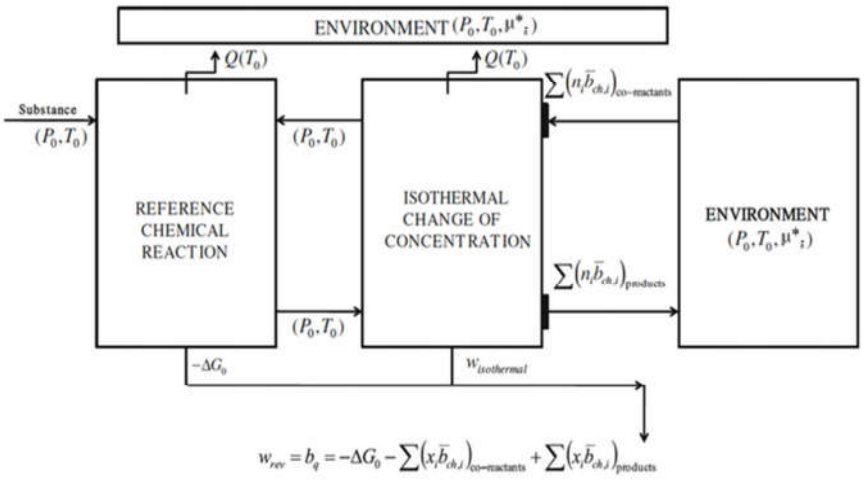

Source: [102]

Firstly, the substance of interest enters the reactor where it is transformed through reversible reactions at P_0, T_0 into products. As an example, say hydrocarbon such as methane may be oxidized in the reactor and becomes CO_2 and H_2O, while heat is released to the environment as to maintain temperature at T_0. The air used for oxidation is extracted from the environment. It goes through an isothermal change in concentration in the second chamber as to meet the exact amount needed for stoichiometric reaction and enters the first reactor at P_0, T_0. The environment of reference here can be modeled after the Earth's atmosphere composed roughly of nitrogen, oxygen, water vapor, carbon dioxide and other inert gases like argon. The oxidation products will do the reverse path made by the air for oxidation, since the methane must be brought to the dead state in order to quantify its chemical exergy. They leave the reactor at the same parameters of pressure and temperature as the environment although probably at a different concentration in which they are present in the reference atmosphere or environment. Therefore, their concentration must be changed in the second box as to meet the environment's values. This transformation must also be isothermal to maintain the same parameters as the environment's, which is achieved by releasing or capturing heat from the environment. Now the methane has been completely transformed into gases that compose the atmosphere and is at the same pressure, temperature and concentration as they are. Thus, it has been

taken from its initial state to the dead state. The energy and/or work necessary to perform these transformations in each reactor can be measured and when added result in the value of chemical exergy of the substance transformed. The ΔG_0 is the value which corresponds to the maximum work available in the conversion process that occurs in the first reactor at P_0 and T_0. In the second chamber, the isothermal change in concentration requires work which is represented in $w_{isothermal}$. If the product gases can be modeled as ideal gases, for instance, compressors and expanders may be used to change their partial pressures as to match environmental values. This isothermal work, can be broken up into standard exergy of co-reactants (air taken from the environment) and products (oxidation of methane). Finally, by adding ΔG_0 and $w_{isothermal}$, the chemical exergy of the substance is calculated.

The assumption that the substance can be modeled as ideal gas is commonly made when referring to air components at normal ambient conditions (25°C, 1 atm). When this assumption can be made and the gases are the same as those found in the reference atmosphere, the chemical exergy can be calculated through the isothermal expansion work in a turbine that takes the substance from P_0 to P_{00}, which is the gas partial pressure in the reference atmosphere.

$$b^{CH} = RT \ln\left(\frac{p_0}{p_{00}}\right) \tag{8}$$

In the case of mixtures of known composition, exergy can be calculated by the following equation. Its second term is called composition exergy and the coefficient of activity (γ) varies from mixture to mixture. However, it is common to consider it to be 1 for hydrocarbons.

$$b^{CH,mix} = \sum_i x_i b_i^{CH} + RT_0 x_i \ln \gamma_i x_i \tag{9}$$

The chemical exergy of fuels with complex composition can be estimated from alternative use of the lower heating value. As reference, the literature presents values of φ for natural gas of about 1.04 [83], and for oil about 1.08 [105].

$$b^{CH} = \varphi(LHV) \quad (10)$$

5.1 Restricted reference state and dead state

Exergy is a property that, in order to be defined and calculated, parameters of the environment the system is surrounded by need to be accounted for and known. These parameters define two states and each one relates to either physical or chemical exergy. The state commonly known as *restricted reference state* relates to physical exergy and is defined as the standard state of the environment characterized by environmental temperature and pressure. When a system of interest reaches the restricted reference state, it is in thermal and mechanical equilibrium with its surroundings. However, no chemical composition equilibrium between them is observed at this point. In that case, theoretically, more work could be obtained in order to bring the system to the same chemical composition as the environment. If chemical equilibrium is indeed achieved additionally to thermal and mechanical equilibrium, this state is defined as the *dead state* and no work can be obtained from the system in that environment anymore.

In order to establish a standard environment to be considered in exergy calculations, the widely used values of 298.15 K for temperature, 101.325 kPa for pressure and standard chemical composition formed by the gases and their respective partial pressures present in the atmosphere (O_2, N_2, CO_2, H_2O, D_2O, Ar, He, Ne, Kr, Xe), solid substances for the Earth's crust, and ionic and molecular reference substances (non-ionizable) in the seas are often considered. The reference temperature, pressure and atmosphere composition are used in the present work.

5.2 Energy integration

The heat exchange network (HEN) design of a system can provide the overall arrangement with energy savings of 20-30%, coupled with capital savings [106]. This area of interest has been the target of efforts towards development of systematic procedures for a long time, but most of the methods that have come before the Energy Integration Method (or Pinch Design Method/Pinch Analysis) have been either fast but prone to failure or dependable but cumbersome. They

would also give stream splitting information which could not be tracked back to the complexity of the problem or inadequacies of the method. That is when, in the 1970's, Bodo Linnhoff formalizes the Pinch Design Method. The Energy Integration or Pinch Design Method would then provide ease and speed of application with near-certainty of finding "best" solutions.

In order to understand how the method works and what it achieves, information on (i) the number of cold and hot streams one wishes to integrate, (ii) their corresponding supply and target temperatures and (iii) respective enthalpy flow rate must be known. With that information, the hot and cold streams are then plotted in a Temperature vs Enthalpy Flow plane, as shown in Figure 21 (a). This systematization will help ascertain the minimum heating and cooling requirements (in other words, where steam and cooling water are needed) of the plant or units one seeks to integrate. As the next step, the multiple hot and cold streams will be merged into a single representation of a hot composite curve and a cold composite curve (CC). It is important to point out that, in constructing this curves, the single streams can be moved horizontally (along the Enthalpy Flow Rate axis) since it represents enthalpy differences, not absolute enthalpy values per se (Figure 21 (b)). The amount of overlap between the curves show the heat transfer match between hot and cold CC and the vertical distances are the temperature differences involved in said heat transfer. A minimum temperature difference ΔT_{min} (Figure 21 (b)), which is represented by the smallest vertical distance between the composite curves, is imposed on the Linnhoff and Flower algorithm [107] for physical and economic reasons (size and cost of the HEN) and it depends on the nature of the fluid that composes the stream and other variables such as pressure, phase, etc. The point at which ΔT_{min} is located is known as the pinch point as shown in Figure 22 (a). The horizontal distance shown in Figure 22 (b) above the pinch point corresponds to the minimum hot utility requirement. In other words, it requires additional heat. Analogously, the difference between the curves below the pinch point represents the minimum cooling requirement.

Figure 21. Construction of cold and hot composite curves. Single hot and cold streams on the left (a) and hot and cold composite curves on the right (b)

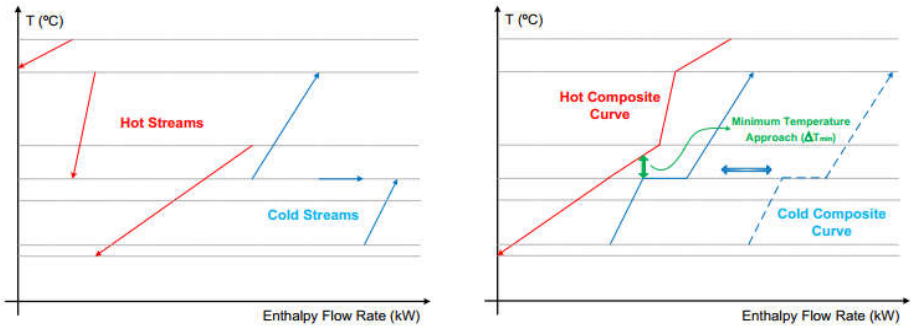

(a) (b)

Source: [108]

Figure 22. Graphical demonstration of minimum temperature difference (a) and minimum hot utility requirement and minimum cooling requirement

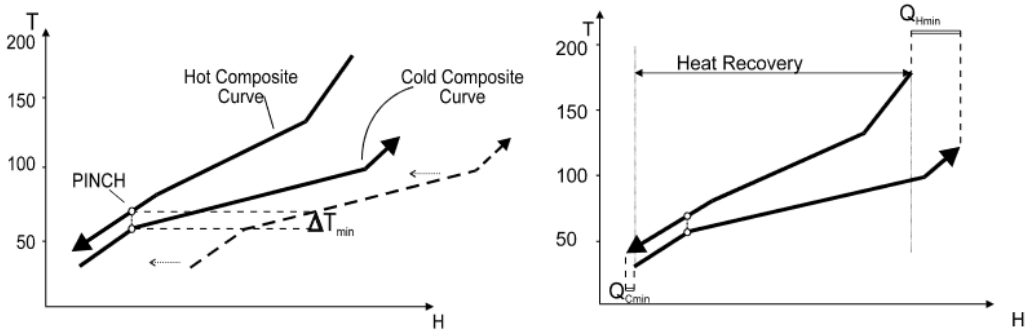

(a) (b)

Source: [109]

The minimum heating and cooling requirements, also known as Minimum Energy Requirements (MER), could be realized through the use of several different utilities. In other words, heating input can be achieved with steam, hot oil circuit or furnace flue gas. Whereas, cooling water might suffice for a cold utility or refrigeration such as a vapor compression refrigeration cycle might be needed. So, from a minimizing capital expenditure standpoint, maximization of the use of cheaper utilities is preferable. For example, Figures 23 (a) and (b) show how a high pressure (HP) steam based hot utility can be partially replaced by a low

pressure (LP) steam based one, given that the minimum temperature difference between the curves is maintained.

Figure 23. Illustrated example of how to manipulate the CC in order to obtain cheaper utilities

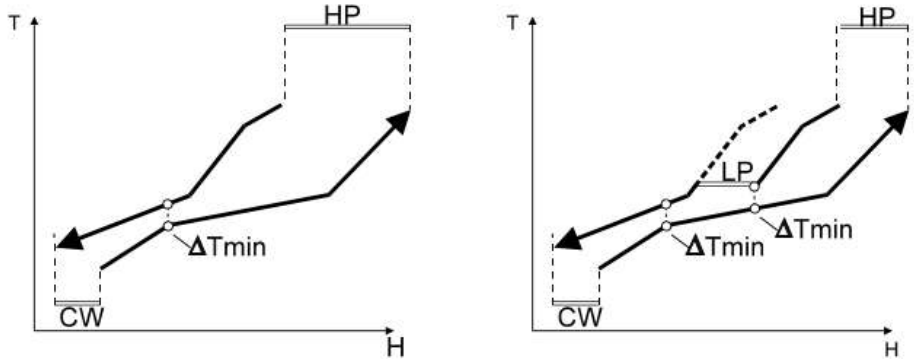

Source: [109]

Although useful, everytime a new utility is added, the composite curve changes thus targeting for multiple utilities may become quite complex and burdensome. A clearer visual representation which encompasses all utilities selected is needed and for this purpose the Grand Composite Curve is used.

The first step taken in order to build the grand composite curve is shifting the composite curves position vertically, i.e. increasing the cold composite curve's temperature by $\frac{1}{2}\Delta T_{min}$ and decreasing the hot composite curve's temperature by $\frac{1}{2}\Delta T_{min}$. By doing this shifting, the curves will touch at the pinch point, as it is the smallest vertical distance between them. The shifted temperatures and the enthalpy differences (α) between the curves will be plotted in a new $T_{shifted}$vs H plane, as shown in Figures 24 (b) and (c). The grand composite curve provides the same energy targets as the composite curves, as shown by the HP (high pressure steam) and Ref. (Refrigeration) indication in Figures 24 (a) and (c), however, it facilitates setting multiple utility targets may the HEN designer wish to.

Figure 24. Turning of the composite curves into the Grand Composite Curve

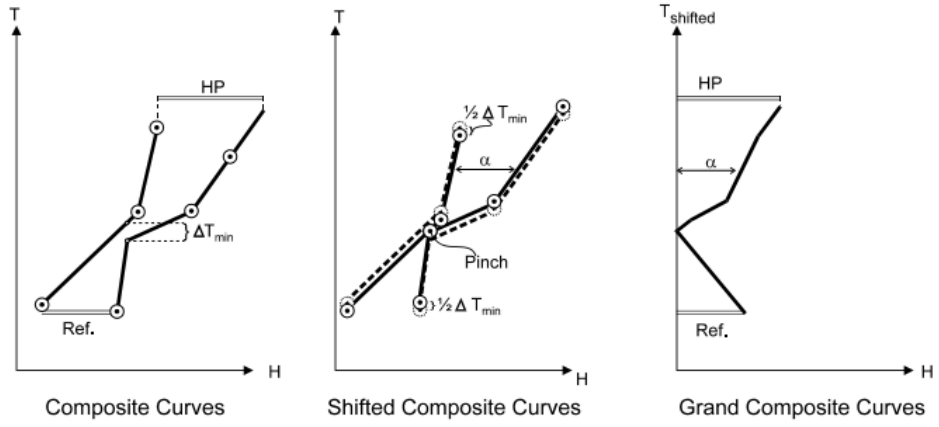

Source: [109]

5.3 Unit exergy cost and CO_2 emissions allocation

Finally, it is worthy noticing that previous works of Oliveira Jr. and van Hombeeck [89], Silva and Oliveira Jr. [110] and Carranza and Oliveira Jr. [34] have already calculated the exergy performance of the offshore petroleum platforms in Brazil, whereas Nguyen et al. [97] wrote extensively about different exergy efficiencies applied to the offshore context. Further studies [111-113] analyzed the processes present in the Brazilian petroleum refineries by using exergy as the efficiency indicator for separation processes. Moreover, the exergy content has been suitably considered as a rational criterion for the allocation of the unit costs among the crude oil and the natural gas produced in offshore platforms that operate under the conventional configuration. For instance, in the work of Nakashima et al. [114], the performance of two energy technologies used for an enhanced petroleum recovery, namely, the gas lifting and the two-phase screw pumping processes are compared in light of the exergoeconomy theory. Those results have been used in turn to calculate the cumulative exergy cost and the specific CO_2 emissions of different fuels, chemicals and transportation services [115] in petrochemical refineries, biorefineries [116], fertilizers complexes [117] and even of the Brazilian electricity mix [118]. The methodology used in those studies relies on the concept of the Total Unit Exergy Cost (cT) [kJ/kJ], defined as the rate of exergy necessary to produce one unit of exergy rate (or flow rate) of a

substance, fuel, electricity, work or heat comprised in the petroleum production platform. Analogously, the specific CO_2 emission cost (cCO_2) [gCO_2/MJ] is defined as the rate of CO_2 emitted to obtain one unit of exergy rate (or flow rate) of the stream analyzed (either material or energy flow). Thus, by considering the control volume embodying each representative process unit (Figures. 24-27) of the offshore platform, the exergoeconomy balance of total exergy costs can be written as in Equation (11):

$$\sum_{j} c_{T,P}^{j} \boldsymbol{B}_{T,P}^{j} = \sum_{i} c_{T,F}^{i} \boldsymbol{B}_{T,F}^{i} \tag{11}$$

where $\dot{B}$ stands for the exergy rate (or flow rate) of the exergy flow inputs (or fuels, F) and products (or byproducts P) of the respective control volume. Similarly, the CO_2 emission cost balances can be written as shown in Equation (12), where the direct CO_2 emissions, either produced by burning the fuel i consumed or arisen/captured from other chemical reactions, are accounted for in the $\boldsymbol{M}_{CO_2,Rxn}^{i}$ and $\boldsymbol{M}_{CO_2,F}^{i}$ terms [gCO_2/s], respectively:

$$\sum_{j} c_{CO_2}^{j} \boldsymbol{B}_{T,P}^{j} = \sum_{i} \left(c_{CO_2,F}^{i} \boldsymbol{B}_{T,F}^{i} + \boldsymbol{M}_{CO_2,F}^{i} \right) + \boldsymbol{M}_{CO_2,Rxn} \tag{12}$$

In the case of the allocation of CO_2 emissions, initial input values for unit CO_2 emissions cost must be considered equal to zero (or known). This differs from the conventional approach of adopting the unity (or a known value from previous analyses) as the unit exergy cost of an external input entering the control volume. Figures A.1-A.4 in APPENDIX A show the simplified control volumes, as well as allocation criteria, adopted for calculating the unit exergy costs and specific CO_2 emissions related to the streams of the offshore petroleum platform. It is important to notice that practitioners often use the specific power consumption ($kWh/t_{crude\ oil}$) or the overall energy intensity ($MJ/t_{crude\ oil}$) in order to quantify the performance of the overall offshore petroleum production platforms and their components. However, the present approach is more advantageous as it allows mapping the generation of the costs along the industrial processes and, consequently, to spotlight the systems responsible for the highest exergy consumption and energy degradation, as well as those entailing the largest non-renewable CO_2 emissions. Furthermore, this methodology allows an improved insight into the influence of the energy demanding CO_2 capture, recompression and sequestration processes on

the overall platform performance. This is possible thanks to an iterative calculation of the unit exergy costs and the specific emissions of the recirculated CO_2-rich streams to the well, as they aim to enhance the petroleum recovery while mitigating the environmental impact.

5.4 Process modeling and performance indicators

Based on the exergy concepts presented, performance indicators were defined as means to help the author compare and judge the different platform configurations studied. Moreover, along the process of modeling the system, assumptions and decisions were made and will be laid out in this section and along the next chapter.

Firstly, the power producing cycle is the major difference between platform configurations. Therefore, it makes intuitive sense to measure the power generation performance of each platforms characteristic power cycle. In order to do so, the power produced in the power generation control volume (Figures. 25-28) is compared to the feed fuel's chemical exergy. The ratio between these two values defines the power exergy efficiency shown in Equation (13). Briefly, it aims to specifically evaluate the ability of the utility system to efficiently convert the chemical exergy of the fuel consumed into net power, required by the ASU and the CO_2 compression unit together with other ancillary equipment in the utility plant.

On either onshore or offshore applications, the ability of a plant to produce combined heat and power is an interesting angle to be assessed. This provides grounds for comparison with other works and allows for estimations such as increase in efficiency in case a bottoming cycles and chemical loops are added. Similarly to the power efficiency definition, Equation (14) also involves ratio between the feed fuel input of chemical exergy and the power generated by the utility system, however it also includes the exergy associated with heat in processes such as intercooling between compression stages. This exergy flow, previously regarded as destroyed exergy, is quantified and looked at as resource that can generate more power or function as a heating source for streams elsewhere in the plant.

Finally, given that the offshore platform most fundamental purpose is to separate petroleum into oil, gas and water, Equation (15) is defined as means to measure the efficiency of separation in exergy terms. It accomplishes said task by measuring the increase in output total exergy relative to the inlet as a result of consumption of the fuel stream exergy. It is important to stress that $\Delta \boldsymbol{B}_{total}$ is calculated with respect to the streams that are not consumed within the utility system. Therefore, the consumed fuel exergy contribution is taken out from the inlet gas stream. Furthermore, the terms $\boldsymbol{W}_{cycle}$, $\boldsymbol{B}^{Q}_{WHRU}$ and $\boldsymbol{B}^{CH}_{fuel}$ refer to the net power produced considering the control volume aforementioned, exergy associated to recovery of flue gas heat from turbine outlet and compression heat also within the control volume, and chemical exergy of the fuel stream, respectively.

Table 4 displays the three exergy efficiency definitions aforementioned. All equations are applied to control volumes that extend from air entering the air compression train to release of flue gas (Power Generation Unit), as in the conventional case, or CO_2 captured leaving for re-injection, as in the case of the S-Graz (Air Separation, Power Generation and CO_2 compression units), amines absorption cycle (Power Generation, MEA loop and CO_2 compression units) and Allam cycle (Air Separation, Power Generation and CO_2 compression units). Mass, energy and exergy balances of each sub-process of interest are carried out by the use of Aspen Hysys® V8.8 software. As for the thermo-physical properties of each flow present in the system, Peng-Robinson and Acid Gas Fluid Packages have been used. Physical and chemical exergy calculations, as well as exergy efficiencies are assessed by using VBA® scripts as *user defined functions* [119].

Table 4. Exergy efficiencies proposed for evaluation of the FPSO

Definition	Formula	Equation
Power	$\eta_{power} = \dfrac{\boldsymbol{B}_{useful,output}}{\boldsymbol{B}_{chemical,fuel}} = \dfrac{\boldsymbol{W}_{cycle}}{\boldsymbol{B}^{CH}_{fuel}}$	(13)
Cogeneration	$\eta_{cogen} = \dfrac{\boldsymbol{B}_{useful,output}}{\boldsymbol{B}_{chemical,fuel}} = \dfrac{\boldsymbol{W}_{cycle} + \boldsymbol{B}^{Q}_{WHRU}}{\boldsymbol{B}^{CH}_{fuel}}$	(14)

Definition	Formula	Equation
Separation	$\eta_{sep} = \frac{\Delta \boldsymbol{B}_{total}}{\boldsymbol{B}_{consumed}} = \frac{\boldsymbol{B}_{total,output} + \boldsymbol{B}_{total,input}}{\boldsymbol{B}_{total,fuel}}$	(15)

Along the modeling process, some decisions regarding simulation have to be made in order to advance the study forward and establish its limitations. The equipment efficiency such as compressor adiabatic efficiency has been set at 85% whereas turbine efficiency at 93%. Intercooling temperature is usually at 40 ºC, unless it is specifically indicated otherwise.

In the following chapters, the configurations studied and respective parameters are presented as well as discussion of the results obtained.

6. Conventional, amine and oxyfuel-based platforms layout

It is important to notice that the conventional platforms operating in Brazil are not yet equipped with carbon capture systems for the sake of mitigation of the atmospheric emissions produced through the combined heat and power generation. Thus, this study is mainly motivated by recent commitments for the introduction of carbon capture systems in the existent and new Brazilian FPSOs [120], due to the increasing environmental regulations in the natural gas and oil industry. For instance, the largest state oil and gas company in Brazil, Petrobras, in its 2040 strategic plan and 2019-2023 business and management plan, aim to keep emissions in the same levels of 2015, even with increase in production. Emissions related to exploitation and production are expected to have a 32% reduction, whereas refining should decrease by 16% [38]. Accordingly, the advantages of three proposed platform configurations with carbon capture systems, namely a chemical absorption-based setup using a typical aqueous amine solution and the other two based on the so-called zero-emissions S-Graz cycle and Allam cycle, are thoroughly compared with the performance of a conventional configuration of an offshore petroleum platform.

Figures 25-28 depict the four types of plants which are assumed to operate at the conditions of highest oil production rates in a mature oilfield located at the Brazilian Pre-salt reservoir [34, 35]. Due to these specific circumstances, the results are not indicative of how the platform will perform throughout its entire lifetime cycle and efficiency is expected to drop once peak oil production passes. It is also noteworthy that water production is not considered at this point of the lifetime of the well, based on the work by Barbosa et al. [121]. The representative production rates of oil, CO_2, and natural gas are based on the reported literature [110, 118, 122] and briefly described in this section. For all the four configurations, petroleum is extracted from the well at a mass flow rate of 196 kg/s, 40ºC and 15 bar, and goes through an energy intensive primary separation unit modeled as a black box. The multiphase separation process of petroleum into natural gas, CO_2 and oil considers the specific energy consumption required to separate the mixture [33, 99, 114] and its numeric value for this work can be

found in the tables of APPENDIX A under the label Primary Separation (Heat Requirement). After the primary separation, oil is pumped and stored at a flow rate of 161 kg/s. Meanwhile, the separated gas phase is compressed to 52 bar [123] and sent through a membrane purification system which separates it into a methane-rich permeate stream and a CO_2-rich stream that still contains a large amount of methane. The stream composition after the membrane separation is such that the methane-rich stream (28 kg/s) is composed of approximately 97% of methane and 3% CO_2 (molar). Next, a fraction of the purified natural gas stream is decompressed to about 40 bar and fed as fuel into the cogeneration system, in the case of the Conventional, S-Graz and Amines-based configuration. For combustion in the Allam cycle, pressure levels are far superior, so the fuel is further compressed to 300 bar. The remaining purified gas is then further compressed to 245 bar and exported to the shore. Meanwhile, the carbon dioxide rich stream (approx. 8 kg/s), which has a molar composition of 70% CO_2 and 30% methane, is compressed up to 450 bar, suitable for injecting it into the well for the sake of enhanced oil recovery.

The conventional configuration shown in Figure 25 is the most common configuration in the commercial scenario of the Brazilian FPSOs. In this design, high temperature gases (1150 °C) are expanded in the simple cycle gas turbine (SCGT) to produce power, whereas the energy available at the turbine exhaust is used to raise hot water that will heat up the petroleum mixture at the primary separation system. The expanded cold flue gases at low pressure are finally discharged to the atmosphere without any other procedure undertaken for flue gas purification purposes.

Figure 25. Conventional simple cycle gas turbine-powered FPSO configuration

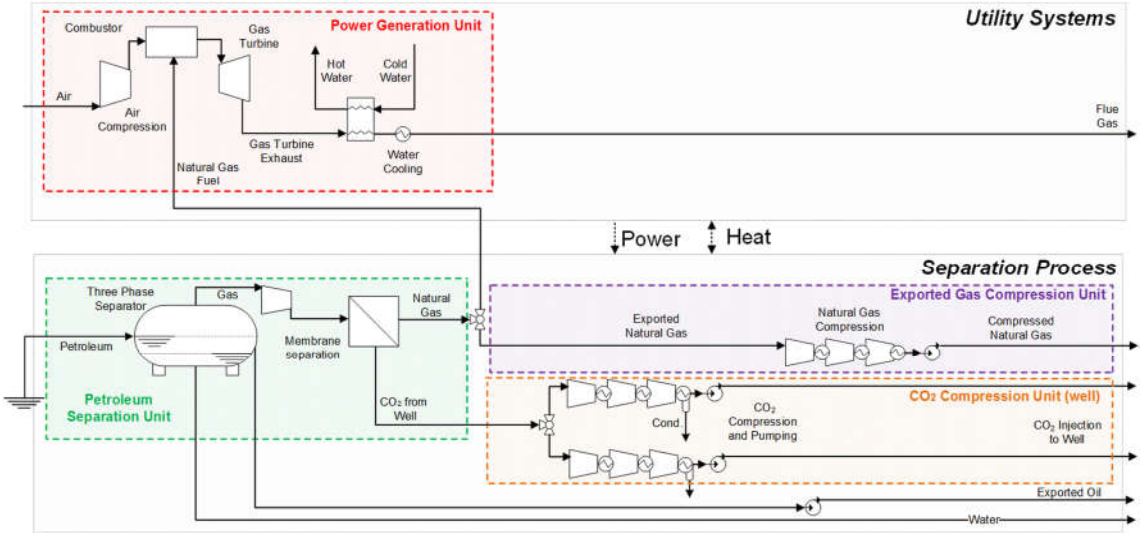

Source: author

As concerns the amine-based configuration (Figure 26), the exergy embodied in the gas turbine exhaust gas is used not only to supply the heat requirement in the primary separation unit but also to raise steam used as the means of providing the reboiler duty in the chemical desorption process for CO_2 purification and subsequent capture. In the monoethanolamine (MEA) loop, amines are used to separate the CO_2 out from the combustion gases before being compressed for re-injection purposes. On the other hand, the purified flue gas that remains is discharged to the environment at close to atmospheric pressure. During the CO_2 compression, the moisture is continuously condensed and separated, and the dried CO_2 gas is compressed to elevated pressures of about 450 bar, so it can be injected back into the well for enhancing the petroleum recovery and mitigating the environmental impact.

Figure 26. Chemical absorption-based (amines), gas turbine-powered FPSO configuration

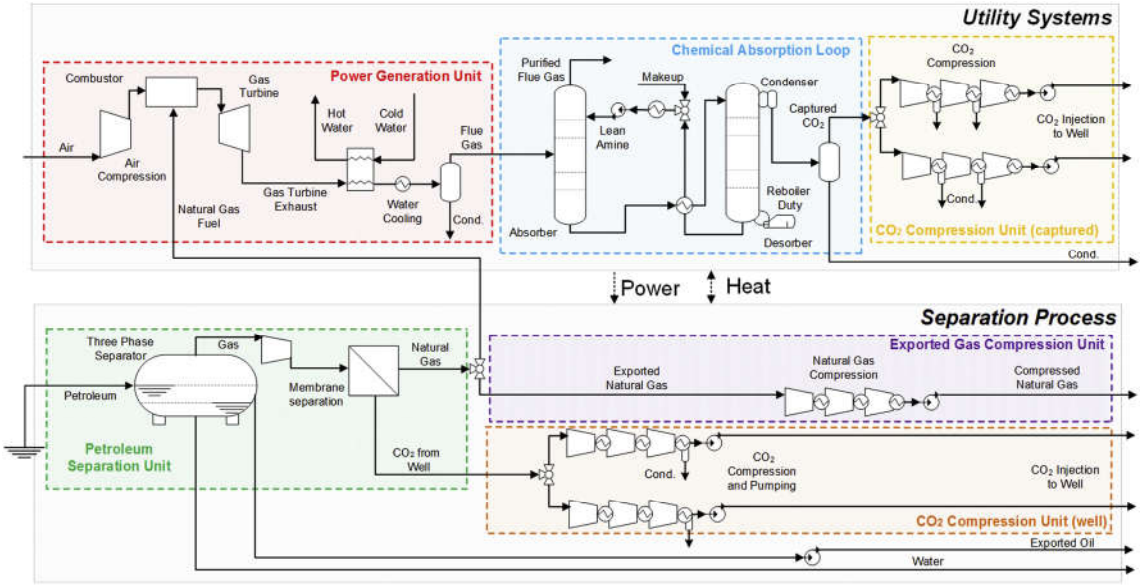

Source: author

Two oxyfuel cycles are studied in this work as alternatives in comparison to the conventional layout and post-combustion CCS technique. The first one presented resembles the S-Graz configuration proposed by Wolfgang Sanz in 2005 and inspired by the original idea of the Graz cycle by Herbert Jericha, 1985 [54, 62]. In the simplified flow sheet of the S-Graz cycle-powered platform (Figure 27), the primary separation of petroleum, the compression process of the exported natural gas and of the CO_2 rich-stream are the same as in the previous configurations.

Figure 27. S-Graz cycle-powered FPSO configuration

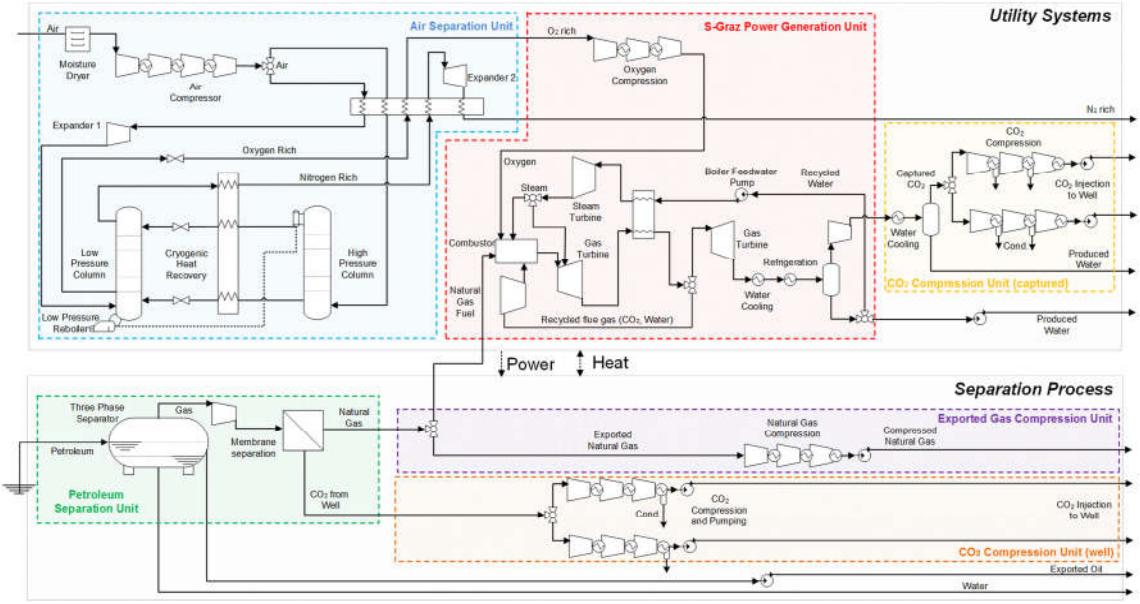

Source: author

However, since pure oxygen is used for combustion instead of normal air, an additional air separation unit (ASU) is required. Differently from the previous offshore platform configurations, a fraction of the natural gas is fired with an oxygen-rich stream at 40 bar. Recycled combustion gases (78% H_2O and 22% CO_2 molar) together with expanded steam are injected into the turbine combustor in order to control the gas turbine inlet temperature (1400°C). Furthermore, superheated steam (565 ºC, 180 bar) is generated in a heat recovery steam generator by using the exhaust gases of the gas turbine, and used to produce further power before the steam injection [68]. It is important to point out that steam is injected not only to the combustor chamber, but also at the admission of the gas turbine itself. Out of the total amount of combustion gases produced, 71.5% of the molar flow is recirculated and compressed back to 40 bar before entering the combustor chamber. The remaining 28.5% of the flue gases are further expanded (0.04 bar) and then cooled to 18ºC by a vapour-compression refrigeration cycle, partially separating the water in a vapor-liquid separator. The captured CO_2 is then recompressed to suitable pressure levels for geological injection and storage, whereas the excess water produced in the combustion

process is discarded to the sea, once it has been treated and carries acceptable levels of contamination.

The second oxyfuel cycle analysed is the Allam or NET Power cycle. In the Allam cycle, the pressure levels involved are much higher than in the previous three designed setups (Figure 28). Oxidant stream is formed by mixing a highly pure O_2 stream with a fraction of the recycled CO_2 flow. It enters the combustor chamber at 300 bar and around 1150 ºC along with pressurized natural gas fuel and some more recycled carbon dioxide. The flue gas resultant from the combustion flows towards the gas turbine inlet where it is joined by the remaining recycled flue gas and expanded to 30 bar. After expansion, the flue gas rich in CO_2 goes through a multiple stream heat exchanger in which heat is recovered by heating up the recycled and oxidant flows. Due to differences in specific heat of carbon dioxide at radically different pressures and temperatures flowing through the heat exchanger, heat from an external source, in this case from the oxygen compressors, must be supplied to balance the heat requirements [20, 53]. In order to separate the water present in the combustion products, further cooling must be performed. Other studies vary in cooling temperature, from 43 ºC to 70 ºC [49, 73]; in the present case, the stream is cooled to 69 ºC. The highly pure CO_2 is thus initially compressed up to 100 bar, and then 96.2% of the compressed stream is recycled back to the power generation unit, as shown in Figure 30, to compose the aforementioned oxidant stream and recycled flows. The remainder is further compressed to re-injection pressures (same as in the previous configurations). Moreover, the air separation unit, the primary petroleum separation, the exported gas compression unit and injected CO_2-rich compression unit operate in a similar manner to all the plant layouts. However, a small amount of natural gas fuel is burnt in an auxiliary boiler to meet the heating requirements of the Allam configuration which could not be satisfied by recovering heat elsewhere.

Figure 28. Allam cycle powered FPSO configuration

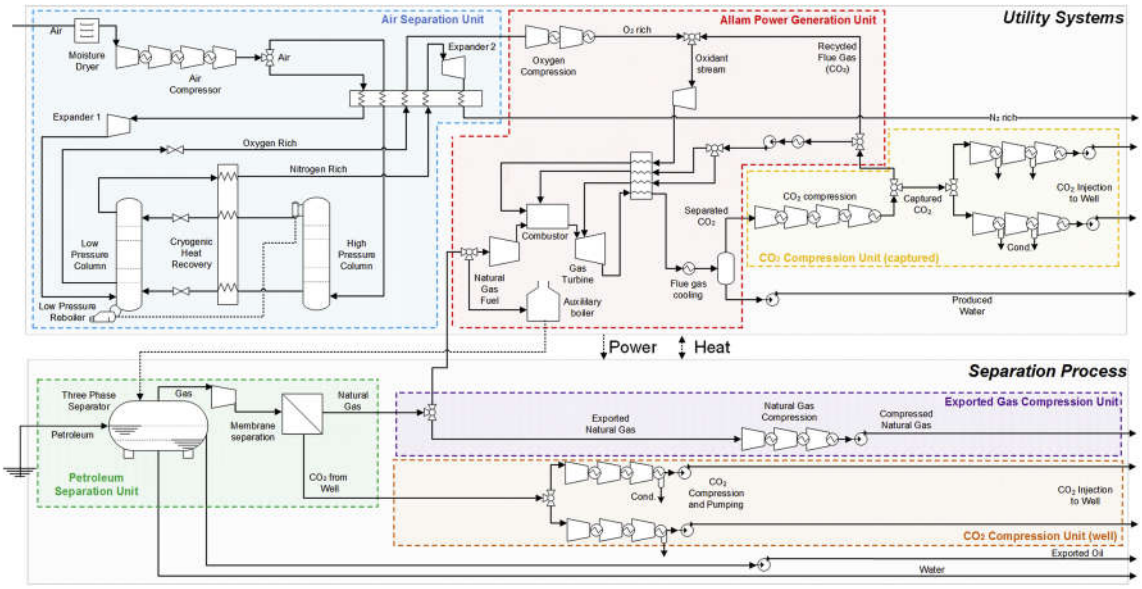

Source: author

The simulations of each of these offshore platform configurations were considered finished once the fuel gas necessary for the turbines to produce power equal to the consumer equipment's demands was found. In other words, once the net power produced by the plant nears zero ($\boldsymbol{W}_{net} = \boldsymbol{W}_{turbines} - \boldsymbol{W}_{consumers} \cong 0$). When that point is reached, the numeric values of the variables corresponding to those in the definition of the exergy efficiencies (Table 4) can be extracted, efficiencies calculated and configurations compared. Furthermore, physical, chemical and total exergy of the streams depicted in Figures 27-30 are also calculated so unit exergy costs, exergy breakdown and exergy destruction and consumption magnitudes are known and located. CO_2 emissions present in the output streams are accounted for so evaluation of pollution levels can be assessed as well as the CO_2 emissions cost of the main hydrocarbon products. Finally, turbines and expanders are set apart from consumers such as compressors and pumps in a simple First Law analysis.

6.1 Air separation

A cryogenic air separation unit (ASU) has been modeled to fulfill the oxygen requirement of the S-Graz and Allam power cycle. This technique was chosen since it is the most adequate when high gaseous oxygen flow rates are required

at high purity [82]. In this unit, normal air at ambient conditions of 25ºC and 1 bar enters and is compressed up to 7.45 bar and 40ºC. The normal air composition considered here is: 78% Nitrogen, 21% oxygen and 1% Argon. Note that it is free from water and carbon dioxide, which can be removed with the use of molecular sieves and is already a pretty common step well known to the cryogenic separation technique. About 95% of the compressed air is cooled down in the main recovery heat exchanger (-170ºC) and then it is fed into a high pressure column (HPC) [124]. The remaining 5% of the compressed air (-139ºC) is expanded to 2.95 bar before entering the low pressure column (LPC). Next, both the liquid bottom and vapor overhead outlet of the HPC are cooled down by using the nitrogen rich stream coming from the LPC overhead, and then expanded and sent to the LPC where further air separation occurs. Both columns are thermally integrated as the HPC condenser provides the duty required by the LPC reboiler. A last expansion step (1 bar) of the nitrogen rich stream produced in the LPC allows for an increased cooling effect in the main heat exchanger [78]. The final ASU product corresponds to an oxygen-rich stream (99.5% molar). This fact adds some advantages in terms of the amount of inert gases in the combustion products, saving an extra inerts removal step later on [125], as well as a nitrogen-rich stream that could be either discharged to the environment or even commercialized. The specific power input is calculated adding all the consumer equipment's demands, such as compressors and pumps power input, and abating the power produced by the expanders present in the air separation unit. For this ASU, specific power input in terms of tons of oxygen produced is calculated as being 286.3 kW/(tO_2/h). Figure 29 shows the schematic representation of the cryogenic ASU in question.

Figure 29. Schematic representation of an air separation unit (ASU)

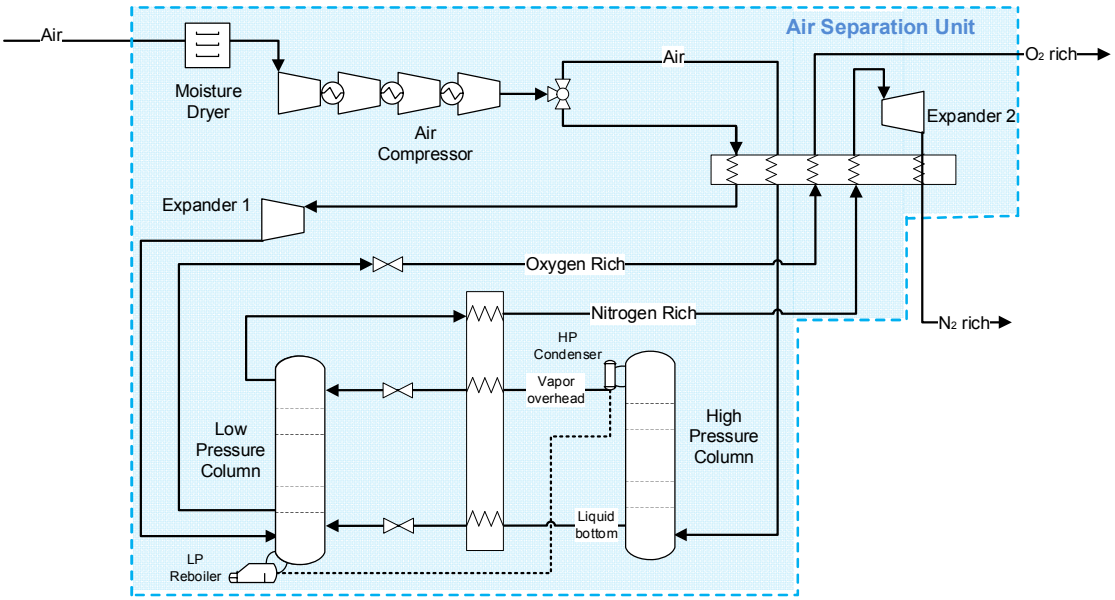

Source: author

7. Results and discussion

In the following sections, the performance of the four FPSO setups, i.e. two consisting of the conventional OCGT with and without an amine-based carbon capture system, and the other two using the oxyfuel S-Graz cycle and Allam cycle, are compared in terms of (i) the specific exergy consumption, (ii) the net amount of CO_2 emissions, (iii) the exergy efficiency, (iv) the specific exergy destruction at the plant wide and subunit levels, as well as (v) the unit exergy cost and specific CO_2 emission cost of the streams pertinent to each process unit.

7.1 Energy consumption remarks

Table 5 summarizes the main design parameters, some of which have also been reported in a specific basis. As stated before all platform configurations intake the same amount of petroleum with the same composition which is why the income streams of oil, gas and CO_2 are the same for all four of them. The natural gas consumption however determines how much gas is exported. On that matter, the configuration which consumes the largest amount of fuel in order to supply power and heat to the process utility is the post-combustion equipped platform. This configuration consists of a conventional setup with an added MEA loop for CO_2 purification and a CO_2 compression step. The additional energy intensive processes and machinery require the power cycle to burn 7% more fuel to support them. On the other hand, one of the advanced configurations is also the smallest fuel consumer. The Allam oxyfuel cycle requires nearly 46% less fuel than the business as usual configuration (conventional), despite the additional equipment. This fact evidences positively towards the increments in efficiency power cycles like these claim to achieve which will be confirmed later through other metrics. Following the Allam cycle is the other oxyfuel cycle investigated, the S-Graz cycle. Furthermore, it is noticeable that the Allam cycle case study is the only one which burns fuel in an auxiliary boiler. The boiler is required in order to provide the heat necessary for the petroleum primary separation which is not found elsewhere in the plant at adequate temperature levels.

The air consumption in the simple cycles is also significantly higher than in the oxyfuel configurations. This is mainly due to the difference in equipment from a

conventional gas turbine and oxyfuel turbines. The latter is able to withstand greater levels of temperature (1400°C) while business-as-usual gas turbines are in the 1100-1200°C range. Hence, more cooling fluid, air in the simple cycle case, is used to help keep the temperature down. Additionally, oxyfuel cycles utilize highly pure oxygen as oxidant, so less air is necessary since it is separated into purified streams of its components. The outstanding case again is the Allam cycle which presents the lowest air intake while operating at the same temperature intervals as conventional gas turbines (see Table 5).

It is noteworthy the striking differences in combustor and exhaust gas pressure among the configurations, which in turn will have ramifications throughout many aspects of the power cycles. Firstly, since the Allam cycle operates at much higher pressures; nearly ten times higher than the levels at the other cycles, the pressure step to achieve appropriate levels for geological storage is much smaller. Also, the cycle's working fluid, which is highly pressurized supercritical CO_2, makes for a fluid that requires compact equipment and less compression power. As for the S-Graz cycle, besides having the highest turbine inlet temperature boosting its efficiency, it counts on close to atmospheric exhaust pressures and even with vacuum pressures on another expander. Its exhaust pressure is then three times lower than the one at conventional and post-combustion configurations, which again contributes to higher efficiencies as more power can be extracted from expansion. The same low exhaust pressures would not be advised for the post combustion set up since lower pressure level render the MEA loop less effective.

Moreover, the lowest cooling requirement also belongs to the Allam cycle, followed by the conventional open gas turbine cycle, the S-Graz cycle and, finally, by the amine-based equipped platform. Graphic representation which allows for the calculation of the cooling requirement of each plant is presented in the pinch analysis section of this chapter. A lower cooling requirement means the plant will also reduce power consumption levels when dissipating excess heat from the facilities. The heat that is actually recovered in the oxyfuel cycles is harnessed at their respective Waste Heat Recovery Unit (WHRU). Table 5 shows how very different the minimum temperature approach is at each oxyfuel configuration. S-Graz cycle presents an 83ºC minimum approach at its WHRU, while the Allam

cycle is at 5ºC. Since larger driving forces lead to greater exergy destruction, this parameter is an indication that closing in on the S-Graz cycle minimum approach is one way to improve its performance efficiency wise. As for the CO_2 captured and emitted, the S-Graz cycle delivers to the pipeline the greatest CO_2 stream, although at the lowest purity levels. The S-Graz configuration also has strikingly lower value of CO_2 emitted in comparison to the other platforms. It surpasses the Allam cycle in this aspect because the latter is incapable of providing primary separation heat without the use of an auxiliary boiler, which in turn makes Allam a more pollutant cycle than the S-Graz. The amine-based setup ends up discharging a lot more CO_2 than the other advanced configurations due to the carbon dioxide present in the purified gas liberated in the MEA loop step. Finally, the conventional platform releases the largest amount of CO_2 into the atmosphere since it has no mechanism of mitigation.

Table 5. Main process variables in the studied configurations

Process parameter	**Amine-based**	**S-Graz Cycle**	**Allam Cycle**	**Conventional**
Oil production flow rate (kg/s)	161	161	161	161
CO_2-rich stream from well (kg/s)	8.2	8.2	8.2	8.2
Natural gas fuel consumed (kg/s)	1.74	1.53	0.88	1.62
Specific natural gas consumption (kg natural gas/ ton oil)	10.85	9.48	6.07	10.09
Natural gas fuel consumed in boiler (kg/s)	-	-	0.094	-
Natural gas exported (kg/s)	26.25	26.47	27.02	26.38
Air consumption (kg/s)	67.76	31.38	19.40	63.03
Oxygen consumption (kg/s)	-	5.79	3.28	-
Oxygen purity (%)	-	99.5	99.5	-
ASU oxygen recovery (%)	-	79.19	79.19	-
ASU spec. power consumption (kWh/t_{O2})	-	286.3	286.3	-
ASU N_2 rich waste gas (kg/s)	-	25.59	14.51	-
Combustor Pressure (kPa)	4,000	4,000	30,000	4,000
Gas Turbine Exhaust Pressure (kPa)	300	100	3,000	300

Process parameter	Amine-based	S-Graz Cycle	Allam Cycle	Conventional
Turbine Inlet Temperature (°C)	1,150	1,400	1,150	1,150
Net power produced (kW)[3]	21,231	27,477	27,238	19,739
Cooling Requirement (kW)[1]	60,815	52,169	22,627	28,367
Spec. Cooling Req. (kJ/t_{Oil})	377,733	324,031	140,540	176,193
Condensate from CO_2 compression (m^3/h)	5.4	6.3	-	-
Combustor/Gas turbine steam splitting (%)	-	91.5/8.5	-	-
Recycled flue gas CO_2 mole fraction	-	0.22	0.98	-
Percentage of recycled flue gas (%)	-	71.52	96.02	-
Oxyfuel total water disposal (m^3/h)	-	11.40	6.82	-
Min. temperature approach - flue gas/HRSG (ºC)	-	83	5	-
Water/CO_2 mixture flash pressure (kPa)	-	4	3,000	-
CO_2 emissions in natural gas export (kg/s)	2.05	2.07	2.11	2.06
CO_2 captured (kg/s)[2]	3.40	3.98	2.25	-
CO_2 captured purity (% mol)	98.90	94.20	98.07	
Spec. CO_2 captured (kg_{CO2}/t_{Oil})[2]	21.1	24.7	14	-
Total CO_2 emitted (kg/s)	1.14	2.3e-3	0.29	4.23
MEA make up water (m^3/h)	3.6	-	-	-
CO_2 recovery using MEA (%)	74.8	-	-	-
CO_2 fed to MEA loop (kg/s)	4.55	-	-	-
MEA loop reboiler duty (kW)	17,012.4	-	-	-
Spec. MEA desorber steam cons.(MJ/kg_{CO2})	4.99	-	-	-

1. Cooling tower water inlet at 18°C, 60% relative humidity; 2.This value only includes the CO_2 produced when burning the natural gas fuel, excluding the original CO_2 already extracted from the well. 3. Net power produced considering the Power Generation control volume (red) in Figures 25-28.

Figure 30 (a)-(d) shows the distribution of power demand among the different consumers of the various designed setups. On both the conventional and the amine-based platform, the normal air compression system is responsible for about 59.4% (approx. 29 and 31 MW, respectively) of the consumption of the overall power generated (considering compressor and expander as separated modules). Meanwhile, in the oxyfuel configurations, the air compression at ASU consumes

11.30% (approx. 7 MW) and 12% (approx. 4MW) of the total power generated in the S-Graz and Allam cycle, respectively. The exported gas compression is the second largest power consumer in all the plants considered, except for the Allam cycle-based FPSO, in which the exported natural gas compression achieves 46% (approx. 15 MW) of all the power produced. Actually, in this configuration that figure surpasses by far the second most power intensive process, namely the power generation unit itself (5.1 MW) as well as the air separation unit. In contrast, the S-Graz internals (i.e. recycle compressors, pumps, and so forth) consume up to 54.14% (33.6 MW) of the power generated by the power cycle, whereas in the Allam cycle, its internal consumption responds for only 16% of the total power produced. The third largest consumption in the plants except for the S-Graz based configuration corresponds to the compression process of the incoming CO_2 from the well to re-injection. The prominent positions occupied by the compression systems might be explained by the large flow rates of gas and particularly elevated pressures for export to shore or reinjection into Pre-Salt reservoirs. It is important to emphasize that, due to the technical regulations of the offshore electricity generation in the Brazilian platforms, no net power export is aimed, and thus, only the platform internal power demands need to be guaranteed. Finally, other ancillary processes represent up to 3.78% (1.9 MW), 3.51% (2.1 MW), 0.92% (447.9 kW) and 1% (447.9 kW) of the overall consumed power in the amine-based, S-Graz, conventional and Allam powered configurations, respectively.

Figure 30. Breakdown of the power supply and demand of the (a) Conventional, (b) Amine-based, (c) S-Graz and (d) Allam in (kW)

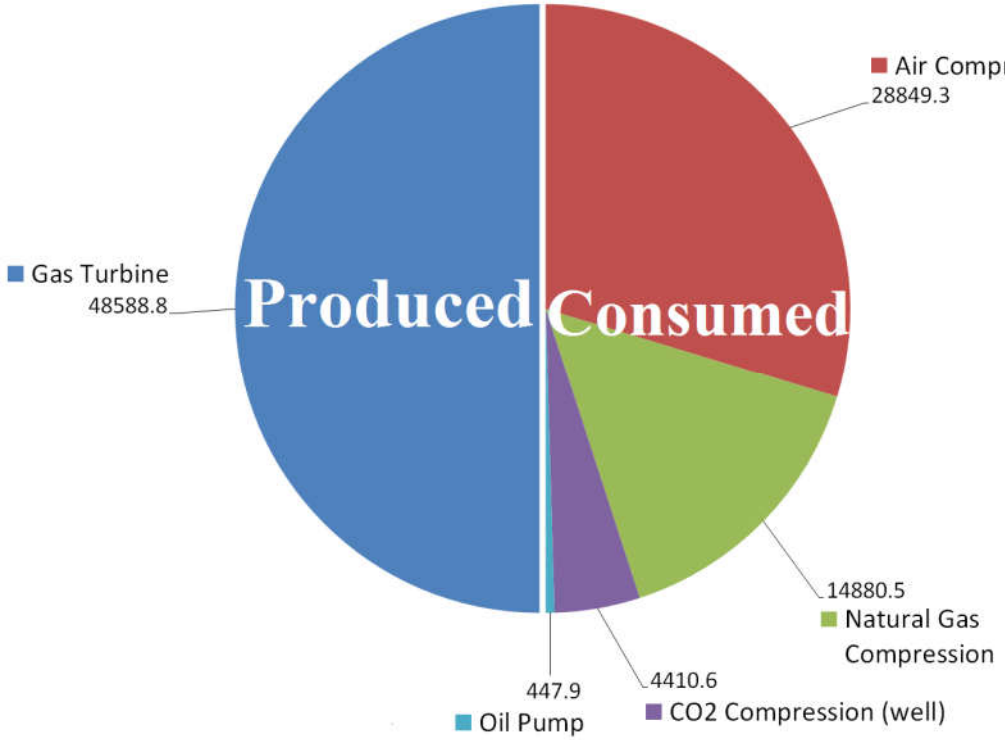

(a) Conventional Configuration

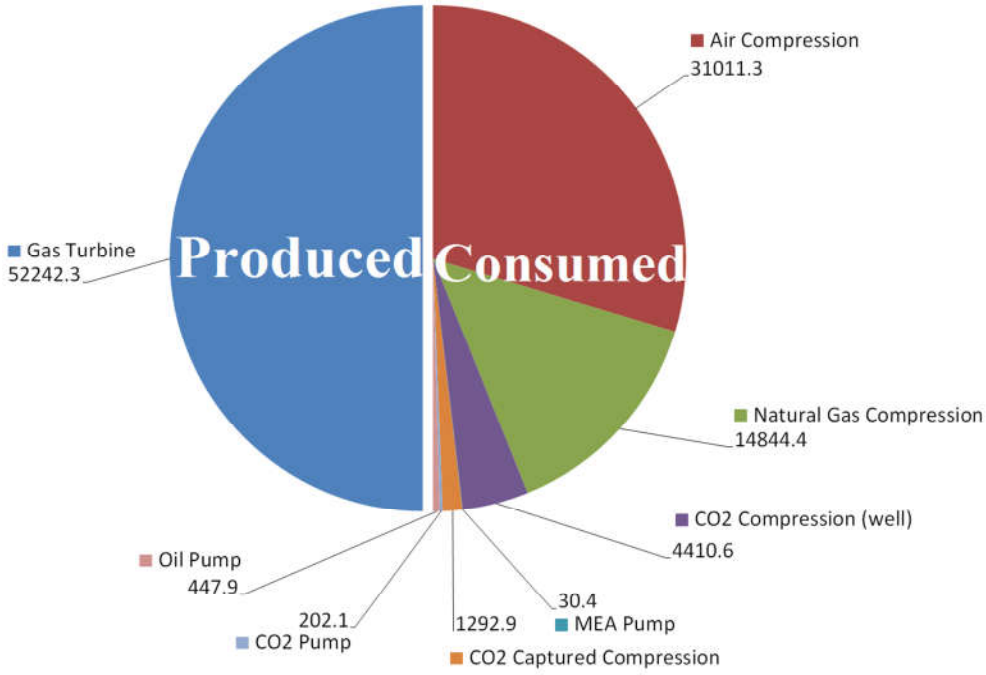

(b) Amines-based Configuration

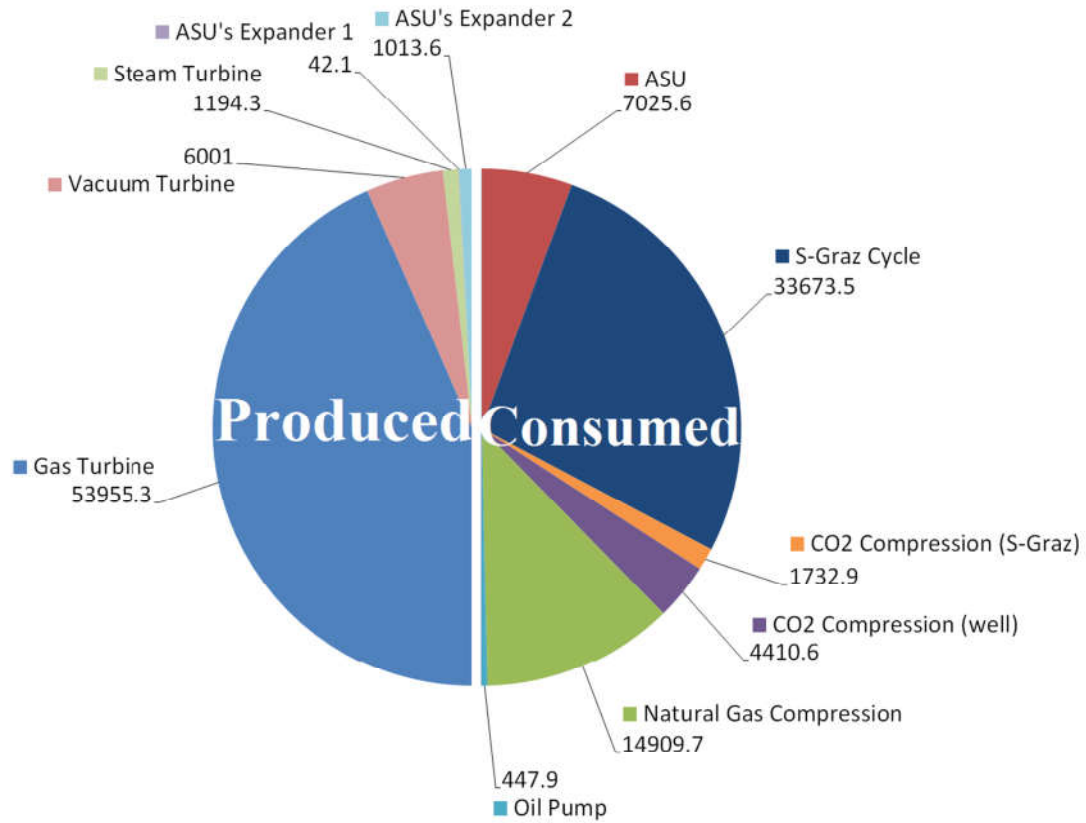

(c) S-Graz based Configuration

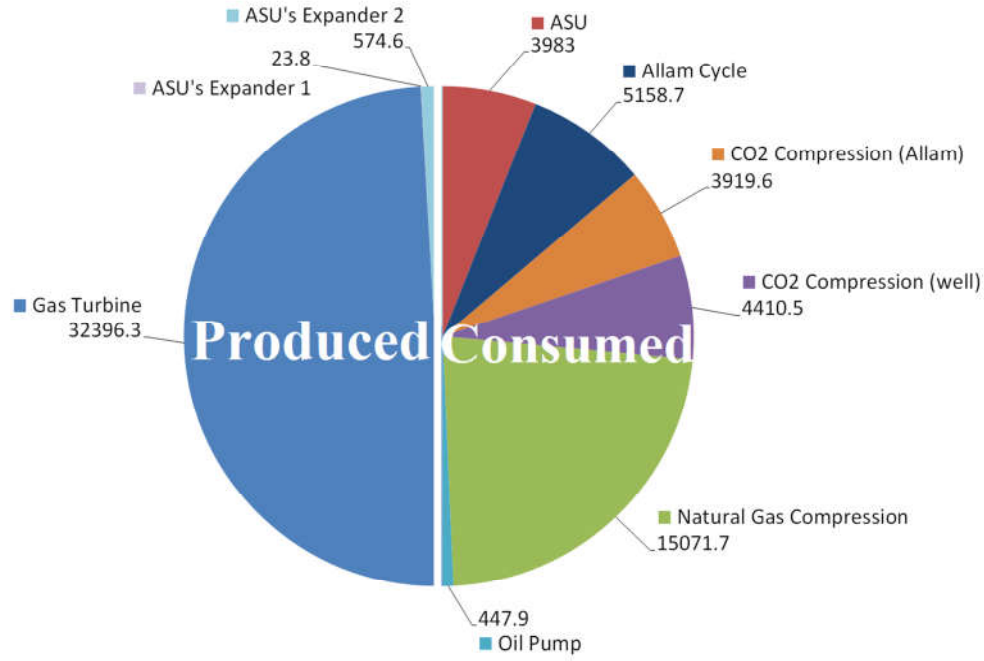

(d) Allam based Configuration

Source: author

7.2 Energy integration analysis

According to the methodology for energy integration previously presented, an energy integration analysis was carried out in order to determine whether the recovery of the waste heat available along the operation units of the platform might reduce the amount of fuel consumed, by either preheating the boiling feed water or raising the steam required in the process, otherwise provided by an auxiliary boiler. To this end, a global approach of 20 ºC is considered, whenever the minimum temperature differences are not specified. Particularly tight minimum temperature differences are selected (2-5°C) in the case of the air liquefaction process and the vapor compression refrigeration system, as heuristically suggested. The red lines (Figure 31 (a)-(d)) account for all the hot streams in the plant, in other words, all the streams that provide heat that could either be harnessed or discharged into the environment. Meanwhile, the blue lines represent cold streams that need to be heated. The supply and target temperatures of each hot and cold curves are plotted against enthalpy flow rate. The enthalpy rate flows plotted are not the individual heat rate flow discharged or absorbed by each individual stream, although the individual heat duty contributions can be used to build the graphic representation as well, but rather the cumulative result, summation of heat duties of either hot or cold streams. The point where the curves are the closest to each other is the pinch point and it is a design parameter that will influence the area through which heat transfer will happen and how much exergy is destroyed in this transfer.

The energy and temperature accounting resultant from the application of the energy integration method culminates in Figure 31 (a)-(d), which shows the integrated composite curves of the four studied configurations. In three of the four configurations, it is theoretically possible to meet the minimum heating requirements (MER) of the platform by recovering the waste heat throughout the facility. The only exception is the Allam cycle–based platform. In this setup, some waste heat is harnessed from the oxygen compression intercooling in order to meet the MER of the recycled flue gases and the oxidant stream (see Figure 28). This is due to the difference in specific heat of the CO_2 at 30 and 300 bar, as shown previously in section 3.2.2 (Table 3 and Figure 16). However, the energy

requirement of the primary separation of petroleum must still be satisfied but supplementary waste heat at the satisfactory temperature is not available elsewhere in the plant. Thus, in order to ensure this demand is tended to, an auxiliary boiler that consumes a fraction of the produced fuel gas is required. It is also worthy noticing that the advanced configurations progressively close in the gap between hot and cold composite curves, which may suggest tighter energy integration built into the advanced cycles design. The rates of exergy destruction in each case could be more easily pictured if the temperature axis were to be replaced by the respective Carnot factor axis. The lower rates of exergy destruction in advanced configurations, particularly in the Allam cycle setup, would result from the reduced driving forces in the heat transfer processes and consequently better performances would ensue. The excess waste heat not recovered is eventually dissipated by using water-cooling. The respective cooling requirement for each configuration in Figure 31 has been indicated in Table 5.

Figure 31. Composite curves for the (a) conventional, (b) amines-based, (c) S-Graz and (d) Allam-based configurations

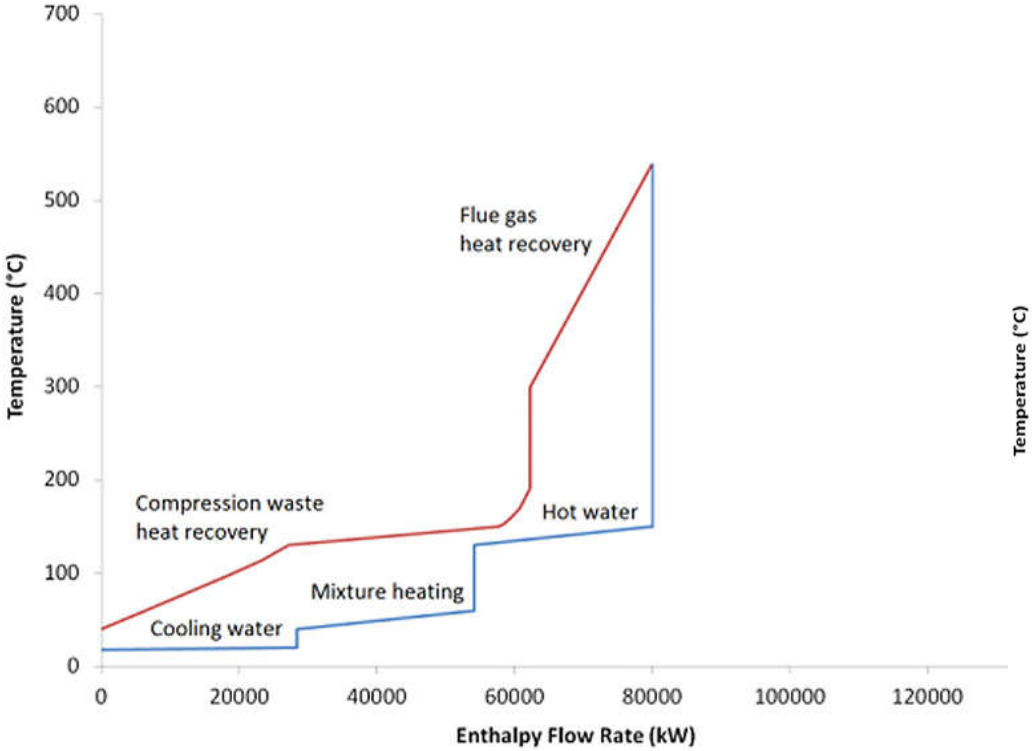

(a) Conventional Configuration

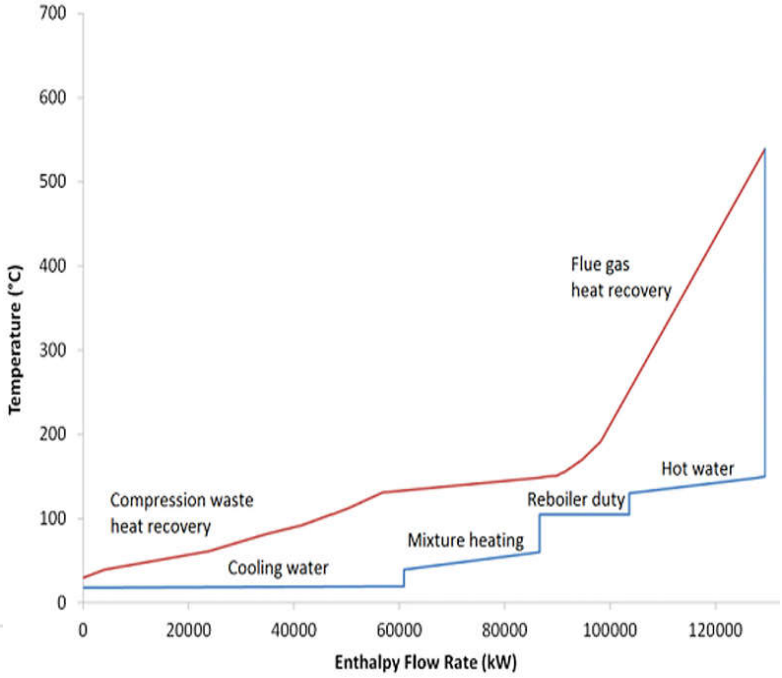

(b) Amines-based Cnfiguration

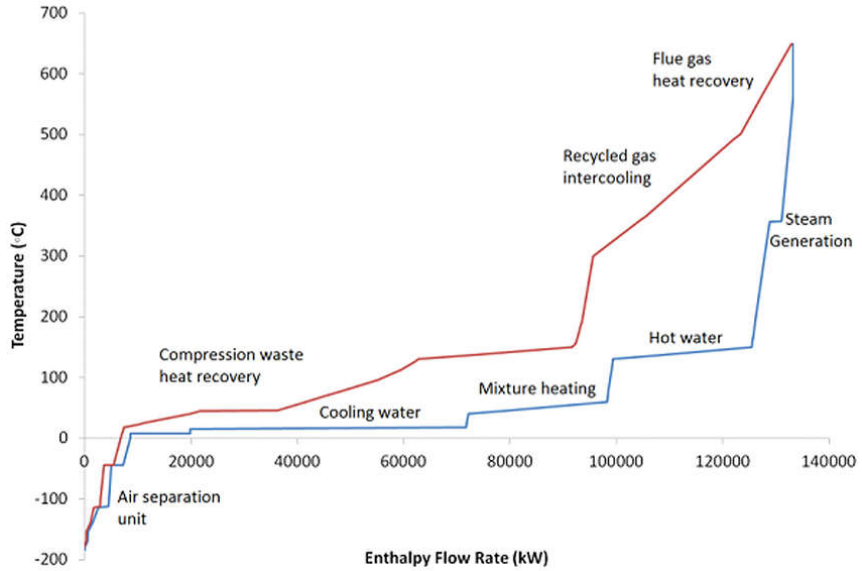

(c) S-Graz Cycle Configuration

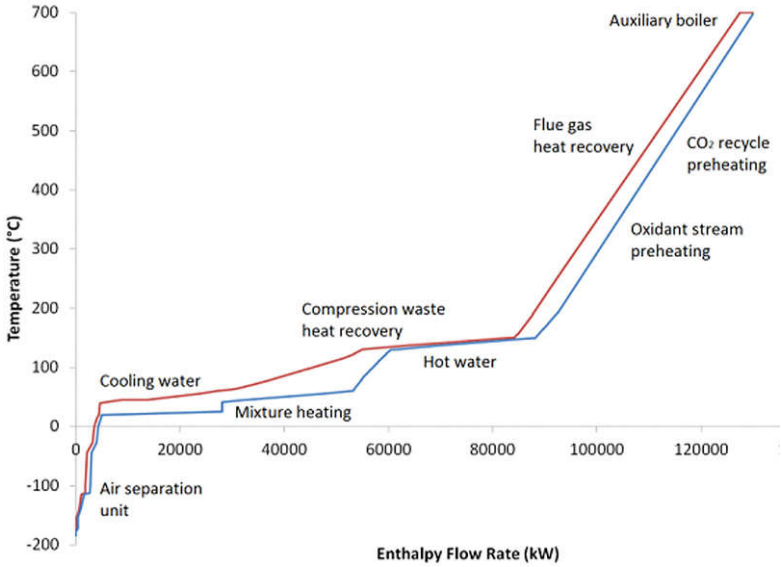

(d) Allam Cycle Configuration

Source: author

7.3 Exergy destroyed and exergy efficiency calculation

The closer a process is to be completely reversible (internally and externally), the lesser the exergy destroyed as it evolves from one given state to another. However, real processes take place on finite-driving forces and, thus, they are inherently irreversible. Accordingly, the exergy analysis gives us means to measure and allocate such irreversibility, accounted for in the amount of exergy destruction, so that the processes with the worst exergy performance can be identified and action to minimize the exergy destruction can be envisaged. Thus, in order to hierarchize the performance of the considered platforms, Figure 32 shows the exergy efficiency as defined in Table 4. It should be noticed that, as the oil virtually goes unchanged through the control volume after the primary separation is performed, it carries with it a large amount of transit exergy. Therefore, if its chemical exergy were to be included in the efficiency calculation, the results may lead to untruthfully large exergy efficiencies, misrepresenting the performance of the actual transformations occurring inside the platform. The same arguments would apply for the large mass exergy flow rate of the natural gas exported, compared to the much lower amount of the mass exergy of the gas consumed to drive the compressors. Accordingly, Figure 32 evidences that the conventional configuration performance experiences drops in all metrics of exergy efficiencies once it is equipped with an amines-based post combustion unit; the sharpest drop happening in the separation efficiency. This is to be expected since the power cycle not only has to supply power and heat for the same processing plant but also for the additional absorption loop and a subsequent CO_2 compression process. As consequence more fuel must be burnt in the amines-based layout. According to Equation (13), the increase in $\boldsymbol{B}_{fuel}^{CH}$ causes a power exergy efficiency drop of roughly two percentage points in the chemical absorption based setup compared to the conventional configuration. The same logic applies when considering the cogeneration exergy efficiency definition, which experiences a similar drop.

Meanwhile, the platform equipped with an S-Graz power cycle exhibits reduction in fuel consumption when compared to the business as usual platform configuration; which raises both the power and cogeneration exergy efficiencies.

The need for less fuel might be explained by the higher temperatures that oxyfuel turbomachinery is able to withstand, lower exhaust pressure and by the layout of the advanced cycle itself. The turbine inlet temperature for some oxyfuel gas turbines is around 1400 °C, as in the case of the S-Graz cycle. Higher inlet temperature such as this coupled with greater pressure differences in the power cycle turbines factor in increases in efficiency. Moreover, the cycle's layout extracts more power lowering working fluid pressure even further to vacuum pressures and by recovering energy from high temperature gases and convert it into more power in a steam turbine (see Figure 27).

Finally, when comparing the conventional platform setup with the Allam cycle equipped one, a very drastic increase in power and cogeneration exergy efficiency is noted. The Allam power cycle requires far less fuel to tend to the demands of the plant. What it shows is that this configuration is far more efficient at converting fuel's chemical exergy into the power and heat the facilities need. The extensive usage of heat integration shown in the composite curves as well as the characteristics of a working fluid comprised of nearly pure CO_2 that warrants such integration might help explain Allam's superiority in these metrics.

The scenario changes trends when analyzing the separation exergy efficiency. Since an offshore platform is primarily a separation process, the separation exergy efficiency correctly points out in Figure 32 the losses that incur when trying to separate the products of combustion even further, which is what happens in the advanced configurations. Therefore, the conventional configuration presents better results than all the advanced configurations in this regard. The Allam cycle still follows as the most efficient among the advanced configurations, followed by the S-Graz cycle and finally by the amines-based layout.

Figure 32. Exergy efficiency definitions for studied configurations as defined in Table 4

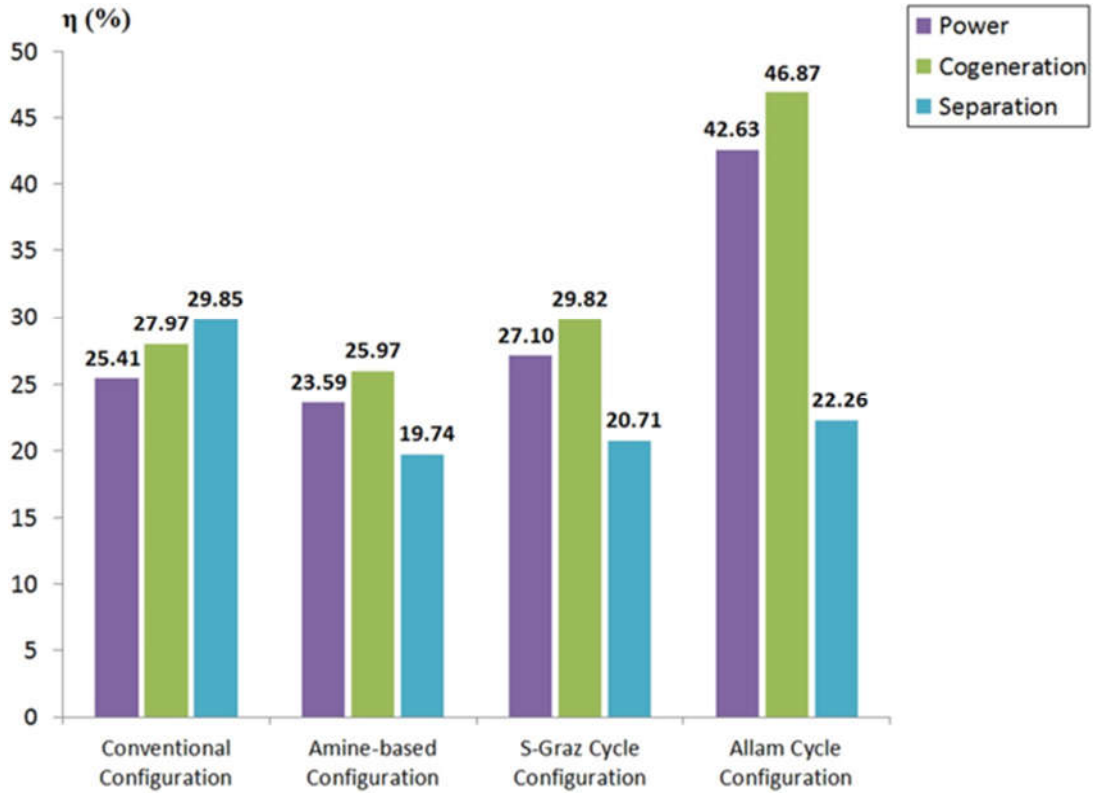

Source: author

The efficiencies presented in Figure 32 are deeply impacted by the additional air separation and CO_2 separation and compression facilities. The CO_2 compression step impacts by 2.38% the power exergy efficiency of the S-Graz cycle, for instance, whereas the ASU causes a drop of 8.19%. In the Allam cycle case, the differences in impact on efficiency of the aforementioned facilities are 8% for the ASU while the cycle CO_2 compression, 9.27%. Although the impact of the ASU is in accordance with estimates given in open literature [80], some measures can be taken to improve upon its performance. The reversible power required by the ASU corresponds to the minimum exergy necessary to separate the air into its main components (namely, oxygen and nitrogen rich streams). Since the system operates irreversibly, the actual power is indeed much higher. The actual exergy power consumed per ton of oxygen produced is calculated as 286.3 kW/(tO_2/h), which is within the ranges (280-340 kW/tO_2/h) reported in the literature for typical ASUs [12]. Equation (16) shows the definition considered to calculate the ASU exergy efficiency:

$$\eta_{ASU} = \frac{\boldsymbol{W}_{sep.consumed,\ reversible}}{\boldsymbol{W}_{sep.consumed,\ actual}} \quad (16)$$

This efficiency definition accounts for how far from the reversible power for air separation the actual power done by the ASU really is. By Equation (16), an exergy efficiency of 17.68% can be calculated. The ASU performance can be further improved by better integrating the dual pressure columns via pump around systems and intermediate heat exchanging sections in the LPC. In this way, the temperature differences are lowered while further decreasing the associated exergy destruction. Another way to achieve the same goal is to use columns HiDIC [126]. These columns are more highly integrated thermally in order to provide a more extended heat exchange area. Lower pressures and better temperature approaches in the contact columns as well as better condenser/reboiler integrations can also improve the ASU's performance. Thus, further research considering particular improvements must still be conducted for this case.

An alternative angle for comparing the performance of the different setups is through the specific exergy destruction per ton of exported oil. In Figure 33, a different trend from that presented in Figure 32 is displayed. The Allam cycle is the configuration which destroys the least amount of exergy in the energy conversion process. This is actually in accordance with Figure 32 when looking at power and cogeneration exergy efficiencies. The Allam cycle is so much more efficient than the others that it is reflected in its much higher natural gas exports and therefore in the Allam cycle's high $\boldsymbol{B}_{out}$, even though 96% of the mass of combustion products is recirculated and remains within the confounds of the control volume. Thus, it follows that the system's $\boldsymbol{B}_{out} - \boldsymbol{B}_{in}$, i.e. exergy destroyed ($\boldsymbol{B}_{dest}$), is the lowest among configurations. The other three configurations have similar efficiencies, but are arranged quite differently in the specific exergy destruction graph. The simple cycle configurations, namely conventional and amines-based, also follow the same pattern when compared to each other as is presented in Figure 32. The amines-based setup is less efficient and therefore should have higher rates of exergy destroyed. This is exactly what it is demonstrated in Figure 33. The same does not happen when looking at the conventional and S-Graz layouts. Despite being more efficient at converting fuel

exergy into power and heat, the S-Graz cycle platform presents higher rates of exergy destruction than the conventional one. Zooming in the accounting of exergy associated to input and output flows of both platforms, it is possible to find that the difference in exergy destruction that causes this is due to the difference in the amount of natural gas export in each platform and the fact that the conventional configuration discharges to the atmosphere all of its high temperature flue gas. The S-Graz, despite being able to export nearly 4800 kW in natural gas related exergy more than the BAU layout, it recirculates most of its would-be flue gas. So, even though the S-Graz cycle's high pressure, low temperature, CO_2 rich stream has higher specific exergy associated to it, because its mass flow is much lower than the conventional configuration's flue gas, the absolute value of the output exergy of the oxyfuel ends up being lower as well, even compensating for its higher efficiency. The gap in exergy is exactly the exergy associated with the recirculated working fluid which is allocated in this metric as destroyed exergy. When accounting for the exergy of the recirculated fluid, the S-Graz configuration scores lower than the BAU setup in specific exergy destruction. Therefore, one can say that the S-Graz cycle equipped FPSO destroys larger amounts of exergy due to the extra steps related to the recirculation of working fluid that remains within the confounds of the control volume.

Figure 33. Specific exergy destruction (kJ/t oil)

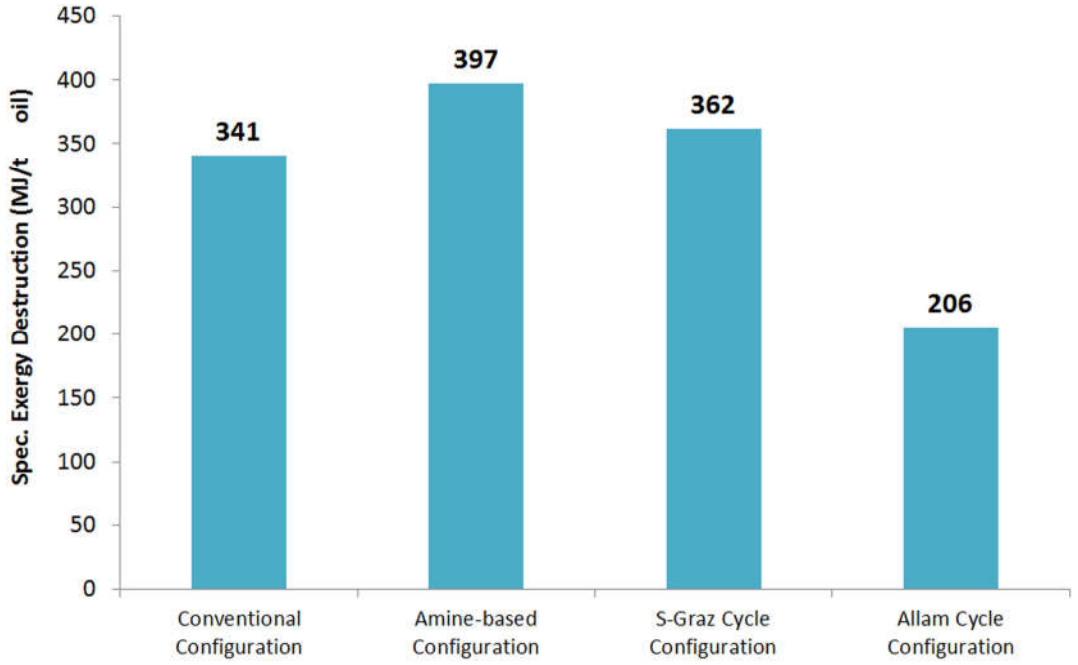

Source: author

Although important for the decision making process, the metrics shown so far should not be the only ones taken into account when evaluating which power cycle should be chosen; especially in the current context of climate emergency and political instability. Therefore, the CO_2 emissions rate of each platform configuration is calculated and shown in Figure 34, as a way to quantify the CO_2 mitigation capabilities of the advanced configurations proposed. As expected, a dramatic cut down of the atmospheric CO_2 emissions can be achieved by employing the advanced configurations. That way, the massive environmental impact of the CO_2 discarded in the conventional platforms may be attenuated by 10 to 1000 times. Moreover, the amines-based and Allam cycle platform discharges 100 times more CO_2 than the S-Graz setup due to release of purified gas resultant from the amines loop, its limited capacity for CO_2 sequestration at post-combustion carbon capture operating conditions and Allam's discharge of CO_2 containing condensate after combustion as well as from its boiler, necessary to meet the Allam cycle heating needs.

Figure 34. Specific CO_2 emission ($kgCO_2$/t oil)

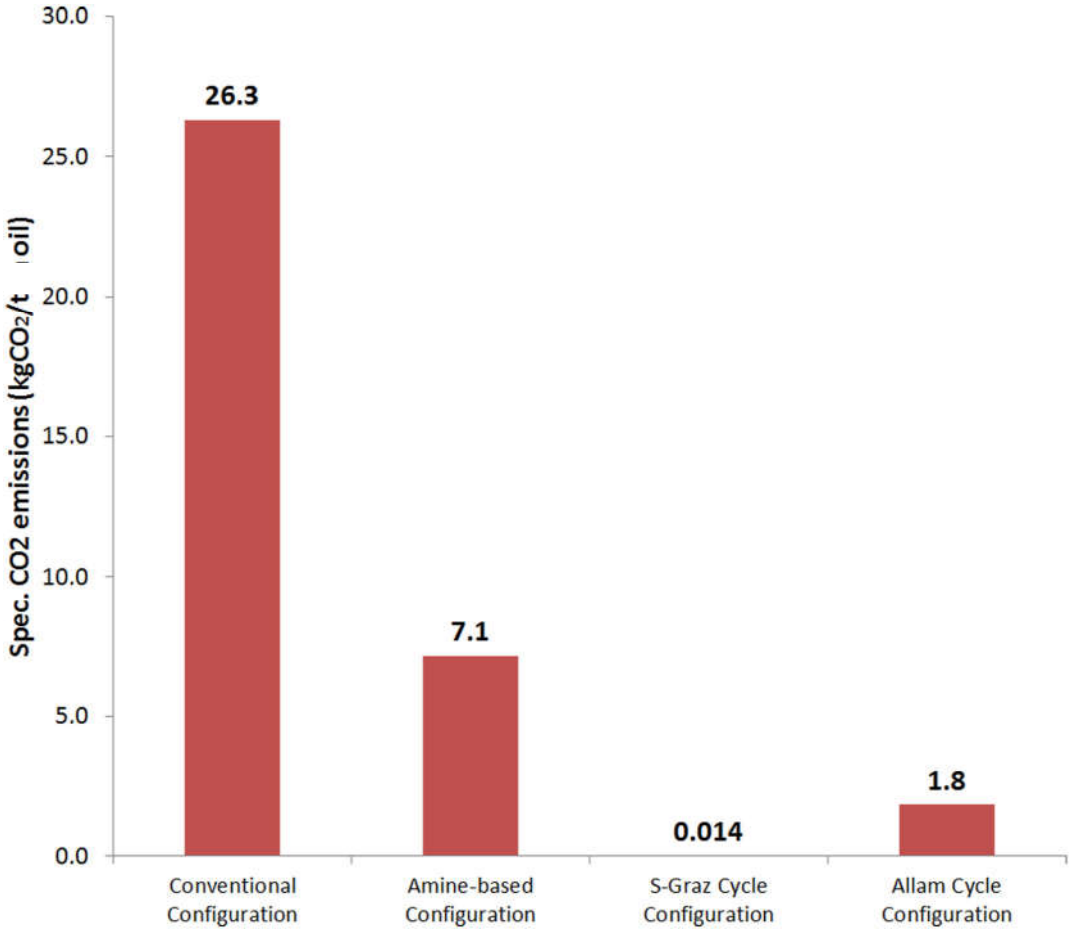

Source: author

Finally, an exergy destruction breakdown informs which among the various subunits composing the offshore petroleum platforms exhibit the highest rates of exergy destruction. This kind of portrayal sheds light upon which processes and components are the main candidates for potential improvements in their operation parameters or even for substitution/revamping. Figure 35 shows that the power generation systems, encompassing the SCGT system with the bottoming waste heat recovery unit (WHRU) as well as the S-Graz combined power and heat transferred entail the largest contributions to the exergy destroyed in all four platforms, corresponding to 67.99% (approx. 37300 kW), 60.35% (approx. 38615 kW), 48.67% (approx. 28300 kW) and 56.64% (approx. 18700 kW) for the conventional, amines-based, S-Graz and Allam cycle-powered configurations, respectively. Combustion reactions is a highly irreversible process which typically destroys at least about 25-30% of the exergy [127]. The conventional and the

amines-based configurations stand out as the setups with the most exergy destroyed during this process, both relatively and in absolute numbers. The energy intensive petroleum separation which takes place at large temperature differences contributes to a large extent to exergy destruction [89, 99] ranging from 9.29 to 20.74% of the total amount of exergy. The units enclosing the processes characteristic to the oxyfuel or chemical absorption units, namely, the air separation unit and the amine loop, follow the primary separation as the most irreversible processes. For instance, the CO2 purification via chemical absorption is responsible for 14.47% (approx. 9000 kW) of the exergy destruction. At the same time, the ASU stands for 8.63% (5000 kW) of the exergy destruction in the S-Graz-powered platform, whereas in the Allam cycle-powered platform this value amounts to 8.61% (2800 kW). As it was shown in Figure 30, the compression processes are quite energy intensive as they manage large mass flows. However, by examining the exergy breakdown, the full picture emerges, and the most energy intensive processes turn not to be necessarily the most exergy-intensive as well. As shown in Figure 35, in most of the cases, the compression units represent less than 5% of the exergy destruction in the platform. Other ancillary equipment, such as the heat exchange network, accounts for the remaining exergy destruction. Notably, in the S-Graz cycle-powered layout, this value climbs to 20% (13000 kW), as it is the power cycle with the most additional equipment. The Allam cycle-powered setup upholds the lowest percentage of ancillary exergy destruction, 4.36% (1400 kW), possibly because of its higher levels of energy integration.

Figure 35. Exergy destruction breakdown

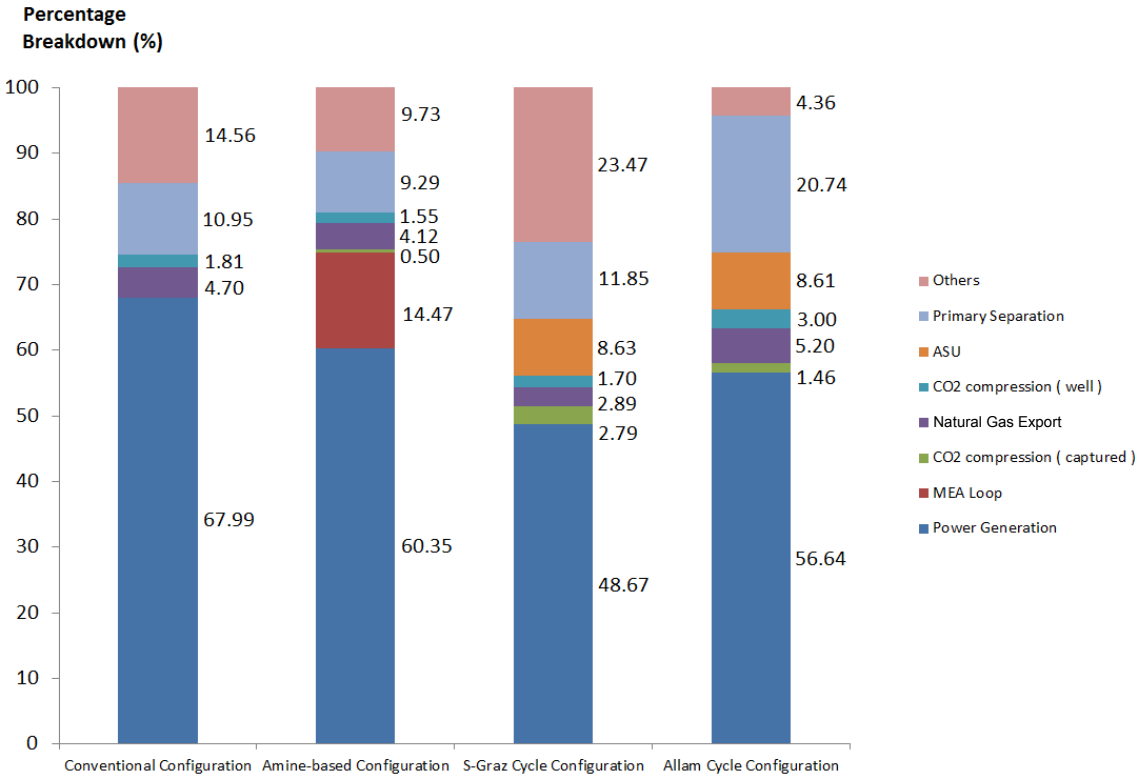

Source: author

7.4 Unit exergy cost and specific CO_2 emissions

In order to evaluate how each stream impacts CO_2 generation and how each of them demands a certain level of exergy expenditure, unit exergy costs and CO_2 emissions costs can be allocated to the streams throughout the processes according to a certain set of criteria. Table A.5 of APPENDIX A shows the criteria chosen for the streams in each subunit of the plant for all configurations, according to Figures A.1 to A.4 of APPENDIX A.

The streams which are considered waste products, such as water from water removal processes and flue gas, of the energy conversion process are attributed the cost value of zero (combine Table A.5 and Figures A.1 to A.4), as the efforts are not driven towards the production of these streams creation. This is most noticeable especially in the Power Cycle unit where a weighted average criterion is also employed for other products. In the conventional configuration (first column of Table A.5), the cost of heat transferred in the power generation unit is a

weighted average of the process inputs, much like the extraction criterion but balancing the multiple entries. The same is true for the other three configurations as well with the addition of flue gas/working fluid stream which is also equated to the weighted average. This is because they have been considered to be useful products since these streams will be further purified into CO_2 rich streams, and defining its cost like this equates it with the heat produced as important products of the power cycle. As for the Primary Separation, the equality criterion is adopted and all products, namely, oil, CO_2 and gas, have their costs equated among themselves. In the Compression and Membrane Separation control volume, the natural gas stream and carbon dioxide rich stream costs are equated as per the equality criterion while input power and output heat costs are equated (extraction criterion). These two criteria are basically applied throughout all the other control volumes in all configurations as they are commonly known, without any other weighted averages. In the Natural Gas Export Compression as well as the CO_2 Injection Compression the extraction criterion is used in the power and heat costs. In the Amines Loop, waste water cost is set to zero, the purified CO_2 as having the same cost as output process heat and the input Reboiler Duty cost is equated to the input heat cost of another process, the Primary Separation input heat cost. In the Captured CO_2 control volume, heat and power costs are equated while waste water cost are set to zero in the S-Graz and post-combustion equipped platforms. However, in the Allam setup, since it does not have a water removal process, the cost of CO_2 sent to injection is equated to the recycled CO_2 that returns to the power cycle. Finally, in the Air Separation control volume of the oxyfuel cycles, the cost of input air and produced nitrogen is equated using the extraction criteria which, in turn, will then heavily transfer the costs to the oxygen stream, the product of interest for oxyfuel cycles. Similarly, the compression power and compression heat costs are also equated in the Air Separation Unit.

These equations are auxiliary equations in an evolutionary algorithm of an Excel spreadsheet which calculates interactively the value of the output costs of each control volume of Figures A.1 through A.4. The results obtained for each configuration are displayed in Figure 38 which shows the calculated values for the crude oil and natural gas produced. Clearly, the highest environmental impact corresponds to the conventional scenario, in which 2.57 gCO_2 are emitted per unit

of exergy (MJ) of natural gas exported, in contrast with the strikingly three to tenfold lower (0.25-0.85 gCO_2/MJ) emissions produced by using the more advanced (amines-based, S-Graz and Allam-powered) platform configurations. Initially, it could be expected increased exergy consumption (kJ/kJ) in the scenario of the production of the natural gas leaving the platforms based on the more advanced, more equipment filled cogeneration and carbon capture systems. However, the unit exergy costs calculated also show a slight reduction of the cumulative exergy consumption of those systems when compared to the conventional configuration, especially in the Allam configuration. This result can be explained, particularly in the case of the oxyfuel configurations, by enhanced energy conversion processes applied in these scenarios. Meanwhile, the difference in the exergy consumption in the production of crude oil is less pronounced, but still the highest specific CO_2 emissions are attributable to the conventional configuration while the unit exergy cost remains quite similar. Furthermore, oxygen production has similar unit exergy cost in both oxyfuel configurations and nearly double the cost of reboiler duty for post-combustion separation. However, the oxyfuel setups present CO_2 emissions costs very different from one another. This might be a reflection of the S-Graz cycle potential to emit 100 times less CO_2 even in comparison to its oxyfuel counterparts. More detailed information about the physical and thermodynamic properties, as well as the unit exergy costs and specific CO_2 emissions of selected streams for each configuration of offshore platform are shown in Figures A.1 - A.4 and in Tables A.1 - A.4.

Figure 36. Unit exergy costs and specific CO2 emissions of the crude oil and natural gas produced

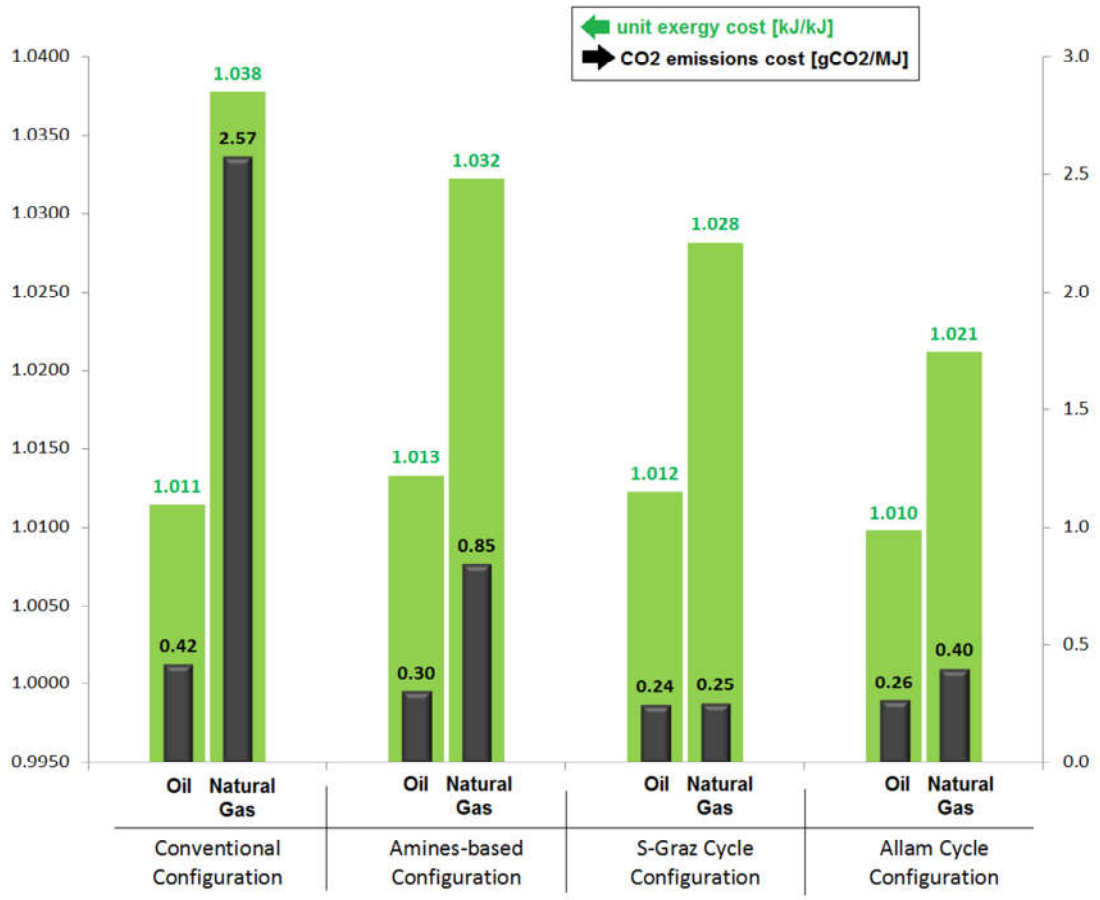

Source: author

7.5 Discussion

In this section, an overall look at the metrics presented so far and discussion of the results are developed. Firstly, a purely energy outlook into power produced and consumed as displayed in Figure 30, shows that in the conventional and post-combustion setups, air compression, natural gas compression and CO_2 compression (incoming from the well) are the most energy intensive processes, in that order. In air-blown combustion, as much as air twenty times (or even more) the amount of fuel needs to be compressed and sent into the combustion chamber to provide enough oxygen and control turbine inlet temperature. That much air requires high values of compression power and explains why air compression is one of the largest energy demands. Natural gas and CO_2 compression deal with large volumes of gas as well

thus also requiring a great deal of power. In the S-Graz cycle case, the first in power demand is the power cycle unit itself revealing that a working fluid composed of over 70% water demands large amounts of power in compression, much larger than Allam's working fluid which is mostly CO_2, even though their flows are comparable. It is also proof of how much equipment the S-Graz power cycle requires. As for the Allam cycle, natural gas compression becomes the greatest demand followed by its power cycle unit, which is still three times lower. This is a good indication of how lean Allam's operation is relative to other vital units and to its oxyfuel counterpart, S-Graz, which consumes five times what Allam does to maintain the power cycle.

Such power dedicated to compress different large gas flows could be an interesting source of heat to other processes elsewhere in the plant. This energy, when recovered, could ultimately result in fuel savings otherwise burnt in an auxiliary boiler in order to meet heating demands. The energy integration analysis depicted in Figure 33 shows the magnitude of the heat transfer and at which temperatures the source and the sink are. Going from Figure 31 (a) through (d) it is possible to notice that the distance between hot and cold curves seem to be decreasing, effectively getting very close in the case of the Allam cycle. One can infer that since the source and sink are closer in temperature, it stands to reason that this possible heat transfer entails lower driving forces and therefore would destroy less exergy if it were to happen. Another way this conclusion can be envisaged is through the transformation of the Temperature axis into a Carnot Factor axis. That way, the exergy destroyed in heat transfer could be calculated much more directly. Although the Allam cycle takes much more advantage of the heat it rejects, when it harvests the heat from oxygen compression to heat up recirculated working fluid, it is not able to meet all heating requirements. Nowhere else in the Allam powered plant there is heat at adequate temperatures to make petroleum separation viable. Therefore, extra fuel must be burnt in an auxiliary boiler; raising Allam's fuel consumption slightly.

Although the energy analyses presented so far are useful, they are not able to quantify the quality of the conversion processes. To understand other bottlenecks that could be troublesome, an exergy analysis must be carried out. The exergy efficiency of the energy conversion processes might be able to shed light into efficiency bottlenecks and ways to solve them. It is expected that the addition of systems to purify and compress CO_2 as well as air separation units for oxyfuel

combustion impact the ability of the system to fulfill its function more efficiently. Unless it is accompanied by an increase in efficiency that compensates the negative effects and that is why the advanced configurations shouldn't be dismissed just yet. When analyzing different definitions of exergy efficiency, helpful insights can be drawn.

For instance, the power efficiency definition conveys the information regarding the capacity of the power plant to transform the chemical exergy of the fuel into net power. To that effect, it is possible to see that the Allam cycle, even though it has to supply power to an air separation unit and a CO_2 compression train, is far more efficient than all the other platform configurations. A clue as to why that might be can be inferred from the working fluid of the cycle which is composed mainly of CO_2 (upwards of 95%) in supercritical state. This fluid composition and properties allow for much lower power demand in compression trains. Moreover, the harvesting of heat from oxygen compression to heat up recycled working fluid avoids further burning of fuel, which keeps the Allam cycle's efficiency up.

The cogeneration efficiency takes into account not only the net power needed to support the processing unit but also its heating requirements, mainly due to petroleum separation. By this metric, the Allam cycle also presents an outstanding performance compared the other layouts, again converting fuel's chemical exergy into power and heat efficiently. Finally, regarding the separation efficiency, it is the only exergy efficiency metric in which the roles are reversed. By this measurement, the conventional configuration is the most efficient setup. This drop in efficiency among the advanced methods reflects the effects of having to separate the combustion products even further, whether it is by attaching a MEA loop or a ASU to the power cycle. Since such extra separation does not occur in the business as usual configuration, its separaton efficiency remains the highest. Among the advanced cycles, the Allam cycle still presents the highest separation efficiency, however still quite lower than the conventional configuration's value.

Another measurement connected to the exergy efficiency is the specific exergy destroyed presented in Figure 33. The Allam cycle appears as the one which destroys the least amount of exergy overall. This result is in accordance with the generally superior performance of the Allam cycle by the exergy efficiency metrics

and its lower consumption of fuel (see Table 5). Interestingly, the S-Graz cycle does not follow as the second configuration to destroy the least amount of exergy, despite being the second most efficient configuration and in fuel consumption. All four platfoms work with the same input, however the output exergy will vary depending on the power cycle layout. Oxyfuel setups recirculate most of the combustion products and therefore present lower exergy values related to output mass flows. Even if said mass flows have higher specific exergy values. Hence, even though the S-Graz cycle exports more natural gas related exergy because it is more efficient, it is not enough to outweigh the effect of partly recycling combustion products. On the other hand, the conventional platform discharges all of its untreated flue gas into the atmosphere, making its $\boldsymbol{B}_{dest} = \boldsymbol{B}_{total,output} - \boldsymbol{B}_{total,input}$ lower than the S-Graz cycle equipped ship. The Allam cycle, on the other hand, is efficient enough to have that effect offset. The one which ranks second lowest specific exergy destroyed is then the conventional configuration. Lastly, a direct correlation can also be drawn from the post combustion equipped platform performance in previous metrics and its specific exergy destroyed. It is expected that the platform with the lowest efficiencies and highest fuel consumption also have the greatest amount of exergy destroyed.

One of these advanced configurations main purposes is to attenuate emissions, particularly carbon dioxide emissions. Accordingly, specific CO_2 emissions values of each platform studied are displayed in Figure 34. The S-Graz cycle has the best performance with 100 to 1000 times lower emission levels than all the other configurations. The burning of fuel in an auxiliary boiler is what prevents the Allam cycle from reaching the same standards as the S-Graz cycle. The post-combustion equipped system also fails to meet S-Graz levels due to the release of purified gas into the atmosphere which still contains some CO_2, though not as much as in the conventional configuration. In Figure 35, an exergy breakdown shows how each subunit contributes to the overall exergy destruction. It is clear that a lot more exergy is destroyed within the power generation unit in all configurations. This makes sense considering the combustion process inevitably destroys at least one fourth of the exergy [116]. The S-Graz cycle seems to be equipped with the most efficient combustion. One reason might be due to its high combustion temperature, consequence of oxyfuel turbine technology. It also extracts more power expanding working fluid to vacuum pressures and having a bottoming steam cycle.

Another large contributor to exergy destruction is the primary separation process, as already mentioned. The multiple heat transfers at large temperature differences are the main causes behind its high rates of exergy destruction. The exergy destroyed allocated to Others can account for the heat exchange network, for instance, and is noticeably very small in the Allam cycle case with the ASU being a much more significant player even though it is not one of the top three most energy intensive units in the Allam equipped platform. Moreover, the air separation and MEA loop are significant contributors to exergy destruction in the carbon capturing plants and can be improved by taking measures such as enlarging heat transfer surface and tweaking of some operational parameters, although these improvements might be limited.

Finally, as expected from looking at the specific CO_2 emissions figures, CO_2 emissions costs are the highest for the conventional layout for both products. Whereas the unit exergy cost is quite similar throughout configurations, with the Allam cycle exhibiting slightly lower values. CO_2 emissions cost of oxygen production are strikingly different from one oxyfuel cycle to another. That might be explained due to the combined factors that CO_2 emissions under the Allam cycle operation, although low, are one hundred times higher than in the S-Graz cycle. And the use of less exergy to produce these Allam's emissions since it is overall more efficient. Furthermore, the amines-based post combustion reboiler duty has CO_2 emissions costs that are more than double the cost of O_2 production in the S-Graz cycle but nearly half the cost to produce oxygen under the Allam cycle. The highest unit exergy cost of net power generation occurs in the conventional configuration and the lowest in the Allam cycle setup. The lower number of products which to attribute costs in the conventional configuration might influence the magnitude of the power costs. Additionally, as the Allam cycle being the most efficient; it will require less fuel exergy to maintain the same facilities, which might also explain the lowest cost value of power.

Overall the work shows that advanced oxyfuel configurations are indeed an alternative to the business as usual way of operating a FPSO unit. The Allam cycle present very high and competitive efficiencies while emitting less CO_2 as its post combustion counterpart. The S-Graz cycle seems to be able to truly achieve near zero emissions, which is drastically lower than works on offshore platforms presented

so far. Nevertheless, some caveats are warranted. These conclusions are coherent as long as the platform functions at this mode of operation and can substantially differ otherwise. Another warning worth mentioning relates to the bigger picture context in which works such as this are immersed into. Although IPCC reports consider CCS and BECCS (bioenergy carbon capture and sequestration) as part of the solution to reach the targets largely agreed upon by the leadership worldwide, several issues surrounding CCS cast doubts and are severely criticized as to whether it is worth it to invest in this path and to which degree. Rockström et al. (2009) [128] proposed nine planetary boundaries (PB) which would limit a safe space for human operation, out of which 3 (rate of biodiversity loss, climate change and nitrogen cycle) have been already exceeded. In 2015, Rockström et al. [129] goes on to include CCS as one of the components of the energy transformation to achieve 80% emissions reduction by 2050 according to their literature review, which they point out is growing but still incomplete. Yet the mitigation achieved with CCS, especially BECCS, which is considered a sink for carbon emissions (negative emissions), seems to create other problems when applied globally. According to Heck et al. [130], although large scale BECCS intends to mitigate the climate change PB, it would most likely steer the pressure towards the limits of freshwater use and transgress on the boundaries for land use, bioshphere integrity and biogeochemical flows.

On another front, civil society has raised valid concerns about the widespread application of CCS techniques which remain largely unpopular [67]. Among the points raised against CCS is timing, given that the technology isn't mature and the latest IPCC report urges for rapid climate change mitigation in the next 10 years to limit average global temperature to 1.5 ºC. Deviation of funds from renewable sources research and deployment is another concern. An option that allows the use of so called "clean" fossil fuel along with the strong political and economic interests that are heavily tied to production of oil and gas has the high potential to generate complacency and prolong the time to reach a truly low carbon solution. It might even stimulate construction of even more fossil fuel based facilities. This would be especially pernicious given the fact that, globally, a third of oil reserves, half of gas reserves and over 80 per cent of current coal reserves should remain unused from 2010 to 2050 in order to meet the target of

2 °C [131]. Besides, CCS related technology costs are still very high and CO_2 storage safety is an unresolved issue. Leakage from underground reservoirs and how responsibility should be placed in case of an accident are debates on progress. And social justice, a concern that permeates all solutions, since under the current system large emitters profit from contributing to climate change but rarely, if ever, are burdened with the consequences [132-136]. Even if some CCS is warranted to reach the targets as some of the cited studies suggest, its employment under neoliberal capitalism does not inspire confidence since the main motivation is to apply what is profitable which not necessarily is what is needed or better for the common wellbeing [137]. Oil and gas companies even acted in delaying effective response to climate change [138]. Gains in efficiency hardly solve the problem since it generally does not result in a more mindful use of a limited resource, but higher exploitation (Jevon's paradox). Since the capitalist system is ever expanding in its goal to accumulate capital, it has no built in breaks short of human extinction. Thus, it drives the rift between human activity and the biosphere rather than repair it [139].

8. Conclusions

Despite of the numerous and well-established onshore generation applications for the oxyfuel process, the use of this technology in offshore platforms has not been pervasively studied. Accordingly, the utilization of a conventional gas turbine system in a FPSO unit is compared to the integration of more advanced cogeneration and carbon capture cycles, such as an S-Graz cycle, a chemical CO_2 absorption unit and Allam cycle, in terms of the exergy and environmental performance. The advanced oxyfuel configurations outperform both the conventional and chemical absorption-based utility systems in terms of the environmental impact, and the power and cogeneration efficiency definitions. In fact, the S-Graz powered platform particularly mitigates nearly all the emissions, while achieving slightly higher power and cogeneration efficiencies than the conventional scenario. As for the scenario in which the platform is equipped with an amine-based post-combustion CCS unit, the energy intensive flue gas purification process demands more fuel to drive the ancillary CCS equipment. Consequently, its performance drops on all fronts and the extent of CO_2 mitigation still falls short in comparison to the oxyfuel powered platforms.

In general, the Allam power cycle presents higher performance in multiple metrics than the other cycles selected, with the added benefit of allowing equipment to be more compact due to the nature of its working fluid and operating pressures. An advantage particularly good for offshore application since the space and weight budgets are tight. Another way to circumvent this issue already under study is the application of centralized power stations (power hubs) that supply power to a cluster of FPSOs operating in the same production field [140-142].

Moreover, as long as other oxygen production methods cannot provide the same level of purity and large throughputs as in the cryogenic distillation process, further improvements can be expected from the use of heat-integrated distillation columns (HIDiC) and other modifications in the operation conditions and layout of the ASUs. Additionally, due to the unavoidable exergy destruction in the combustion processes, lower driving forces associated to narrower temperature differences in the heat recovery network may help reducing the amount of irreversibility in the petroleum production facilities, especially in the utility plant. Furthermore, the use of the exergy concept for rationally allocating the cumulative exergy consumption and the specific

CO_2 emissions among the various intermediate and final products of the platform allowed mapping the largest sources of exergy destruction and the process of the exergy costs formation.

Finally, although CCS might be regarded as a promising and even necessary technique in the transitional period to a decarbonized future [7, 143], many issues concerning these techniques still need to be addressed. Time necessary for proper development, security of carbon storage, public acceptance, and how it might stray investment from renewable energy, thus allowing for extended use of fossil fuels and how it the factors into the already tight global carbon budget are some issues called into question [67, 134, 143]. It is already known that most fossil fuel reserves should remain unexploited if global warming below 2 °C is to be achieved [131]. It follows that carbon capture, if implemented, should be used towards taking out carbon from the already carbon loaded atmosphere, instead of being used to further extract hydrocarbons that will, in turn, require even more effort to mitigate. Substantial gains in efficiency as shown here and in many studies will doubtfully lead to more mindful use of the fossil fuel reserves as long as it is employed under a neoliberal capitalist system. A revolutionary change in the social, economic and political systems is necessary in order for these techniques to be applied in a way that harmonize human activity with the biosphere instead of driving a rift between them [137, 139].

References

1. Figueroa, J.D., Fout, T., Plasynski, S., McIlvried H., Srivastava, R. D., *Advances in CO2 capture technology—The U.S. Department of Energy's Carbon Sequestration Program.* International Journal of Greenhouse Gas Control, 2008(2): p. 9-20.
2. IPCC, *Climate Change 2014: Mitigation of Climate Change*, in *Working Group III Contribution to the Fifth Assessment Report of the Intergovernmental Panel on Climate Change*. 2014, UN. p. 1454.
3. IPCC, *Global Warming of 1.5°C. An IPCC Special Report on the impacts of global warming of 1.5°C above pre-industrial levels and related global greenhouse gas emission pathways, in the context of strengthening the global response to the threat of climate change, sustainable development, and efforts to eradicate poverty*. 2018.
4. UNEP, *The Emissions Gap Report 2018*. 2018, United Nations: Nairobi.
5. Hannah Ritchie; Max Roser. *CO2 and other Greenhouse Gas Emissions*. 2017 [cited 2019 January 12]; Available from: https://ourworldindata.org/co2-and-other-greenhouse-gas-emissions.
6. IEA, *Energy and Climate Change, World Energy Outlook Special Report*. 2015, International Energy Agency. p. 1-200.
7. Zappa, W., Junginger, M., van den Broek, M., *Is a 100% renewable European power system feasible by 2050?* Applied Energy, 2019. **233-234**: p. 1027-1050.
8. Leung, D.Y.C., Caramanna, G., Mercedes Maroto-Valer, M. , *An overview of current status of carbon dioxide capture and storage technologies.* Renewable and Sustainable Energy Reviews, 2014. **39**: p. 426-443.
9. IEA, *World Energy Outlook - Outlook for Natural Gas*. 2017, International Energy Agency. p. 450.
10. Boait, P., Advani, V., Gammon, R., *Estimation of demand diversity and daily demand profile for off-grid electrification in developing countries.* Energy for Sustainable Development, 2015. **29**: p. 135-141.
11. Zhang, Q., Li, H., Mclellan, B., *An Integrated Scenario Analysis for Future Zero-Carbon Energy System.* Energy Procedia, 2014. **61**: p. 2801-2804.
12. Florez-Orrego, D., Nascimento Silva, F., Oliveira Jr., S. *Syngas Production with Thermo-Chemically Recuperated Gas Turbine Systems: An Exergy Analysis and Energy Integration Study*. in *31th International Conference on Efficiency, Cost, Optimization, Simulation and Environmental Impact of Energy Systems - ECOS 2018*. 2018. Guimaraes, Portugal: University of Minho.
13. Nagy, T., Koczka, K., Haáz E., Tóth, A.J., Rácz, L., Mizsey, P., *Efficiency Improvement of CO2 Capture.* Periodica Polytechnica Chemical Engineering, 2016: p. 51-58.
14. Yi Zhao, Y.S., Guoyi Ma, Rongjie Hao, *Adsorption Separation of Carbon Dioxide from Flue Gas by a Molecularly Imprinted Adsorbent.* Environmental Science & Technology, 2014. **48**(3): p. 1601-1608.
15. Ewa Knapik; Piotr Kosowski; Jerzy Stopa, *Cryogenic liquefaction and separation of CO2 using nitrogen removal unit cold energy.* Chemical Engineering Research and Design, 2018. **131**: p. 66-79.
16. Stephanie Burt; Andrew Baxter; Larry Baxter; Sustainable Energy Solutions, *Cryogenic CO2 Capture to Control Climate Change Emissions*. 2009: Sustainable ES Clearwater web page.
17. Gibbins, J., Chalmers, H., *Carbon capture and storage.* Energy Policy, 2008. **36**(12): p. 4317-4322.
18. IEAGHG, *CO2 Capture As a Factor in Power Station Investment*. 2006: IEA Greenhouse Gas R&D Programme.
19. Heitmeir, F., Sanz, W., Jericha, H., *1.3.1.1. Graz Cycle – a Zero Emission Power Plant of Highest Efficiency, in The Gas Turbine Handbook*, U.D.E. Office, Editor. 2006, National Energy Technology Laboratory.

20. Allam et al., *High efficiency and low cost of electricity generation from fossil fuels while eliminating atmospheric emissions, including carbon dioxide.* Energy Procedia, 2013. **37**: p. 1135-1149.
21. Anderson, R.E., MacAdam, S., Viteri, F., Davies, D.O., Downs, J.P., Paliszewski, A. *Adapting gas turbines to zero emission oxy-fuel power plants*. in *ASME Turbo Expo 2*. 2008.
22. Stanger et al, *Oxyfuel combustion for CO2 capture in power plants.* International Journal of Greenhouse Gas Control, 2015. **40**: p. 55-125.
23. Devanna, L., *Advanced Turbine Developments for Oxy-Combustion TriGenTM Plants*. 2012, CES Inc.: Rancho Cordova, CA.
24. SINTEF Energi A/S, *Oxyfuel feasibility project*. 2014.
25. Simpson, A., Lutz, A., *Exergy analysis of hydrogen production via steam methane reforming.* International Journal of Hydrogen Energy, 2007. **32**(18): p. 4811-4820.
26. Fu Chao; Truls Gundersen, *Thermodynamic Analysis of an Oxy-Combustion Process for Coal-Fired Power Plants with CO2 Capture*. 2010.
27. Jie Xiong; Haibo Zhao; Meng Chen; Chuguang Zheng, *Simulation and Exergy Analysis of a 600 MWe Oxy-Combustion Pulverized Coal-Fired Power Plant*. 2016: Cleaner Combustion and Sustainable World.
28. Kristin Jordal; Rahul Anantharaman; Øyvind Langorgen, *Novel oxy-combustion gas turbine concepts for off-shore application*, in *International CCS Research Centre*. 2013.
29. Equinor ASA. *Sleipner area*. [cited 2020 July 20th]; Available from: https://www.equinor.com/en/what-we-do/norwegian-continental-shelf-platforms/sleipner.html.
30. R.A.Chadwick, *Offshore CO2 storage: Sleipner natural gas field beneath the North Sea*, in *Geological Storage of Carbon Dioxide (CO2)*. 2013. p. 227-250.
31. Anne-Kari Furre; Ola Eiken; Håvard Alnes; Jonas Nesland Vevatne; Anders Fredrik Kiær, *20 years of monitoring CO2-injection at Sleipner.* Energy Procedia 2017. **114** (13th International Conference on Greenhouse Gas Control Technologies): p. 3916 – 3926
32. R. Chadwock et. al, *Geological reservoir characterization of a CO2 storage site: The Utsira Sand, Sleipner, Northern North Sea.* Energy, 2004. **29**: p. 1371-1381.
33. Nguyen, T.V., Voldsund, M., Breuhaus, P., Elmegaard, B., *Energy efficiency measures for offshore oil and gas platforms.* Energy, 2016. **117**: p. 325-340.
34. Carranza-Sánchez, Y., Oliveira Jr, S., *Exergy analysis of offshore primary petroleum processing plant with CO2 capture.* Energy, 2015. **88**: p. 46-56.
35. Carranza-Sánchez, Y.A., Oliveira Junior, S., da Silva, J.A.M., Nguyen, T.V. *Energy and exergy performance of three FPSO operational modes*. in *Proceedings of the 23rd ABCM International Congress of Mechanical Engineering*. 2015.
36. Luca Riboldi; Lars O.Nord, *Concepts for lifetime efficient supply of power and heat to offshore installations in the North Sea.* Energy Conversion and Management, 2017. **148**: p. 860-875.
37. IEA. *Not on track*. 2019 [cited 2019 February 6]; Available from: https://www.iea.org/tcep/power/ccs/.
38. Petrobras. *Plano de Negócios e Gestão 2019-2023*. 2019.
39. Petrobras. *Vamos operar o quarto sistema de separação e reinjeção de gás carbônico no pré-sal*. Fatos e Dados 2016 [cited 2019 August 15th].
40. PETROBRAS. *Tipos de Platafromas*. 2014 [cited 2019 March 15]; Available from: http://www.petrobras.com.br/infograficos/tipos-de-plataformas/desktop/index.html.
41. PETROBRAS. *Fatos e dados: entenda por que investimos em fertilizantes [In Portuguese]*. 2014 14-12-2014]; Available from: http://www.petrobras.com.br/fatos-e-dados/entenda-por-que-investimos-em-fertilizantes.htm.
42. PETROBRAS. *P-51 – Construção e Montagem*. 2014 [cited 2019 March 23]; Available from: https://www.youtube.com/watch?v=jmrjv436-ml.

43. Carranza-Sanchéz, Y.O.J., S.;. *Assessment of the exergy performance of a floating, production, storage and offloading (FPSO) unit: Influence of three operational modes*. in *EFFICIENCY, COST, OPTIMIZATION, SIMULATION AND ENVIRONMENTAL IMPACT OF ENERGY SYSTEMS*. 2015. France.
44. D'aloia, F.A., *Análise exergética de sistemas de compressão de gás em plataformas offshore de produção de petróleo*, in *Mechanical Engineering*. 2017, University of São Paulo: São Paulo.
45. Forum Energy Technologies. 2014 [cited 2019 February 14]; Available from: https://www.youtube.com/watch?v=AUJQBb6OpuI&list=PLO4ODcscbp0AlTE3FnLNOQ2SEra36mHnF.
46. Conselho Nacional do Meio Ambiente, *Resolução CONAMA nº 393/07*, CONAMA, Editor. 2007, Ministério do Meio Ambiente: Diário Oficial da União. p. 72-73.
47. Sampaio, J.A., Oliveira, G.P., da Silva, A.O., *ENSAIOS DE CLASSIFICAÇÃO EM HIDROCICLONE*, in *Tratamento de Minérios: Práticas Laboratoriais*.
48. Makagon, Y.F., *Natural gas hydrates – A promising source of energy.* Journal of Natural Gas Science and Engineering, 2010. **2**(1): p. 49-59.
49. IEAGHG, *Oxy-combustion Turbine Power Plants*. 2015.
50. Hanne M. Kvamsdal, K.J., Olav Bolland, *A quantitative comparison of gas turbine cycles with CO2 capture.* Energy, 2007. **32**(1): p. 10-24.
51. Allam et al., *SYSTEMAND METHOD FOR HIGH EFFICIENCY POWER GENERATION USING A CARBON DIOXDE CIRCULATING WORKING FLUID*. 2011, Palmer Labs, LLC.
52. Fernando Climent Barba; Guillermo Martínez-Denegri; Blanca Soler Segui; Edward Anthony, *A Technical Evaluation, Performance Analysis and Risk Assessment of Multiple Novel Oxy-Turbine Lower Cycles with Complete CO2 Capture.* Journal of Cleaner Production, 2016.
53. Allam et al., *Demonstration of the Allam Cycle: An update on the development status of a high efficiency supercritical carbon dioxide power process employing full carbon capture.* Energy Procedia, 2017. **114**: p. 5948-5966.
54. Sanz, W., Jericha, H., Luckel, F., Göttlich, E., Heitmeir, F. *A FURTHER STEP TOWARDS A GRAZ CYCLE POWER PLANT FOR CO2 CAPTURE*. in *ASME Turbo Expo 2005: Power for Land, Sea and Air*. 2005. Reno-Tahoe, Nevada, USA.
55. IEAGHG, *Post-Combustion CO2 Capture Scale-up Study*. 2013.
56. Carbon Capture and Sequestration Technology MIT. *Kimberlina Fact Sheet: Carbon Dioxide Capture and Storage Project* 2016 [cited 2019 August 22nd].
57. Proske, K.L. *Carbon-Negative Energy and Renewable Hydrogen Projects: An Opportunity for California*. 2019 [cited 2021 February 19]; Presentation].
58. NET POWER. *DEVELOPMENT STATUS*. 2018 [cited 2020; Available from: https://www.netpower.com/technology/#eor.
59. Rengarajan Soundararajan; Rahul Anantharaman; Truls Gundersen, *Design of Steam Cycles for Oxy-combustion Coal based Power Plants with Emphasis on Heat Integration.* Energy Procedia, 2014. **51**: p. 119-126.
60. Jericha, H., Göttlich, E. *CONCEPTUAL DESIGN FOR AN INDUSTRIAL PROTOTYPE GRAZ CYCLE POWER PLANT*. in *ASME TURBO EXPO 2002*. 2002. Amsterdam.
61. NET POWER., *NET Power Achieves Major Milestone for Carbon Capture with Demonstration Plant First Fire*, in *The Company Is Now Operating Its Low-Cost, Emissions-Free Natural Gas Power System*. 2018.
62. Jericha, H., *EFFICIENT STEAM CYCLES WITH INTERNAL COMBUSTION OF HYDROGEN AND TOICHIOMETRIC OXYGEN FOR TURBINES AND PISTON ENGINES.* International Journal Hydrogen Energy, 1985. **12**(5): p. 345-354.
63. Aoki S.; Uematsu K.; Suenaga K.; Mori H.; Sugishita H. *A Study of Hydrogen Combustion Turbines*. in *ASME 1998 International Gas Turbine and Aeroengine Congress and Exhibition* 1998. Stockholm.

64. W. Sanz; Carl-W. Hustad; H. Jericha. *FIRST GENERATION GRAZ CYCLE POWER PLANT FOR NEAR-TERM DEPLOYMENT*. in *ASME Turbo Expo 2011*. 2011. Vancouver, Canada.
65. Franz Heitmeir; Wolfgang Sanz; Emil Göttlich; Herbert Jericha. *The Graz Cycle – a Zero Emission Power Plant of Highest Efficiency*. in *XXXV Kraftwerkstechnisches Kolloquium*. 2003. Dresden.
66. EEA, *Trends and projections in the EU ETS in 2017 - The EU Emissions Trading System in numbers*. 2017, European Environmental Agency.
67. Kevin P.F.Broecks; Sandervan Egmond; Frank J.van Rijnsoever; Marlies Verlinde-van den Berg; Marko P.Hekkert, *Persuasiveness, importance and novelty of arguments about Carbon Capture and Storage.* Environmental Science & Policy, 2016. **59**: p. 58-66.
68. Jericha, H., Sanz, W. , Göttlich, E. *DESIGN CONCEPT FOR LARGE OUTPUT GRAZ CYCLE GAS TURBINES*. in *ASME Turbo Expo 2006: Power for Land, Sea and Air*. 2006. Barcelona, Spain.
69. Herbert Jericha; Wolfgang Sanz; Emil Göttlich; Fritz Neumayer. *Design Details of a 600 MW Graz Cycle Thermal Power Plant for CO2 Capture*. in *ASME Turbo Expo 2008*. 2008. Berlin, Germany.
70. W. Sanz; M. Mayr; H. Jericha. *THERMODYNAMIC AND ECONOMIC EVALUATION OF AN IGCC PLANT BASED ON THE GRAZ CYCLE FOR CO2 CAPTURE*. in *ASME Turbo Expo 2010*. 2010. Glasgow, UK.
71. Wolfgang Sanz; Martin Braun; Herbert Jericha; Max F. Platzer, *Adapting the zero-emission Graz Cycle for hydrogen combustion and investigation of its part load behavior.* International Journal Hydrogen Energy, 2018. **43**: p. 5737-5746.
72. Allam et al., *SYSTEMAND METHOD FOR HIGH EFFICIENCY POWER GENERATION USING A CARBON DIOXDE CIRCULATING WORKING FLUID*. 2013, 8 RIVERS CAPITAL, LLC, Durham, NC (US); PALMER LABS, LLC, Durham, NC (US).
73. Penkuhn, M., Tsatsaronis, G., *Exergy Analysis of the Allam Cycle*, in *The 5th International Symposium – Supercritical CO2 Power Cycles*. 2016: San Antonio, Texas.
74. Rodney Allam, S.M., Brock Forrest, Jeremy Fetvedt, Xijia Lu, David Freed, G. William Brown Jr., Takashi Sasaki, Masao Itoh, James Manning, *Demonstration of the Allam Cycle: An update on the development status of a high efficiency supercritical carbon dioxide power process employing full carbon capture.* Energy Procedia, 2017. **114**: p. 5948-5966.
75. Smith, R., *Chemical Process: Design and Integration*. 2005, Manchester: Wiley and Sons.
76. Fan Wu, M.D.A., Paul A. Dellenback, Maohong Fan, *Progress in O2separation for oxy-fuel combustionA promising way forcost-effective CO2capture: A review.* Progress in Energy and Combustion Science, 2018. **67**: p. 188-205.
77. van der Ham, L.V., J. Gross, and S. Kjelstrup, *Two performance indicators for the characterization of the entropy production in a process unit.* Energy, 2011. **36**(6): p. 3727-3732.
78. Fu, C., Gundersen, T., *Using exergy analysis to reduce power consumption in air separation units for oxy-combustion processes.* Energy, 2012. **44**: p. 60-68.
79. Cornelissen, R., Hirs, G., *The value of the exergetic Life Cycle Assessment besides the LCA.* Energy Conversion and Management, 2002. **43**: p. 1417-1424.
80. Beysel, G. *Enhanced Cryogenic Air Separation: A proven Process applied to Oxyfuel. The Linde Group.* in *1st Oxyfuel Combustion Conference*. 2009. Cottbus.
81. A.R. Smith; J. Klosek, *A review of air separation technologies and their integration with energy conversion processes.* Fuel Processing Technology, 2001. **70**: p. 115-134.
82. Ham, L.v.d., *Improving the Second law efficiency of a cryogenic air separation unit*, in *Department of Chemistry*. 2011, Norwegian University of Science and Technology.

83. Kotas, T., *The exergy method of thermal planta analysis*. 2 ed. 1995, Malabar, Florida: Krieger Publishing Company.
84. The Linde Group. *Air separation plants - History and technological progress in the course of time*. 2017.
85. SM CHear. *Continuous Distillation - McCabe-Thiele method*. 2000 [cited 2018 October 29th]; Available from: http://www.separationprocesses.com/Distillation/DT_Chp04g.htm.
86. Arne Dugstad, M.H., Bjørn Morland, *Testing of CO2 specifications with respect to corrosion and bulk phase reactions.* Energy Procedia, 2014. **63**: p. 2547-2556.
87. NETL, *Cost and Performance Baseline for Fossil Energy Plants - Volume 2: Coal to Synthetic Natural Gas and Ammonia. DOE/NETL-2010/1402*, N.E.T.L. (NETL), Editor. 2011.
88. Zeina Abbas, T.M., Mohammad R.M.Abu-Zahra, *CO2 purification. Part I: Purification requirement review and the selection of impurities deep removal technologies.* International Journal of Greenhouse Gas Control, 2013. **16**: p. 324-334.
89. Oliveira Júnior, S., Van Hombeeck, M., *Exergy analysis of petroleum separation processes in offshore platforms.* Energy Conversion and Management, 1997. **38**(15-17): p. 1577-1584.
90. Pal Kloster, *Reduction of Emissions to Air Through Energy Optimisation on Offshore Installations*, in *SPE International Conference on Health, Safety and Environment in Oil and Gas Exploration and Production*. 2000: Stavanger, Norway.
91. Mari Voldsund; Ivar Ståle Ertesvåg; Wei He; Signe Kjelstrup, *Exergy analysis of the oil and gas processing on a North Sea oil platform a real production day.* Energy, 2013. **55**: p. 716-727.
92. Mari Voldsund; Tuong-Van Nguyen; Brian Elmegaard; Ivar S.Ertesvåg; Audun Røsjorde; Knut Jøssang; Signe Kjelstrup, *Exergy destruction and losses on four North Sea offshore platforms: A comparative study of the oil and gas processing plants.* Energy, 2014. **74**: p. 45-58.
93. Rodrigo Dias, *Exergoeconomic Analysis of a Cogeneration Plant on a Brazilian Pre-Salt FPSO Considering Different Fuel Gas Compositions*, in *CILAMCE 2015*. 2015: Rio de Janeiro.
94. Marit Jagtøyen Mazzetti; Petter Nekså; Harald Taxt Walnum; Anne Karin T. Hemmingsen, *Energy-Efficient Technologies for Reduction of Offshore CO2 Emmissions*, in *Offshore Technology Conference*. 2013: Houston.
95. L. Pierobon; A. Benato; E. Scolari; F.Haglind; A.Stoppato, *Waste heat recovery technologies for offshore platforms.* Applied Energy, 2014. **136**: p. 228-241.
96. Tuong-Van Nguyen; Laurence Tock; Peter Breuhaus; François Maréchal; Brian Elmegaard, *CO2-mitigation options for the offshore oil and gas sector.* Applied Energy, 2016. **161**: p. 673-694.
97. Tuong-Van Nguyen; Mari Voldsund; Brian Elmegaard; Ivar Ståle Ertesvåg; Signe Kjelstrup, *On the definition of exergy efficiencies for petroleum systems: Application to offshore oil and gas processing.* Energy, 2014. **73**: p. 264-281.
98. Luca Riboldi; Lars O. Nord, *Lifetime Assessment of Combined Cycles for Cogeneration of Power and Heat in Offshore Oil and Gas Installations.* Energies, 2017.
99. Tuong-Van Nguyen; Tamás Gábor Fülöp; Peter Breuhaus; Brian Elmegaard, *Life performance of oil and gas platforms: Site integration and thermodynamic evaluation.* Energy, 2014. **73**: p. 282-301.
100. da Silva, J.A.M., Oliveira Junior, S.,, *Unit exergy cost and CO2 emissions of offshore petroleum production.* Energy, 2018. **147**: p. 757-766.
101. Dincer, I., Cengel, Y. A.,, *Energy, Entropy and Exergy Concepts and Their Roles in Thermal Engineering.* Entropy, 2001: p. 116-149.
102. de Oliveira Jr, S., *Exergy Analysis of Energy Conversion Processes Course*. 2019.
103. Ortiz, P.A.S., Flórez-Orrego, D. A., *Exergia - Conceituação e Aplicação*. 2013, Escola Politécnica da Universidade de São Paulo: Academia web site.

104. Szargut, J., Morris, D, Steward, F, *Exergy analysis of thermal, chemical, and metallurgical processes*. 1988, New York: Hemisphere Publishing Corporation.
105. RIVERO, R.R., C.; MONROY, L.,, *The exergy of crude oil mixtures and petroleum fractions: calculation and application.* International Journal of applied thermodynamics, 1999. **2**(3): p. 116-123.
106. Linnhoff, B., Hindmarsh, E., *The pinch design method for heat exchanger networks.* Chemical Engineering Science, 1983. **38**(5): p. 745-763.
107. Linnhoff, B., Flower, J., *Synthesis of heat exchanger networks: I. Systematic generation of energy optimal networks.* AIChE Journal, 1978. **24**(4): p. 633-642.
108. Flórez-Orrego, D.A., *Process Sysnthesis and Optimization of Syngas and Ammonia Production in Nitrogen Fertilizers Complexes: Exergy, Energy and CO2 Emissions Assessment*, in *Mechanical Engineering*. 2018, University of São Paulo: São Paulo.
109. Linnhoff, B., *Introduction to Pinch Technology*. 1998. p. 63.
110. Silva, J.A.M., Flórez-Orrego, D., Oliveira Jr, S., *An exergy based approach to determine production cost and CO2 allocation for petroleum derived fuels.* Energy, 2014. **67**(0): p. 490-495.
111. Oliveira Jr., S., *Exergy: Production, Cost and Renewability*. 2013, Sao Paulo: Springer.
112. Silva, J.A.M., Oliveira, Jr., S., Pulgarin, J., Velasquez, H., Molina, A., *On the exergy determination for petroleum fractions and separation processes efficiency.* Heat Transf. Eng, 2015. **36**(11): p. 974-983.
113. Silva, J.A.M., *Exergoenvironmental Performance of Petroleum Processing [In Portuguese]*. 2017: Novas Edicoes Academicas.
114. Nakashima, C., Oliveira Jr, S., Caetano, E. F, *Subsea multiphase pumping system x gas lift: an exergo-economic comparison.* Thermal Engineering, 2004. **3**: p. 1676-1790.
115. Flórez-Orrego, D., Silva, J. A. M., Oliveira Jr, S., *Exergy and environmental comparison of the end use of vehicle fuels: The Brazilian case.* Energy Conversion and Management, 2015. **100**: p. 220-231.
116. Flórez-Orrego, D., *Comparação Termodinâmica e Ambiental (Emissões de CO2) das Rotas de Produção e Utilização de Combustíveis Veiculares Derivados de Petróleo e Gás Natural, Biocombustíveis, Hidrogênio e Eletricidade (Veículos Elétricos) [In Portuguese]*, in *Department of Mechanical Engineering*. 2014, University of São Paulo: São Paulo. p. 229.
117. Flórez-Orrego, D., Oliveira Jr, S. *On the Allocation of the Exergy Costs and CO2 Emission Cost for an Integrated Syngas and Ammonia Production Plant*. in *28th International Conference on Efficiency, Cost, Optimization, Simulation and Environmental Impact of Energy Systems, ECOS 2015*. 2015. Pau, France.
118. Flórez-Orrego, D., Silva, J.A.M., Velásquez, H., Oliveira Jr., S., *Renewable and non-renewable exergy costs and CO2 emissions in the production of fuels for Brazilian transportation sector.* Energy, 2015.
119. Abdollahi-Demneh, F., Moosavian, M., Omidkhah, M., Bahmanyar, H., *Calculating exergy in flowsheeting simulators: A HYSYS implementation.* Energy, 2011. **36**(8): p. 5320-5327.
120. Beck, B., Cunha, P., Ketzer, M., Machado, H., Rocha, Paulo S., Zancan, F., de Almeida, A. Pinheiro, D., *The current status of CCS development in Brazil.* Energy Procedia, 2011. **4**: p. 6148-6151.
121. Barbosa, Y.M., da Silva, J.A.M., de Oliveira, S., Torres, E.A., *Performance assessment of primary petroleum production cogeneration plants.* Energy, 2018. **160**: p. 233-244.
122. Silva, J.A.M., Oliveira Junior, S., *Unit exergy cost and CO2 emissions of offshore petroleum production.* Energy, 2018. **147**: p. 757-766.
123. Baker, R., Lokhandwala, K., *Natural Gas Processing with Membranes: An Overview.* Industrial & Engineering Chemistry Research, 2008. **47**(7): p. 2109-2121.

124. Agrawal, R., Herron, D., *Air Liquefaction: Destillation, in Encyclopedia of Separation Science*, ed. P. I. Wilson, C., Cooke, M. 2000: Academic Press.
125. National Energy Technology Laboratory., *QUALITY GUIDELINES FOR ENERGY SYSTEM STUDIES - CO2 Impurity Design Parameters*, US Department of Energy., Editor. 2012, Office of Program Planning and Analysis.
126. Suphanit, B., *Design of internally heat-integrated distillation column (HIDiC): Uniform heat transfer area versus uniform heat distribution.* Energy, 2010. **35**(3): p. 1505-1514.
127. Dunbar, W.R., Lior, N., *Sources of combustion irreversibility.* Combustion Science and Technology, 1994. **103**(1-6): p. 41-61.
128. Johan Rockström, *A safe operating space for humanity.* Nature, 2009. **461**: p. 472-475.
129. Johan Rockström; Jeffrey D. Sachs; Marcus C. Öhman; Guido Schmidt-Traub, *Sustainable Development and Planetary Boundaries - BACKGROUND RESEARCH PAPER*. 2015.
130. Heck, V., Gerten, D., Lucht, W. and Popp, A., *Biomass-based negative emissions difficult to reconcile with planetary boundaries.* Nature Climate Changae, 2018. **8**: p. 151-155.
131. McGlade, C., Ekins, P., *The geographical distribution of fossil fuels unused when limiting global warming to 2 °C.* Nature, 2015. **517**: p. 187–190.
132. Tess Riley, *Just 100 companies responsible for 71% of global emissions, study says*, in *The Guardian*. 2017, The Guardian web site.
133. CBS News. *Big oil asks government to protect its Texas facilities from climate change*. 2018; Available from: https://www.cbsnews.com/news/texas-protect-oil-facilities-from-climate-change-coastal-spine/.
134. NOAH Friends of the Earth Denmark., *10 arguments against CCS*: NOAH Friends of the Earth Denmark webpage.
135. Cordes et al., *Environmental Impacts of the Deep-Water Oil and Gas Industry: A Review to Guide Management Strategies.* Frontiers in Environmental Science, 2016.
136. Fuss et al., *Betting on negative emissions.* Nature Climate Changae, 2014. **4**: p. 850-853.
137. Jonathan T. Park; University of Utah, *Climate Change and Capitalism.* The Journal of Sustainable Development, 2015. **14**(2): p. 189-206.
138. Benjamin, F., *Shell and Exxon's secret 1980s climate change warnings*, in *The Guardian*. 2018.
139. Clark, B., York, R., *Carbon metabolism: Global capitalism, climatechange, and the biospheric rift.* Theory and Society, 2005. **34**: p. 391-428.
140. Freire, R., De Oliveira Junior, S.,. *Lifetime Exergy Analysis of Electricity and Hot Water Production Systems in Offshore Projects with Multiple Platforms*. in *ENCIT*. 2018. Águas de Lindóia, SP, Brazil.
141. Florez-Orrego D, F.R., Silva JAM, Albuquerque Neto C, Oliveira Junior S. *Centralized power generation with carbon capture on decommissioned offshore petroleum platforms*. in *International Conference On Efficiency, Cost, Optimization, Simulation And Environmental Impact Of Energy Systems*. 2020. Osaka, Japan.
142. Freire, R., Florez-Orrego, D., Silva, J., Albuquerque Neto, C., Oliveira Junior, S. *Optimizing the power hub in multi-platform offshore oil and gas production development projects*. in *International Conference On Efficiency, Cost, Optimization, Simulation And Environmental Impact Of Energy Systems*. 2020. Osaka, Japan.
143. Biello, D., *Can Carbon Capture Technology Be Part of the Climate Solution?*, in *Yale Environment 360*. 2014, Yale Environment 360 webpage: Yale School of Forestry & Environmental Studies.

APPENDIX A

Figure A.1. Unit exergy costs and specific CO_2 emissions of the crude oil and natural gas produced

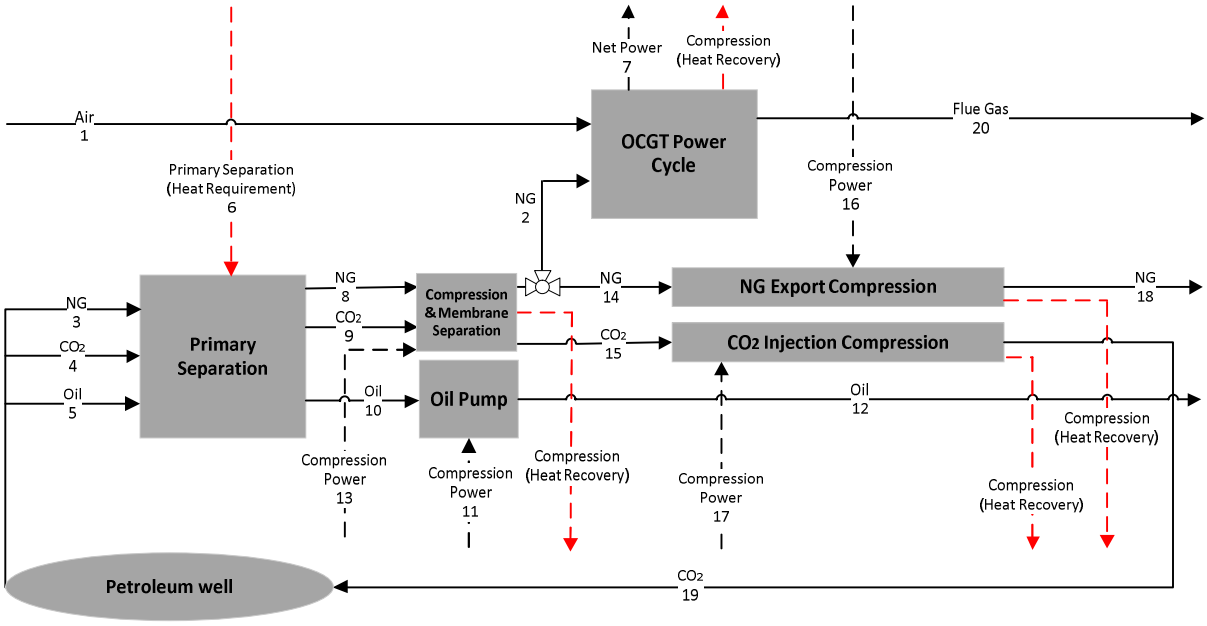

Source: author

Table A.1. Conventional Offshore platform configuration. Thermodynamic properties and exergy cost of selected streams in Fig A.1

N°	Name	T (°C)	P (kPa)	m (kg/s)	B_T (kW)	c (kJ/kJ)	c_{CO2} (g_{CO2}/MJ)
1	Combustion air	25	101	63.0	0.0	1.0000	0.00
2	Natural gas (fuel)	38	4,800	1.6	78,572	1.0235	1.38
3	Natural gas (well)	40	1,500	28.0	1,349,493	1.0083	0.32
4	CO_2 (well)	40	1,500	8.2	63,442	1.0083	0.32
5	Oil (well)	40	1,500	161.0	7,211,029	1.0083	0.32
6	Primary separation (Heating requirement)	150	–	–	1,985	12.5183	360.42
7	**Net power (to compression systems)**	–	–	–	1,9739	3.3538	219.61
8	NG to compression & membrane	40	1,500	28.0	1,349,493	1.0112	0.40

9	CO_2 to compression & membrane	40	1,500	8.2	61,856	1.0112	0.40
10	Oil to pump	60	1,500	161.0	7,211,029	1.0112	0.40
11	Oil pump power	–	–	–	447	3.3538	219.61
12	**Oil export to shore**	60	2,300	161.0	7,211,029	1.0114	0.42
13	Gas compression power	–	–	–	8,039	3.3538	219.61
14	Methane-rich exported natural gas	38	4,800	26.4	1,276,307	1.0235	1.38
15	CO_2 rich-permeate	38	300	8.2	60,975	1.0235	1.38
16	NG export compression power	–	–	–	7,793	3.3538	219.61
17	CO_2 compression power to injection	–	–	–	3,458	3.3538	219.61
18	**Natural gas export**	113	24,500	26.4	1,281,524	1.0377	2.57
19	CO_2 (from well) to injection	130	45,000	8.2	63,442	1.1332	11.11
20	Flue gas	300	300	64.7	11,753	0.0000	0.00

Figure A.2. Offshore platform configuration with a chemical absorption carbon capture unit. Unit exergy cost and specific CO_2 emissions calculation scheme

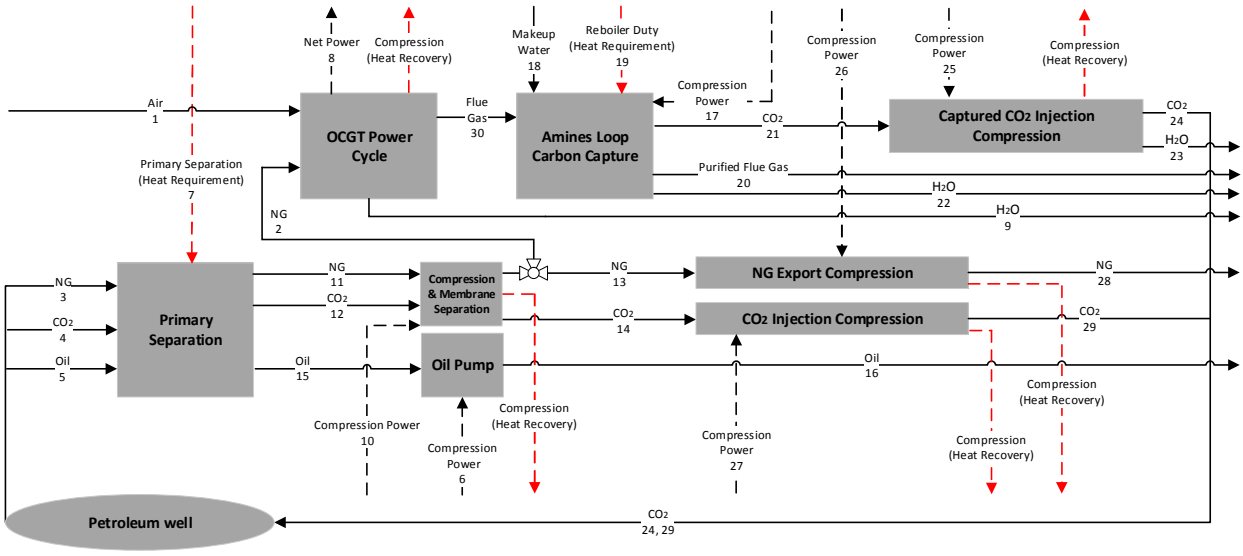

Source: author

Table A.2. Offshore platform configuration with a chemical absorption carbon capture unit. Thermodynamic properties and exergy cost of selected streams in the Fig A.2

N°	Name	T (°C)	P (kPa)	m (kg/s)	B^T (kW)	c (kJ/kJ)	c_{CO2} (g_{CO2}/MJ)
1	Combustion air	25	101	67.8	0	1.0000	0.00
2	Natural gas (fuel)	38	4,800	1.7	84,490	1.0221	0.54
3	Natural gas (well)	40	1,500	28.0	1,349,493	1.0108	0.28
4	CO_2 (well)	40	1,500	8.2	61,856	1.0108	0.28
5	Oil (well)	40	1,500	161.0	7,211,029	1.0108	0.28
6	Oil pump power	–	–	–	447	2.6014	56.10
7	Primary Separation (Heating requirement)	150	–	–	1,985	9.9620	58.15
8	**Net power (to compression systems)**	–	–	–	21,231	2.6014	56.10
9	Waste water	40	300	2.6	133	0.0000	0.00
10	Gas compression power	–	–	–	8,039	2.6014	56.10
11	Natural gas to compression & membrane	40	1,500	28.0	1,349,493	1.0131	0.29
12	CO_2 to compression & membrane	40	1,500	8.2	61,856	1.0131	0.29
13	Methane-rich exported natural gas	38	4,800	26.3	1,270,456	1.0221	0.54
14	CO_2 rich-permeate	38	300	8.2	60,975	1.0221	0.54
15	Oil to pump	60	1,500	161.0	7,211,029	1.0131	0.29
16	**Oil export to shore**	60	2,300	161.0	7,211,029	1.0133	0.30
17	Amine loop power consumption	–	–	–	30	2.6014	56.10
18	Makeup water	25	130	1.0	49	1.0000	0.00
19	**Reboiler duty (Heating requirement)**	104	–	–	3,566	9.9620	58.15
20	Purified flue gas	30	300	63.0	5,987	0.0000	0.00
21	Captured CO_2 to compression	42	100	3.6	1,488	13.9292	69.36
22	Waste water	42	100	1.4	71	0.0000	0.00
23	Waste water	40	multiple	1.2	30	0.0000	0.00
24	Captured CO_2 to injection	90	45,000	3.4	2,439	9.6762	67.31
25	Captured CO_2 injection	–	–	–	1,495	2.6014	56.10

	compression power						
26	NG export compression power	–	–	–	7,756	2.6014	56.10
27	CO_2 (well) to injection compression power	–	–	–	3,458	2.6014	56.10
28	**Natural gas export**	113	24,500	26.3	1,275,577	1.0322	0.85
29	CO_2 (from well) to injection	130	45,000	8.2	63,442	1.0983	3.02
30	Flue gas	40	300	66.9	6,925	1.0220	0.54

Figure A.3. Offshore platform configuration integrated to an S-Graz power cycle. Unit exergy cost and specific CO_2 emissions calculation scheme

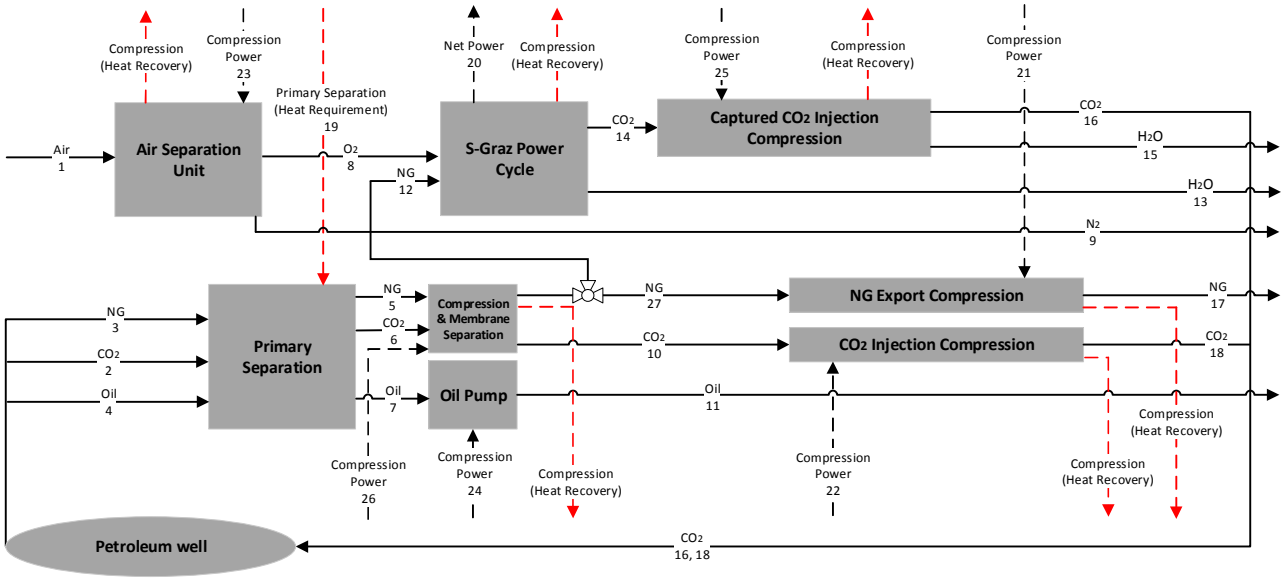

Source: author

Table A.3. Offshore platform configuration integrated to an S-Graz power cycle. Thermodynamic properties and exergy cost of selected streams in the Fig A.3

N°	Name	T (°C)	P (kPa)	m (kg/s)	B^T (kW)	c (kJ/kJ)	c_{CO2} (g_{CO2}/MJ)
1	Combustion air	25	101	31.4	0	1.0000	0.00
2	CO_2 (well)	40	1,500	8.2	61,856	1.0084	0.24
3	Natural gas (well)	40	1,500	28.0	1,349,493	1.0084	0.24
4	Oil (well)	40	1,500	161.0	7,211,029	1.0084	0.24
5	NG to compression &	40	1,500	28.0	1,349,493	1.0121	0.24

	membrane						
6	CO_2 to compression & membrane	40	1,500	8.2	61,856	1.0121	0.24
7	Oil to pump	60	1,500	161.0	7,211,029	1.0121	0.24
8	**Oxygen rich**	25	101	5.8	711	16.7759	7.86
9	Nitrogen rich	1	101	25.6	344	1.0000	0.00
10	CO_2 rich-permeate	40	300	8.2	60,975	1.0200	0.25
11	**Oil export to shore**	60	2,300	161.0	7,211,029	1.0123	0.24
12	Natural gas (fuel)	38	4,800	1.5	73,798	1.0200	0.25
13	Waste water	18	4	1.4	70	0.0000	0.00
14	Captured CO_2 to compression	366	100	5.9	2,901	1.1704	0.32
15	Waste water	23	multiple	1.8	5	0.0000	0.00
16	Captured CO_2 to injection	101	45,000	4.2	2,901	1.1839	0.33
17	**Natural gas export**	113	24,500	26.5	1,286,320	1.0282	0.25
18	CO_2 (from well) to injection	130	45,000	8.2	63,442	1.0861	0.29
19	Primary separation (Heating requirement)	150	–	–	1,985	16.1784	5.70
20	**Net power (to compression systems)**	–	–	–	27,477	2.3708	1.08
21	NG export compression power	–	–	–	7,822	2.3708	1.08
22	CO_2 (well) to injection compression power	–	–	–	3,458	2.3708	1.08
23	Air separation compression power	–	–	–	5,970	2.3708	1.08
24	Oil pump power	–	–	–	447	2.3708	1.08
25	Captured CO_2 injection compression power	–	–	–	1,732	2.3708	1.08
26	Gas compression power	–	–	–	8,039	2.3708	1.08
27	NG to compression	38	4,800	26.5	1,280,183	1.0200	0.25

Figure A.4. Offshore platform configuration integrated to an Allam power cycle. Unit exergy cost and specific CO_2 emissions calculation scheme

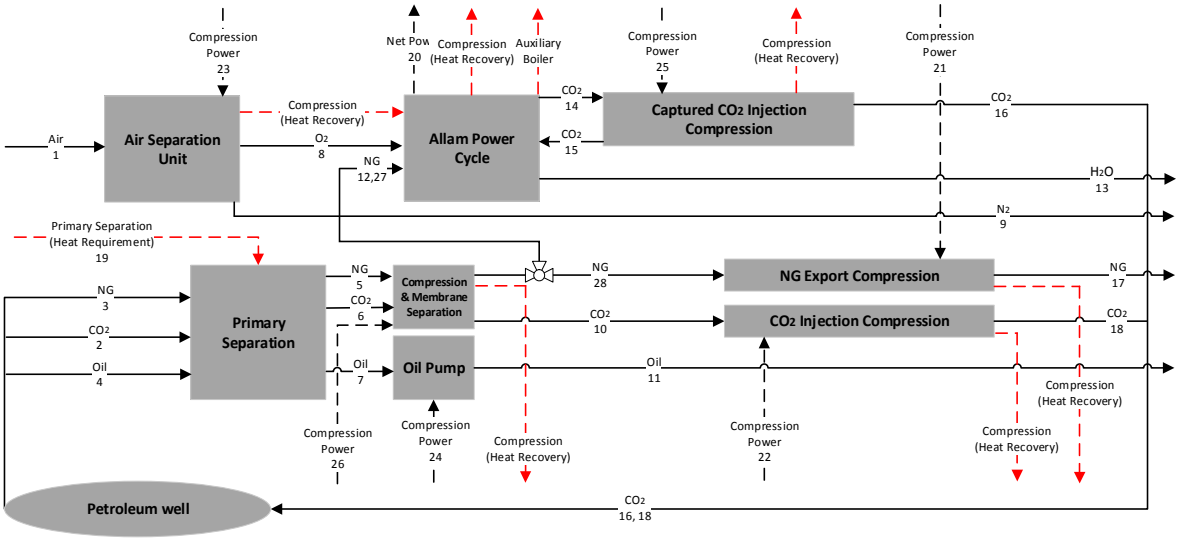

Source: author

Table A.4. Offshore platform configuration integrated to an Allam power cycle. Thermodynamic properties and exergy cost of selected streams in the Fig A.4

N°	Name	T (°C)	P (kPa)	m (kg/s)	B^T (kW)	c (kJ/kJ)	c_{CO2} (g_{CO2}/MJ)
1	Combustion air	25	101	17.8	0	1.0000	0.00
2	CO_2 (well)	40	1,500	8.2	61,856	1.0081	0.25
3	Natural gas (well)	40	1,500	28.0	1,349,493	1.0081	0.25
4	Oil (well)	40	1,500	161.0	7,211,029	1.0081	0.25
5	NG to compression & membrane	40	1,500	28.0	1,349,493	1.0096	0.26
6	CO_2 to compression & membrane	40	1,500	8.2	61,856	1.0096	0.26
7	Oil to pump	60	1,500	161.0	7,211,029	1.0096	0.26
8	**Oxygen rich**	25	101	3.3	403	13.4496	103.51
9	Nitrogen rich	1	101	14.5	195	1.0000	0.00
10	CO_2 rich-permeate	40	300	8.2	60,975	1.0155	0.32
11	**Oil export to shore**	60	2,300	161.0	7,211,029	1.0098	0.26

12	Natural gas (fuel)	38	4,800	0.9	42,758	1.0155	0.32
13	Waste water	30	3,000	1.9	112	0.0000	0.00
14	Captured CO_2 to compression	30	3,000	60.2	37,543	1.1721	1.89
15	CO_2 recycled	40	10,000	57.9	38,311	1.2361	2.76
16	Captured CO_2 to injection	78	45,000	2.3	1,611	1.3170	3.75
17	**Natural gas export**	113	24,500	27.0	1,312,951	1.0212	0.40
18	CO_2 (from well) to injection	130	45,000	8.2	63,442	1.0614	0.94
19	Primary separation (Heating requirement)	150	–	–	1,985	6.8843	37.64
20	**Net power (to compression systems)**	–	–	–	27,237	1.9139	14.22
21	NG export compression power	–	–	–	7,984	1.9139	14.22
22	CO_2 (well) to injection compression power	–	–	–	3,458	1.9139	14.22
23	Air separation compression power	–	–	–	3,384	1.9139	14.22
24	Oil pump power	–	–	–	447	1.9139	14.22
25	Captured CO_2 injection compression power	–	–	–	3,919	1.9139	14.22
26	Gas compression power	–	–	–	8,039	1.9139	14.22
27	Auxiliary boiler fuel	38	4,800	0.09	4,536	1.0155	0.32
28	NG to compression	38	4,800	27.0	1,306,687	1.0155	0.32

Table A.5. Auxiliary equations considered in order to calculate unit exergy and CO_2 emissions costs

	Conventional Configuration	Amines-based Configuration	S-Graz Cycle Configuration	Allam Cycle Configuration
Power Cycle	$c_{20} = 0$ $c_q = \frac{c_1 B_1 + c_2 B_2}{B_1 + B_2}$	$c_9 = 0$ $c_q = \frac{c_1 B_1 + c_2 B_2}{B_1 + B_2} = c_{30}$	$c_{13} = 0$ $c_{14} = \frac{c_8 B_8 + c_{12} B_{12}}{B_8 + B_{12}} = c_q$	$c_{13} = 0$ $c_{14} = \frac{c_8 B_8 + c_{12,27} B_{12,27} + c_{15} B_{15}}{B_8 + B_{12,27} + B_{15}} = c_q$
Primary Separation	$c_{10} = c_9 = c_8$	$c_{11} = c_{12} = c_{15}$	$c_7 = c_5$ $c_6 = c_5$	$c_5 = c_6 = c_7$
Compression & Membrane Separation	$c_{15} = c_{14}$ $c_q = c_{13}$	$c_{13} = c_{14}$ $c_q = c_{10}$	$c_{10} = c_{27}$ $c_{26} = c_q$	$c_q = c_{26}$ $c_{10} = c_{28}$
NG Export Compression	$c_q = c_{16}$	$c_q = c_{26}$	$c_q = c_{21}$	$c_q = c_{21}$
CO_2 Injection Compression	$c_q = c_{17}$	$c_q = c_{27}$	$c_q = c_{22}$	$c_q = c_{22}$
Amines Loop Carbon Capture	-	$c_{22} = 0$ $c_{21} = c_q$ $c_{19} = c_7$	-	-
Captured CO_2 Injection Compression	-	$c_q = c_{25}$ $c_{23} = 0$	$c_{15} = 0$ $c_q = c_{25}$	$c_q = c_{25}$ $c_{15} = c_{16}$
Air Separation Unit	-	-	$c_9 = c_1 = 1$ $c_{23} = c_q$	$c_1 = c_9 = 1$ $c_q = c_{23}$